

MARTIN MARIETTA ENERGY SYSTEMS LIBRARIES



3 4456 0333847 6

ORNL/TM-11812

oml

**OAK RIDGE
NATIONAL
LABORATORY**

MARTIN MARIETTA

Computed Secondary-Particle Energy Spectra Following Nonelastic Neutron Interactions With ^{12}C for E_n Between 15 and 60 MeV: Comparisons of Results from Two Computational Methods

J. K. Dickens

OAK RIDGE NATIONAL LABORATORY
CENTRAL RESEARCH LIBRARY
CIRCULATION SECTION
NSM 2008 171
LIBRARY LOAN COPY
DO NOT TRANSFER TO ANOTHER PERSON
If you wish someone else to use this
report, send in name with report and
the library will arrange a loan.

MANAGED BY
MARTIN MARIETTA ENERGY SYSTEMS, INC.
FOR THE UNITED STATES
DEPARTMENT OF ENERGY

This report has been reproduced directly from the best available copy.

Available to DOE and DOE contractors from the Office of Scientific and Technical Information, P.O. Box 62, Oak Ridge, TN 37831; prices available from (615) 578-8401, FTS 628-8401.

Available to the public from the National Technical Information Service, U.S. Department of Commerce, 5285 Port Royal Rd., Springfield, VA 22161.

This report was prepared as an account of work sponsored by an agency of the United States Government. Neither the United States Government nor any agency thereof, nor any of their employees, makes any warranty, express or implied, or assumes any legal liability or responsibility for the accuracy, completeness, or usefulness of any information, apparatus, product, or process disclosed, or represents that its use would not infringe privately owned rights. Reference herein to any specific commercial product, process, or service by trade name, trademark, manufacturer, or otherwise, does not necessarily constitute or imply its endorsement, recommendation, or favoring by the United States Government or any agency thereof. The views and opinions of authors expressed herein do not necessarily state or reflect those of the United States Government or any agency thereof.

ORNL/TM-11812

Engineering Physics and Mathematics Division

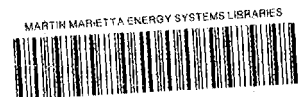
**COMPUTED SECONDARY-PARTICLE ENERGY
SPECTRA FOLLOWING NONELASTIC NEUTRON
INTERACTIONS WITH ^{12}C FOR E_n BETWEEN
15 AND 60 MeV: COMPARISONS OF RESULTS
FROM TWO CALCULATIONAL METHODS**

J. K. Dickens

DATE PUBLISHED — April 1991

Prepared for the
Office of Energy Research
Division of Nuclear Physics

Prepared by the
OAK RIDGE NATIONAL LABORATORY
Oak Ridge, Tennessee 37831
managed by
MARTIN MARIETTA ENERGY SYSTEMS, INC.
for the
U.S. DEPARTMENT OF ENERGY
under contract DE-AC05-84OR21400



3 4456 0333847 6

CONTENTS

ABSTRACT	viii
1. INTRODUCTION	1
2. COMPARISONS OF THE COMPUTATIONAL METHODS	2
3. COMPARISONS OF SECONDARY PROTON PRODUCTION	5
4. COMPARISONS OF SECONDARY DEUTERON PRODUCTION	14
5. COMPARISONS OF SECONDARY TRITON PRODUCTION	22
6. COMPARISONS OF ^3He -ION PRODUCTION	29
7. COMPARISONS OF ALPHA PARTICLE PRODUCTION	36
8. COMPARISONS OF SECONDARY NEUTRON PRODUCTION	46
9. COMPARISONS OF TOTAL PARTICLE PRODUCTION CROSS SECTIONS	57
10. CONCLUSIONS AND RECOMMENDATIONS	61
ACKNOWLEDGMENTS	63
REFERENCES	64

LIST OF FIGURES

<u>Fig.</u>		<u>Page</u>
1	Distribution of kinetic energies of the outgoing proton in a $^{12}\text{C}(n,p)^{12}\text{B}$ reaction for $E_n = 40$ MeV	6
2	Comparison of outgoing secondary-proton energy spectra for an incident neutron energy of 20 MeV	7
3	Comparison of outgoing secondary proton energy spectra for an incident neutron energy of 25 MeV	8
4	Comparison of outgoing secondary-proton energy spectra for an incident neutron energy of 30 MeV	9
5	Comparison of outgoing secondary-proton energy spectra for an incident neutron energy of 35 MeV	10
6	Comparison of outgoing secondary-proton energy spectra for an incident neutron energy of 40 MeV	11
7	Comparison of outgoing secondary-proton energy spectra for an incident neutron energy of 50 MeV	12
8	Comparison of outgoing secondary-proton energy spectra for an incident neutron energy of 60 MeV	13
9	Comparison of outgoing secondary-deuteron energy spectra for an incident neutron energy of 20 MeV	15
10	Comparison of outgoing secondary-deuteron energy spectra for an incident neutron energy of 25 MeV	16

<u>Fig.</u>		<u>Page</u>
11	Comparison of outgoing secondary-deuteron energy spectra for an incident neutron energy of 30 MeV	17
12	Comparison of outgoing secondary-deuteron energy spectra for an incident neutron energy of 35 MeV	18
13	Comparison of outgoing secondary-deuteron energy spectra for an incident neutron energy of 40 MeV	19
14	Comparison of outgoing secondary-deuteron energy spectra for an incident neutron energy of 50 MeV	20
15	Comparison of outgoing secondary-deuteron energy spectra for an incident neutron energy of 60 MeV	21
16	Comparison of outgoing secondary-triton energy spectra for an incident neutron energy of 25 MeV	23
17	Comparison of outgoing secondary-triton energy spectra for an incident neutron energy of 30 MeV	24
18	Comparison of outgoing secondary-triton energy spectra for an incident neutron energy of 35 MeV	25
19	Comparison of outgoing secondary-triton energy spectra for an incident neutron energy of 40 MeV	26
20	Comparison of outgoing secondary-triton energy spectra for an incident neutron energy of 50 MeV	27
21	Comparison of outgoing secondary-triton energy spectra for an incident neutron energy of 60 MeV	28
22	Comparison of outgoing secondary- ³ He-ion energy spectra for an incident neutron energy of 25 MeV	30

<u>Fig.</u>		<u>Page</u>
23	Comparison of outgoing secondary- ³ He-ion energy spectra for an incident neutron energy of 30 MeV	31
24	Comparison of outgoing secondary- ³ He-ion energy spectra for an incident neutron energy of 35 MeV	32
25	Comparison of outgoing secondary- ³ He-ion energy spectra for an incident neutron energy of 40 MeV	33
26	Comparison of outgoing secondary- ³ He-ion energy spectra for an incident neutron energy of 50 MeV	34
27	Comparison of outgoing secondary- ³ He-ion energy spectra for an incident neutron energy at 60 MeV	35
28	Comparison of outgoing secondary-alpha energy spectra for an incident neutron energy of 15 MeV	38
29	Comparison of outgoing secondary-alpha energy spectra for an incident neutron energy of 20 MeV	39
30	Comparison of outgoing secondary-alpha energy spectra for an incident neutron energy of 25 MeV	40
31	Comparison of outgoing secondary-alpha energy spectra for an incident neutron energy of 30 MeV	41
32	Comparison of outgoing secondary-alpha energy spectra for an incident neutron energy of 35 MeV	42
33	Comparison of outgoing secondary-alpha energy spectra for an incident neutron energy of 40 MeV	43
34	Comparison of outgoing secondary-alpha energy spectra for an incident neutron energy of 50 MeV	44

<u>Fig.</u>		<u>Page</u>
35	Comparison of outgoing secondary-alpha energy spectra for an incident neutron energy of 60 MeV	45
36	Comparison of outgoing secondary-neutron energy spectra for an incident neutron energy of 15 MeV	48
37	Comparison of outgoing secondary-neutron energy spectra for an incident neutron energy of 20 MeV	49
38	Comparison of outgoing secondary-neutron energy spectra for an incident neutron energy of 25 MeV	50
39	Comparison of outgoing secondary-neutron energy spectra for an incident neutron energy of 30 MeV	51
40	Comparison of outgoing secondary-neutron energy spectra for an incident neutron energy of 35 MeV	52
41	Comparison of outgoing secondary-neutron energy spectra for an incident neutron energy of 40 MeV	53
42	Comparison of outgoing secondary-neutron energy spectra for an incident neutron energy of 50 MeV	54
43	Comparison of outgoing secondary-neutron energy spectra for an incident neutron energy of 60 MeV	55
44	Distribution of kinetic energies of the outgoing secondary neutron in a $^{12}\text{C}(n, n')^{12}\text{C}$ reaction for $E_n = 40$ MeV and for the residual ^{12}C in a highly excited continuum state.	56

ABSTRACT

The organic scintillation detector response code SCINFUL has been used to compute secondary-particle energy spectra, $d\sigma/dE$, following nonelastic neutron interactions with ^{12}C for incident neutron energies between 15 and 60 MeV. The resulting spectra are compared with published similar spectra computed by Brenner and Prael who used an intranuclear cascade code, including alpha clustering, a particle pickup mechanism, and a theoretical approach to sequential decay via intermediate particle-unstable states. The similarities of and the differences between the results of the two approaches are discussed.

1. INTRODUCTION

In a recently published paper¹ Brenner and Prael reported on calculated differential secondary-particle production cross sections following nonelastic neutron interactions with ^{12}C . Their calculations utilized a Monte-Carlo-based intranuclear cascade code called INCA including alpha clustering and particle pickup. They used a second program called FBRK to compute deexcitation of a highly-excited compound nucleus which included a Fermi breakup mechanism² to account for decay via intermediate particle-unstable states. Calculated spectra were reported for $E_n = 15, 20, 25, 30, 35, 40, 50$ and 60 MeV.

At about the same time as their paper was published, the present author was completing documentation on a Monte-Carlo-based code to compute responses of organic scintillators to incident monoenergetic neutrons having energies between 0.1 and 80 MeV. This program,³ called SCINFUL for SCINtillator FULL energy response, is divided into three, rather distinct, calculational phases. These are: (1) computing characteristics of energetic charged particles following neutron interactions with the carbon and hydrogen constituents of the detecting medium; (2) multiple scattering in and geometrical aspects of a finite-sized detector, including partial or complete absorption of the energy of the charged particles; and (3) the transformation of the total absorbed charged-particle energy into fluorescent light.

The nuclear data published¹ by Brenner and Prael are the same type of data resulting from the first phase of the SCINFUL calculation. The methods of obtaining these secondary-particle production cross sections are quite different, however, and it is of some interest to compare results of these two programs.

It should be emphasized at the outset that it is not the purpose of this comparison to enter into any discussion on the validity of the use of the intranuclear cascade concept for calculations herein presented. Rather, the point is that the data deduced by Brenner and Prael are published,¹ and it is reasonable to inquire what effects, if any, might have been observed in the total detector-response output had the data published by Brenner and Prael been used in the first phase of the SCINFUL calculation instead of the data actually generated by the SCINFUL programming.

One way to have done the comparison would have been to replace the first-phase SCINFUL results with some method of utilizing the tabular values of the Brenner-Prael data of ref. 1. This way would have entailed a considerable amount of reprogramming of SCINFUL, and it would have the added disadvantage that if differences were observed, the source or sources of those differences probably would not be readily apparent.

The way the comparison was done was to add several arrays to SCINFUL and then to save results of what are intermediate calculations in SCINFUL in these arrays. At the end of the total calculation the data saved in these arrays were output for direct comparison with Brenner-Prael tabulated values. Any source of potential calculated response difference is quickly apparent; however, the potential calculated detector response difference can be only qualitatively discussed.

2. COMPARISONS OF THE COMPUTATIONAL METHODS

The basis of the INCA-FBRK code family is primarily theoretical, using mostly fundamental physics concepts. In the first stage of the calculation the nuclear processes are modeled with an intranuclear cascade code, which, in turn, relies on modeling two-body interactions. The carbon nucleus is considered to be made up of α particles, neutrons and protons which interact with the incident neutron. Because secondary deuterons are observed experimentally⁴ a pickup model was devised and incorporated which complements the intranuclear cascade. Deexcitation of a highly-excited compound nucleus is computed using a Fermi-breakup model,² in which channel probabilities depend upon statistical weights generated by the model. Decay of highly-excited states is sequential as secondary particles are “boiled” off. Coulomb-barrier penetration factors are computed explicitly. Up to seven-body breakups are allowed. The only experimental data used are those for mass excesses and nuclear properties of low-lying and ground states of residual nuclei of Li, Be, B, and C.

The basic methods used in the nuclear part of SCINFUL have been published.⁵ Some comparisons with data of Subramanian et al.⁴ are given in that paper; a more complete set of comparisons with experimental data is given in a laboratory report.⁶ The nuclear portion of SCINFUL is definitely semi-empirical. All available experimental data were utilized in developing the code, for example, published cross sections and angular distributions of reaction particles. For some quantities, e.g. angular distributions, parametric representations of the data are devised and used for ease of interpolation and Monte-Carlo sampling. For cross sections not available from experiment, evaluated data from the U. S. ENDF/B evaluation⁷ for $n + {}^{12}\text{C}$ reactions were used when available for $E_n \leq 20$ MeV. Other data, particularly for $E_n \geq 20$ MeV, were adapted from calculations using the statistical model code TNG.⁸ Except for the



reaction assigned as an “instantaneous” breakup of the ${}^{12}\text{C}$ into three α particles, the initial interaction is treated as a binary system:



where x represents a light reaction product, n , p , d , t , ${}^3\text{He}$, or α , and Y represents the heavy residual particle, Be, B, or C. SCINFUL computes deexcitation of a highly-excited Y particle using probabilities available from evaluations⁹ or experimental data where available or statistical-model code calculations⁸ when experimental data are not available.

Some comparisons of the calculational methods of the Brenner-Prael codes INCA-FBRK *vis-a-vis* SCINFUL are given in Table 1.

Table 1. Comparisons of Two Methods for Calculating Secondary-Particle Production Cross Sections after Nonelastic Neutron Interactions with ^{12}C

Calculation	INCA-FBRK ^a	SCINFUL ^b
Overall	Primarily theoretical	Semi-empirical
Experimental Cross Sections	Two-body interactions	All $n + ^{12}\text{C}$ experimental data available.
Direct interactions	Only for (n, d) reactions, which are modeled	Implied in all channels by use of cross section data
Continuum-particle spectrum	Intranuclear cascade model	Parametrization of statistical model calculations
Alpha clustering of ^{12}C	Included specifically	Not included
Outgoing nucleon angular distributions	Calculated as part of the cascade model	Parametric representation of experimental data; otherwise isotropic in center of mass
Deexcitation of highly-excited residual nucleus	Fermi breakup model; some experimental data used; sequential	Experimental data when available; parametrized statistical model estimates; sequential, except for 3α breakup of ^{12}C
Number of breakup modes	Seven	Four charged particles and two neutrons

^aRef. 1.^bRef. 3.

In the next sections, comparisons of differential energy cross sections, $d\sigma/dE$, determined by INCA-FBRK and by SCINFUL will be presented. As originally written in the SCINFUL code,³ angular and energy distributions of secondary particles were completely internal to the code. However, when the double differential data of Subramanian et al.⁴ were provided¹⁰ as angle-integrated charged-particle energy spectra, SCINFUL was modified to output calculated results of energy spectra (in 1-MeV-wide bins) for comparison purposes.

For the present comparisons, the SCINFUL output is compared with the angle-integrated data given in the last column of the tables in the Brenner-Prael report.¹ In principle angular distributions could also be extracted from SCINFUL; however, there would be a substantial increase in computed uncertainties associated with the computed angular distributions. The comparisons that follow are likely sufficient

4 *COMPARISONS OF THE COMPUTATIONAL METHODS*

to demonstrate approximate equivalences and/or definite differences in the output from the two different programs.

3. COMPARISONS OF SECONDARY PROTON PRODUCTION

In SCINFUL the secondary proton spectra are very important since it is these protons that contribute much of the detector response due to $n+^{12}\text{C}$ interactions. Initial reactions of the type



are divided into two groups — those that leave the ${}^{12}\text{B}$ in a bound state and those that don't. Separate excitation functions are included in SCINFUL, and that for the bound state group is tailored to give at least moderate agreement with the Subramanian et al.⁴ high-energy response data up to $E_n = 60$ MeV.

To represent a proton continuum, SCINFUL uses a parametrized analytic function as used in an earlier detector response code O5S:¹¹

$$\Phi(E_p) = E_p * \text{EXP}(-E_p/\text{Temp}) * [1.0 - \text{EXP}(-K * E_p/B)] \quad (4)$$

where $K = 1.5$ and $B = 2.9$ to approximate the effects of Coulomb repulsion, and Temp is a "temperature" given by:

$$\text{Temp} = E_n * [0.1245 + 0.001 * \text{ABS}(E_n - 45)] \quad (5)$$

The parametrization of the variable Temp was deduced empirically not only to reproduce the data of Subramanian et al.⁴ but also the data of Lockwood et al.¹² A comparison of this function, Eq. (4), with a statistical model⁸ calculation is exhibited in Fig. 1.

Figures 2 to 8 exhibit comparisons between the calculated data given in the Brenner-Prael report¹ and the SCINFUL computations. The normalization is absolute. The agreement for $E_p > 6$ MeV and $E_n \geq 30$ MeV is quite good, being different only in the detail that SCINFUL computes more ${}^{12}\text{B}$ bound-state yield than does INCA-FBRK and somewhat less middle- to high-energy continuum. The major difference is for the low-energy response $E_p < 5$ MeV. This difference is most likely due to the intranuclear cascade of the continuum, since at $E_n = 30$ MeV, there is, for practical purposes, insufficient energy for reactions leading to a final state having two separate protons.

ORNL-DWG 88-6088

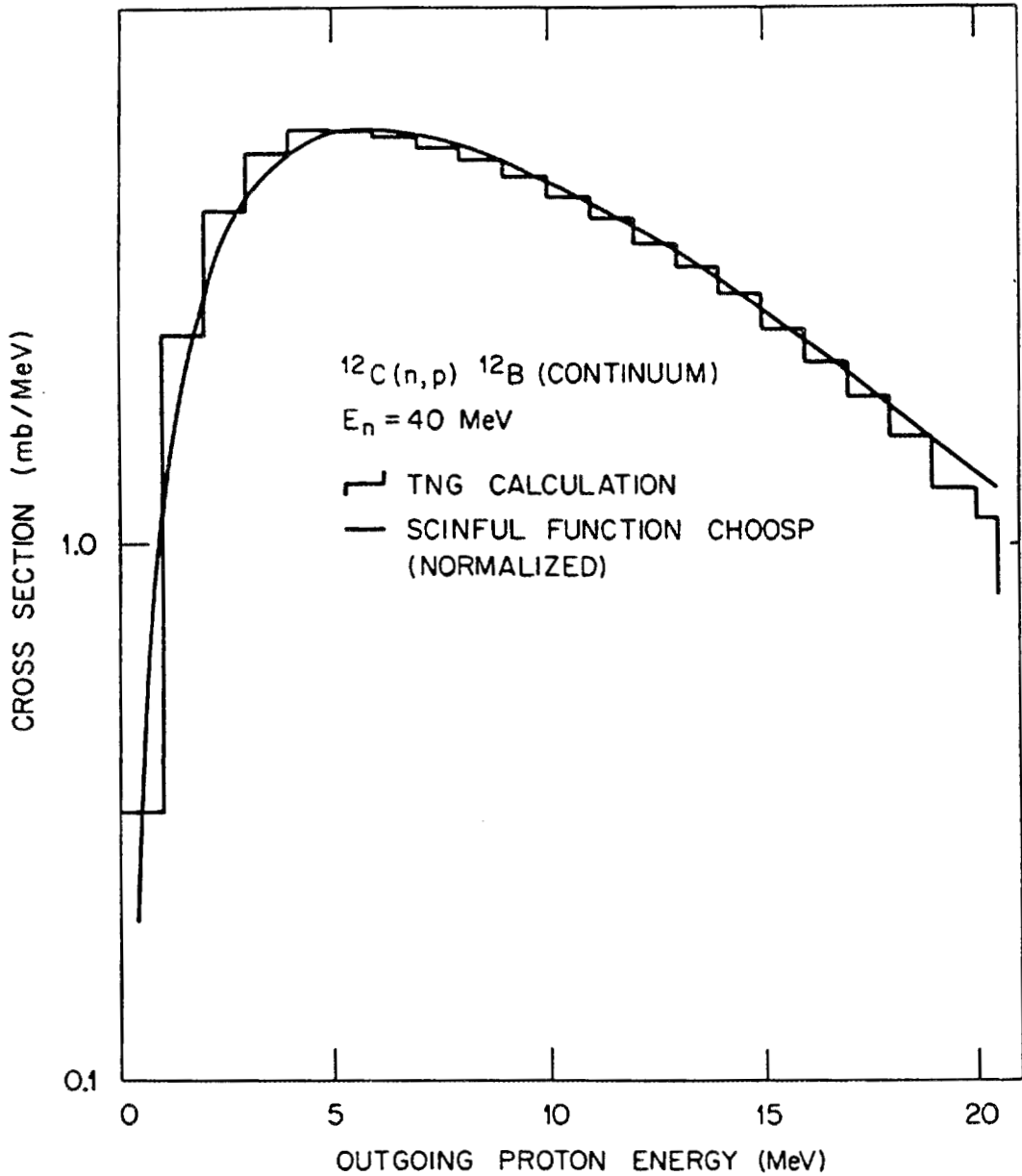


Fig. 1. Distribution of kinetic energies of the outgoing proton in a $^{12}\text{C}(n,p)^{12}\text{B}$ reaction for $E_n = 40$ MeV. The histogram was computed using the statistical-model code TNG (ref. 8). The normalized curve is the analytic function used in the author's code SCINFUL (ref. 3) and is given in Eqs. (4) and (5) of the text.

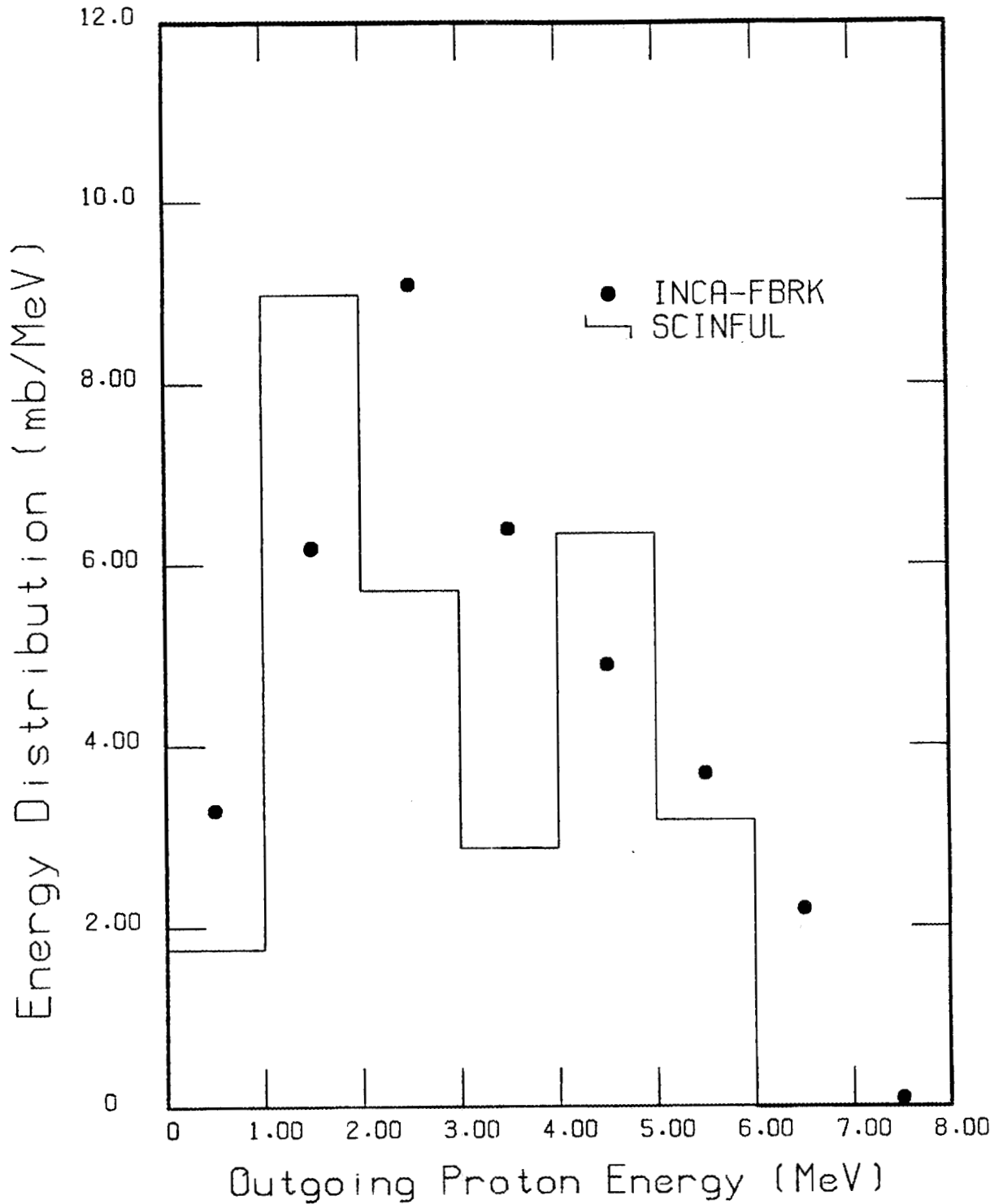


Fig. 2. Comparison of outgoing secondary-proton energy spectra for an incident neutron energy of 20 MeV. The solid points represent the spectrum computed using the intranuclear-cascade model code family INCA-FBRK; the data shown for this spectrum are reported in ref. 1. The histogram represents the same spectrum computed using the author's SCINFUL code which is described in ref. 3.

8 COMPARISONS OF SECONDARY PROTON PRODUCTION

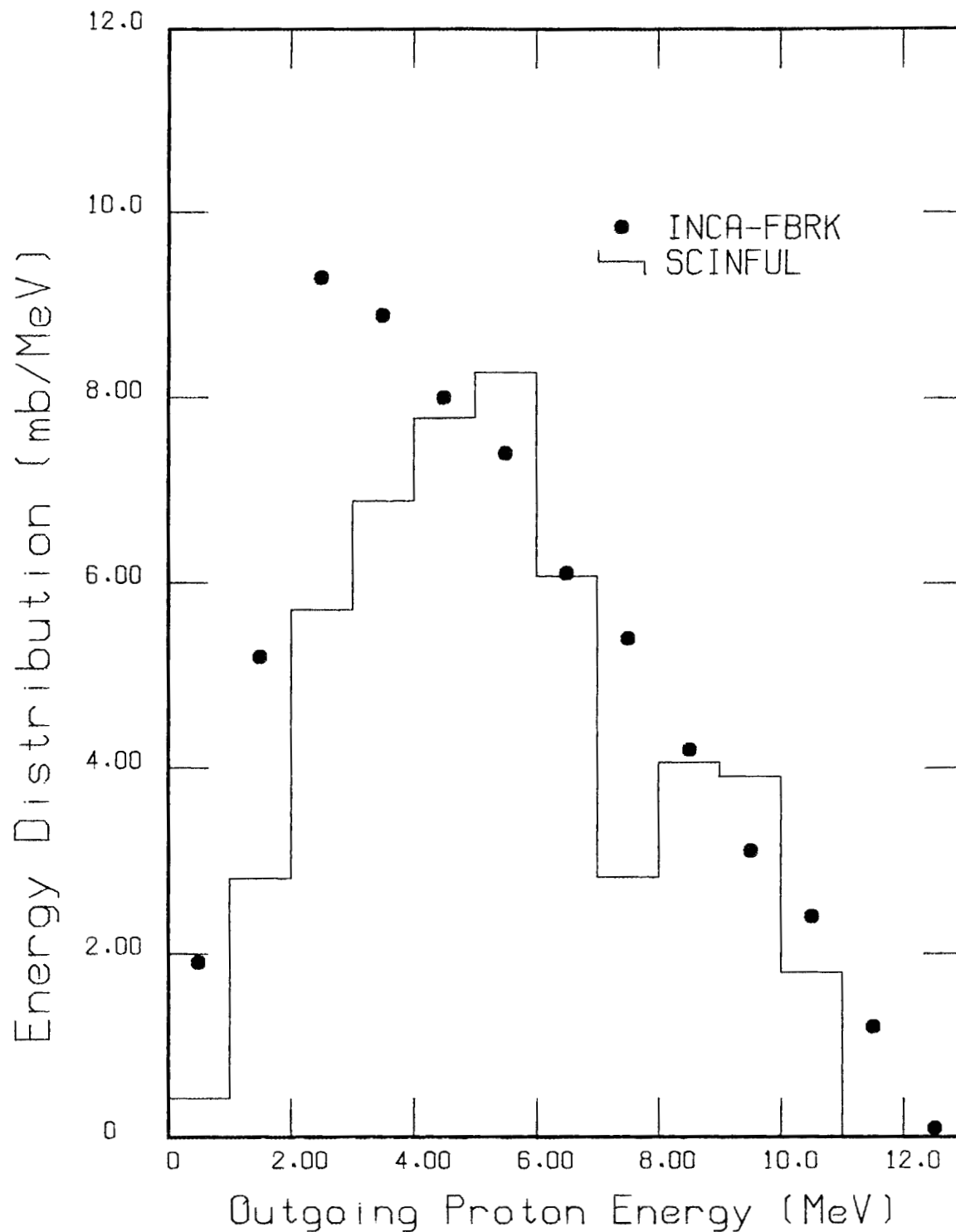


Fig. 3. Comparison of outgoing secondary proton energy spectra for an incident neutron energy of 25 MeV. The solid points represent the spectrum computed using the intranuclear-cascade model code family INCA-FBRK; the data shown for this spectrum are reported in ref. 1. The histogram represents the same spectrum computed using the author's SCINFUL code which is described in ref. 3.

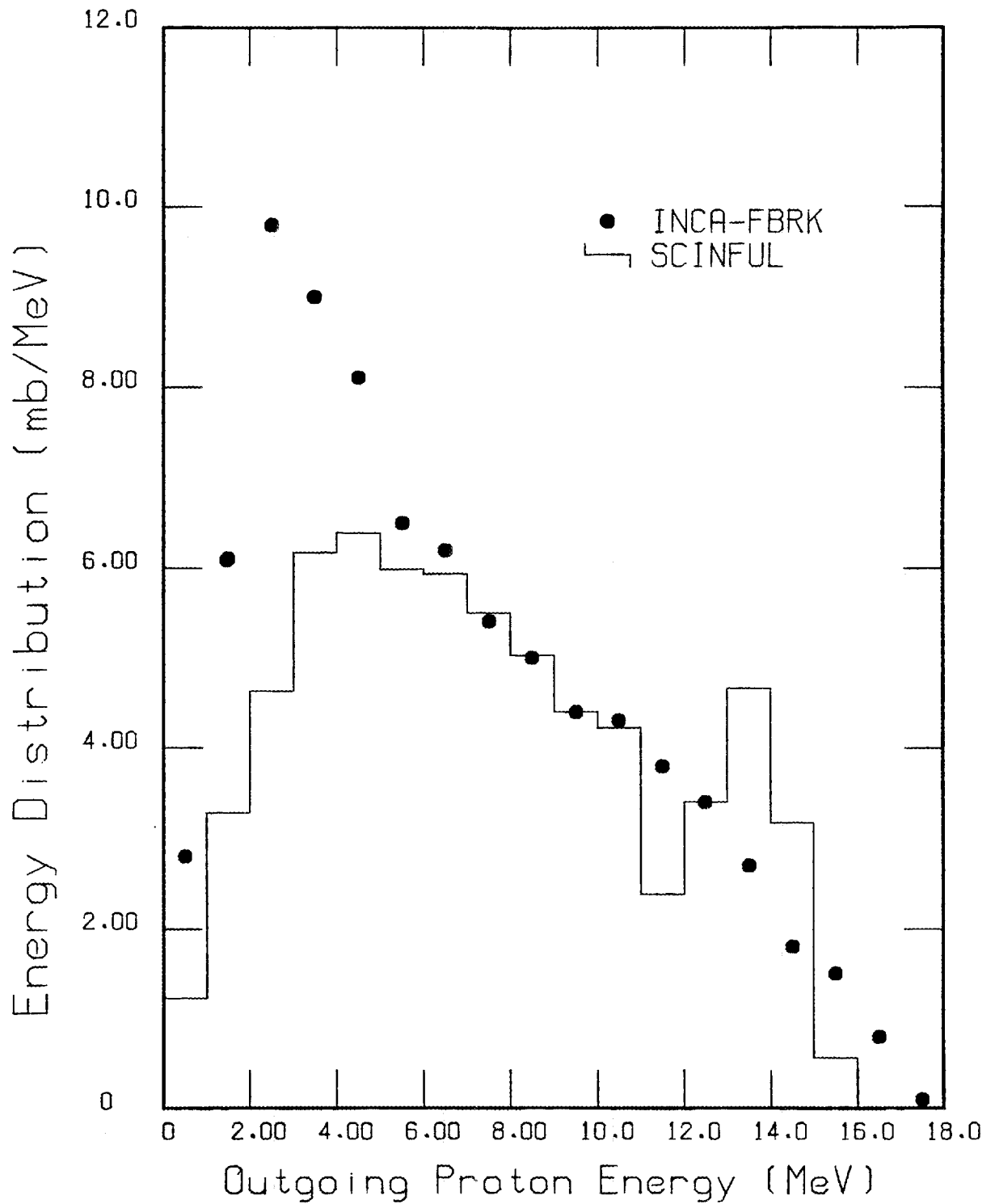


Fig. 4. Comparison of outgoing secondary-proton energy spectra for an incident neutron energy of 30 MeV. The solid points represent the spectrum computed using the intranuclear-cascade model code family INCA-FBRK; the data shown for this spectrum are reported in ref. 1. The histogram represents the same spectrum computed using the author's SCINFUL code which is described in ref. 3.

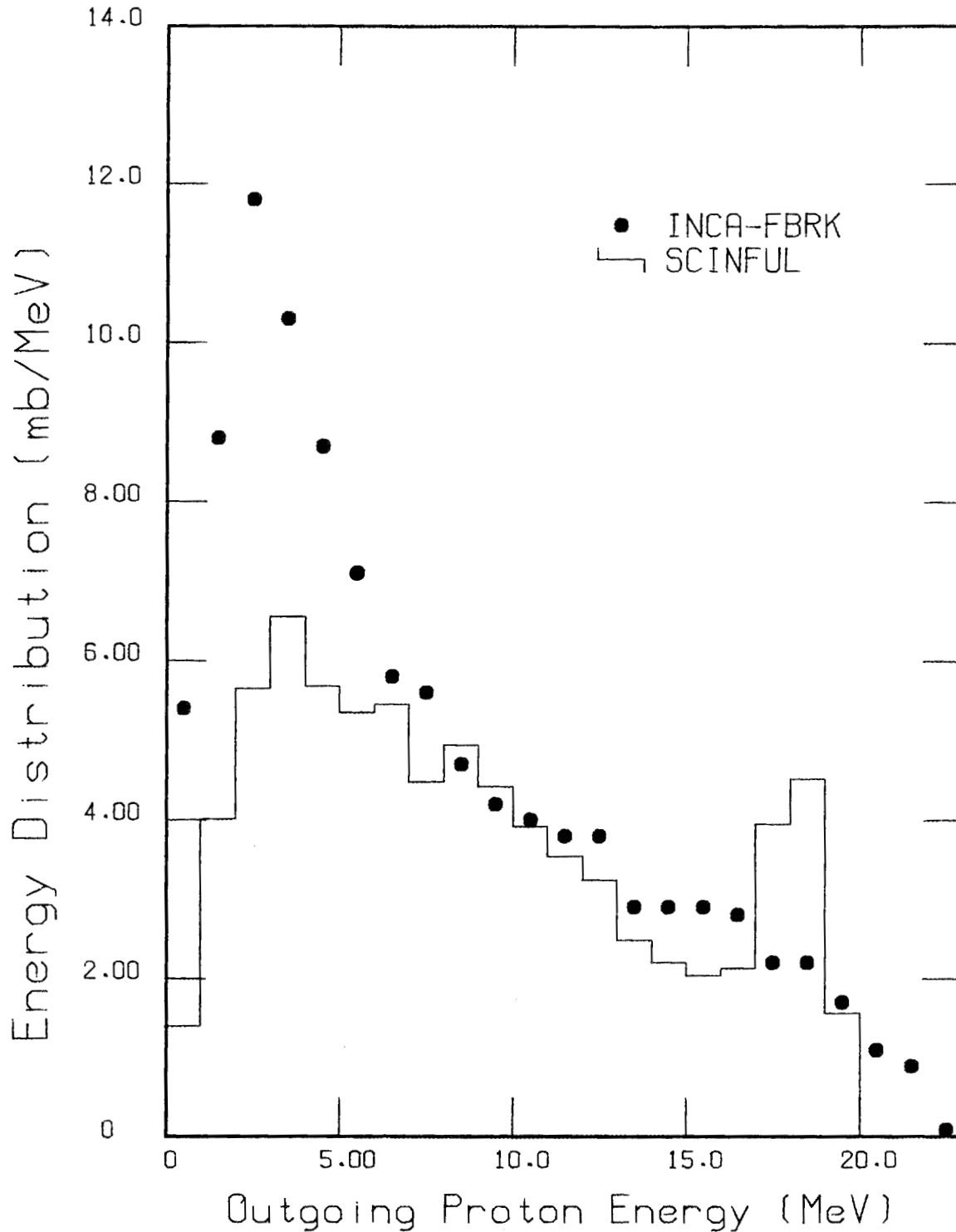


Fig. 5. Comparison of outgoing secondary-proton energy spectra for an incident neutron energy of 35 MeV. The solid points represent the spectrum computed using the intranuclear-cascade model code family INCA-FBRK; the data shown for this spectrum are reported in ref. 1. The histogram represents the same spectrum computed using the author's SCINFUL code which is described in ref. 3.

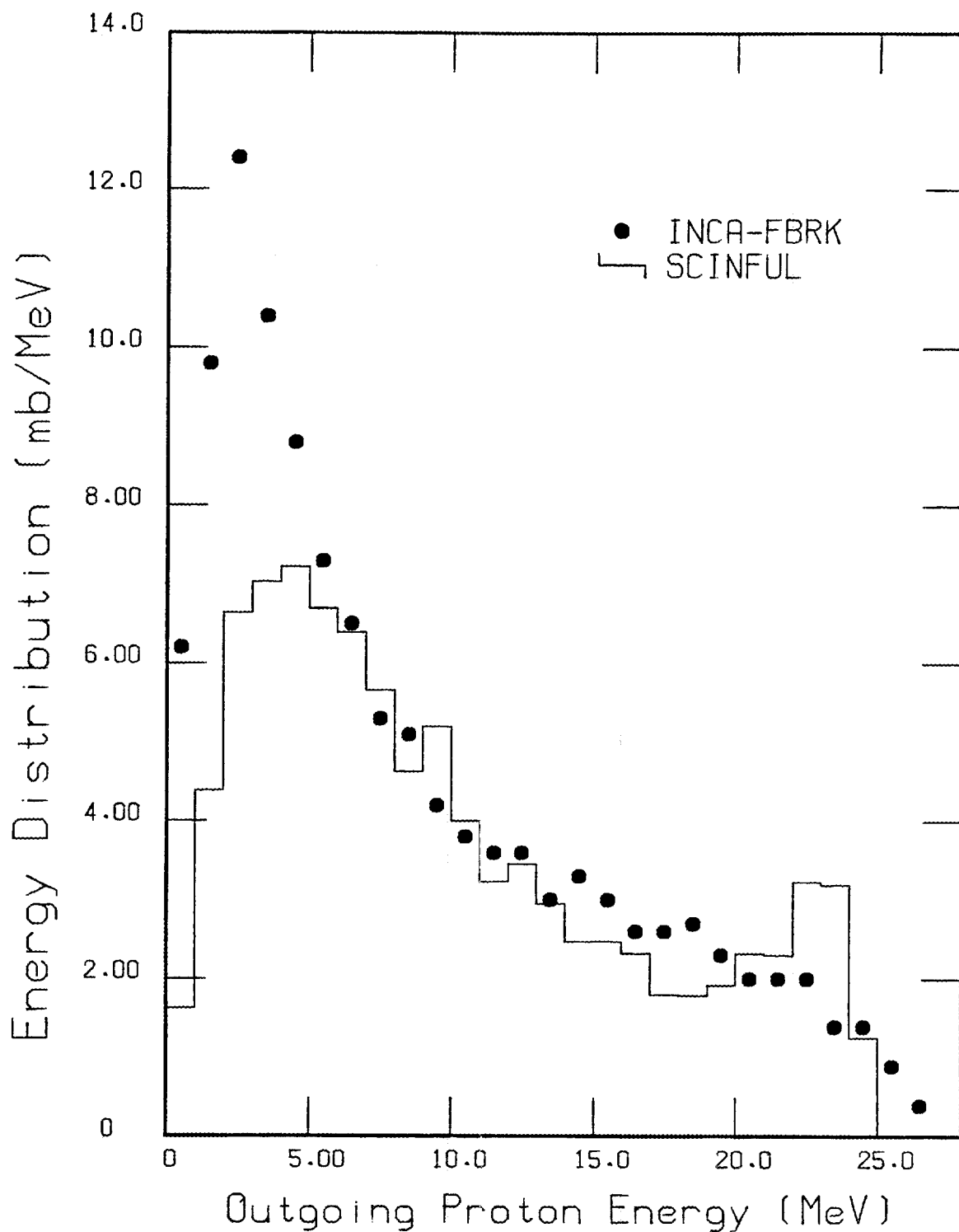


Fig. 6. Comparison of outgoing secondary-proton energy spectra for an incident neutron energy of 40 MeV. The solid points represent the spectrum computed using the intranuclear-cascade model code family INCA-FBRK; the data shown for this spectrum are reported in ref. 1. The histogram represents the same spectrum computed using the author's SCINFUL code which is described in ref. 3.

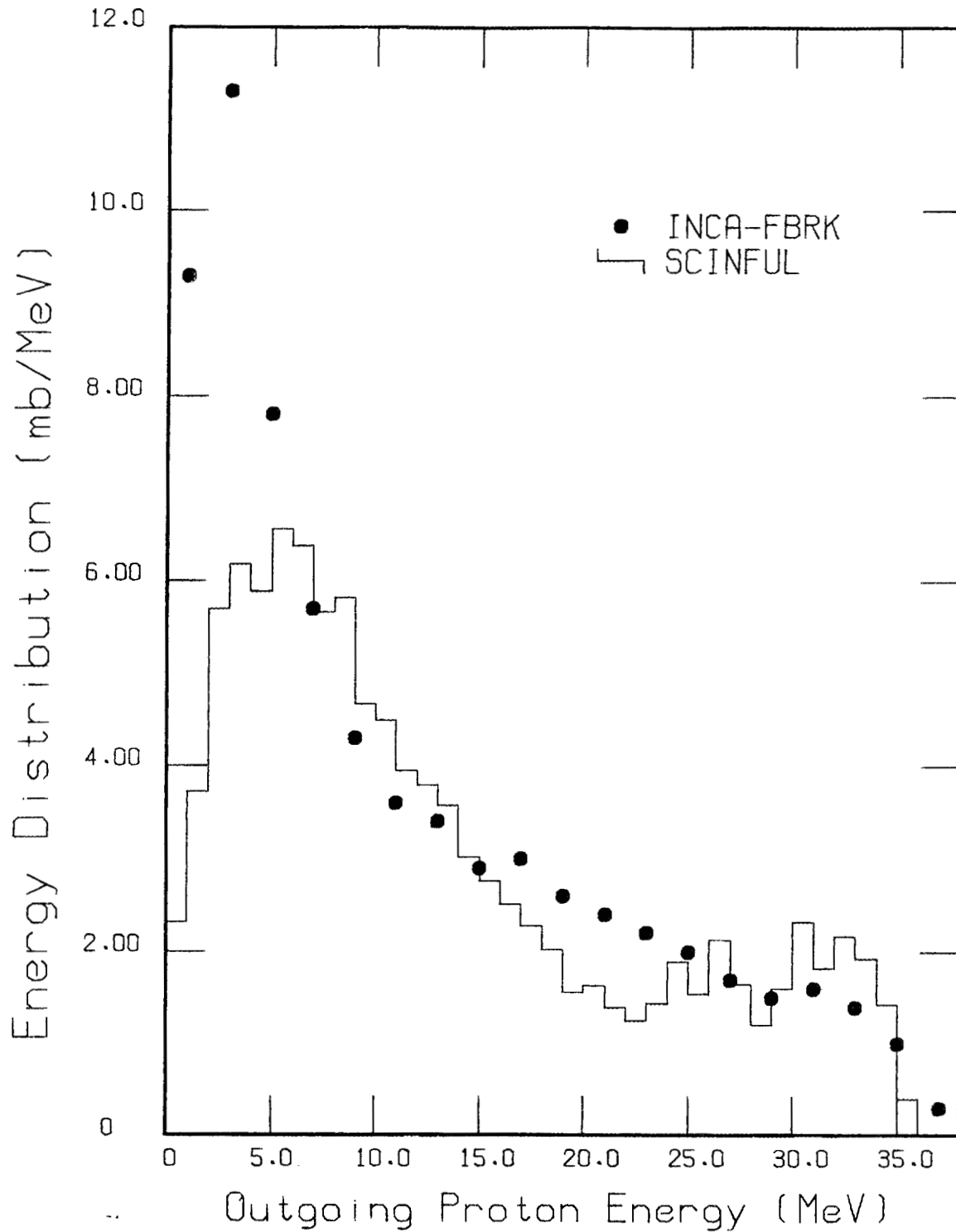


Fig. 7. Comparison of outgoing secondary-proton energy spectra for an incident neutron energy of 50 MeV. The solid points represent the spectrum computed using the intranuclear-cascade model code family INCA-FBRK; the data shown for this spectrum are reported in ref. 1. The histogram represents the same spectrum computed using the author's SCINFUL code which is described in ref. 3.

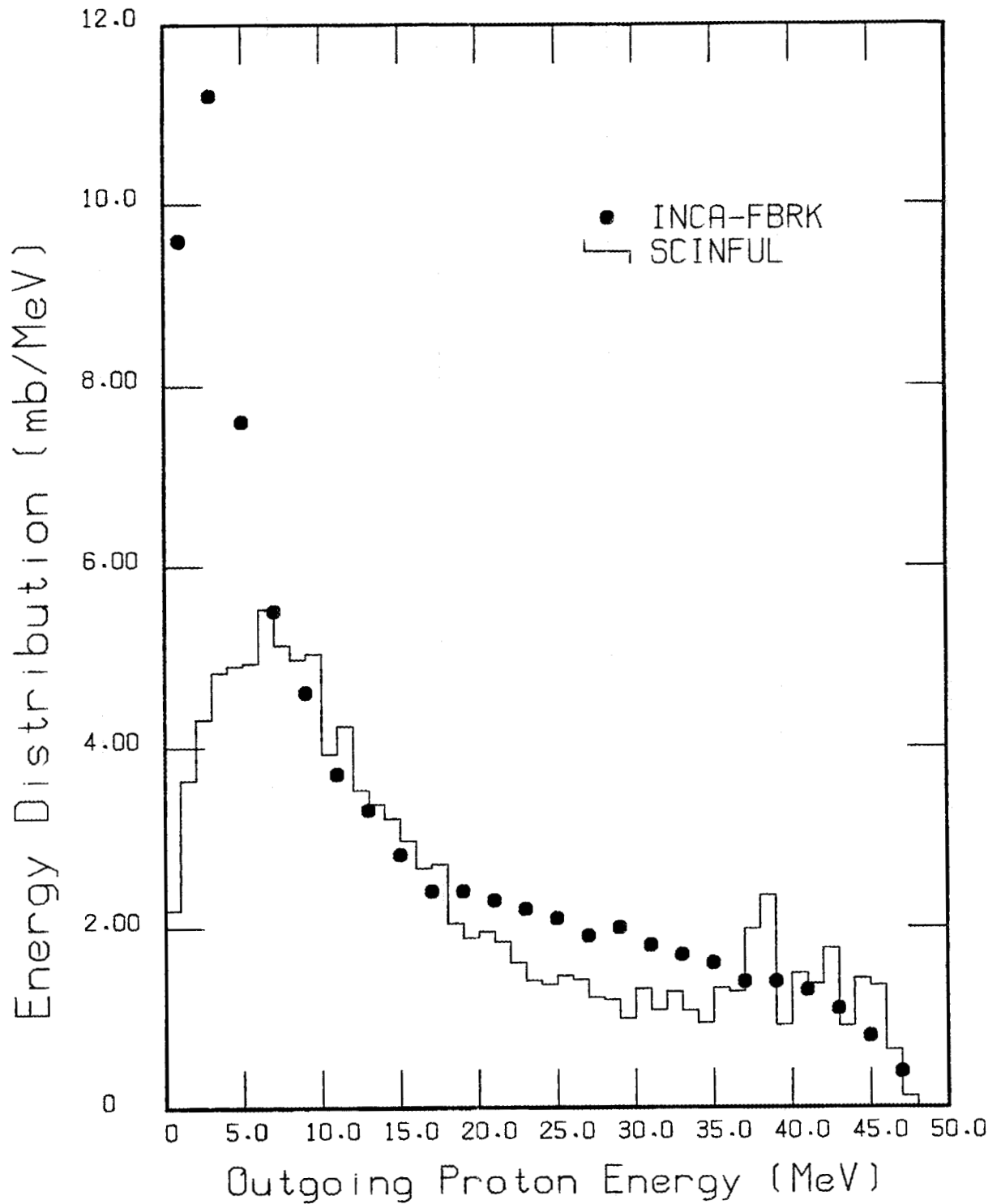


Fig. 8. Comparison of outgoing secondary-proton energy spectra for an incident neutron energy of 60 MeV. The solid points represent the spectrum computed using the intranuclear-cascade model code family INCA-FBRK; the data shown for this spectrum are reported in ref. 1. The histogram represents the same spectrum computed using the author's SCINFUL code which is described in ref. 3.

4. COMPARISONS OF SECONDARY DEUTERON PRODUCTION

Secondary deuterons are also important in SCINFUL because, as the experiment of Subramanian et al.⁴ exhibited, and Brenner and Prael^{1,4} found they had to account for by a separate pickup mechanism not in their intranuclear cascade calculation, the secondary deuteron spectra are dominated by high energy deuterons. This high-energy deuteron group has a distinct light output in the full SCINFUL calculation, and the position of this group in the total computed response agrees with a similar peak in experimental responses¹² observed for E_n from 40 to 75 MeV.

For the continuum portion of the secondary deuteron spectrum the formula of Eq. (4) is used. However, a different ad hoc parametrization of the variable $Temp$ is used:

$$Temp = \begin{cases} 0.13 * E_n & \text{for } E_n > 30 \text{ MeV} \\ 12.6 - 1.07 * E_n + 0.026 * E_n^2 & \text{for } E_n < 30 \text{ MeV} \end{cases} \quad (6a)$$

$$(6b)$$

Because of the domination of the secondary deuteron spectra by the high-energy deuterons, detector response calculations are not very sensitive to the variable $Temp$.

Comparisons of deuteron calculations are shown in Figs. 9 to 15. The major differences are for the high-energy portion of the responses and (similar to the secondary proton spectra) the preponderance of low energy deuterons in the INCA-FBRK calculation. This feature is also likely due to the intranuclear cascade model treatment. Interestingly, for $E_n = 60.7$ MeV, the deuteron data of Subramanian et al.⁴ exhibit a peak for $E_{d'} \leq 5$ MeV having a yield about twice the SCINFUL calculation (see Fig. 4 of ref. 5). For $E_{d'} > 7$ MeV, the SCINFUL computation reproduces the Subramanian et al.⁴ spectrum at $E_n = 60.7$ MeV quite well.

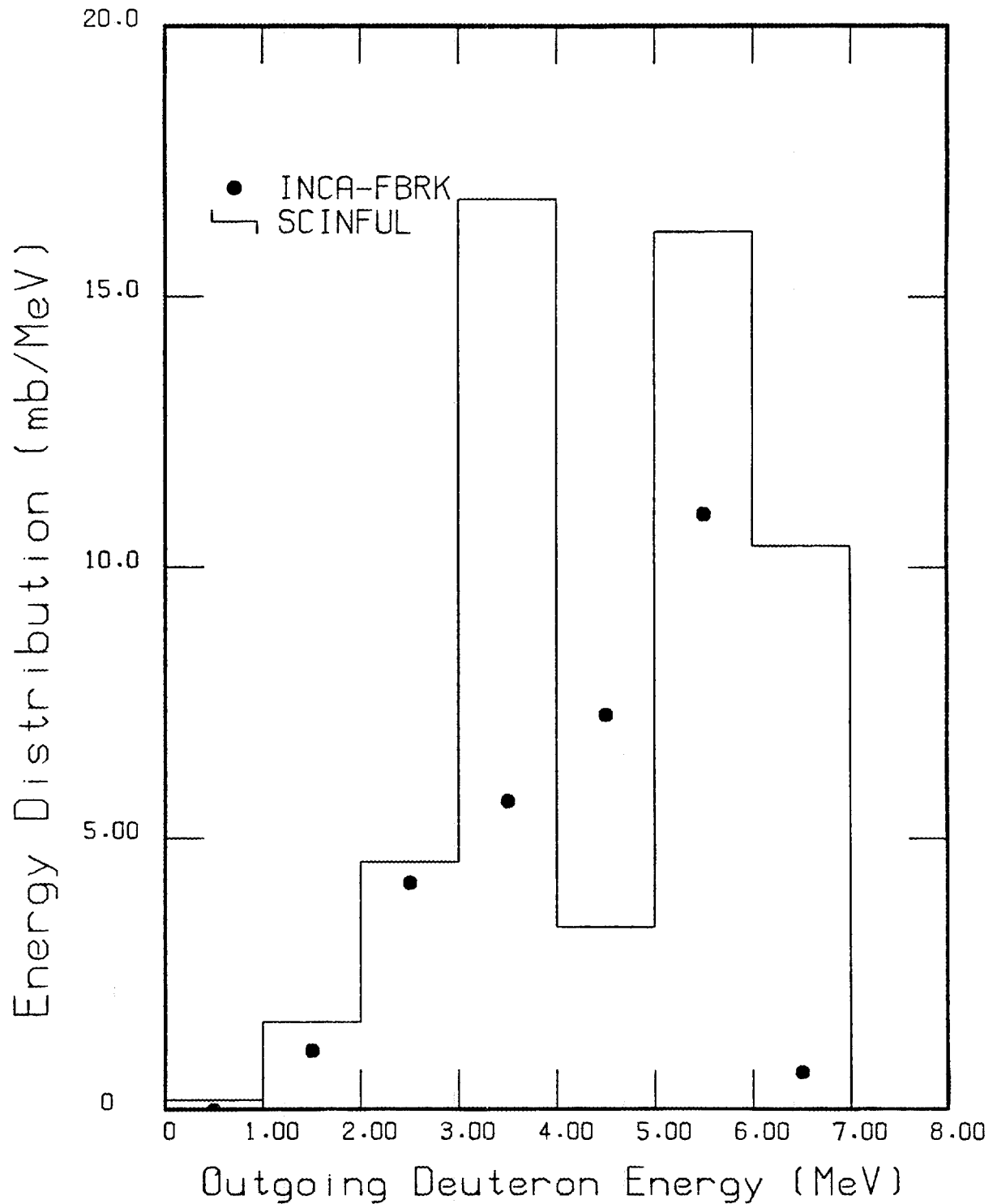


Fig. 9. Comparison of outgoing secondary-deuteron energy spectra for an incident neutron energy of 20 MeV. The solid points represent the spectrum computed using the intranuclear-cascade model code family INCA-FBRK; the data shown for this spectrum are reported in ref. 1. The histogram represents the same spectrum computed using the author's SCINFUL code which is described in ref.3.

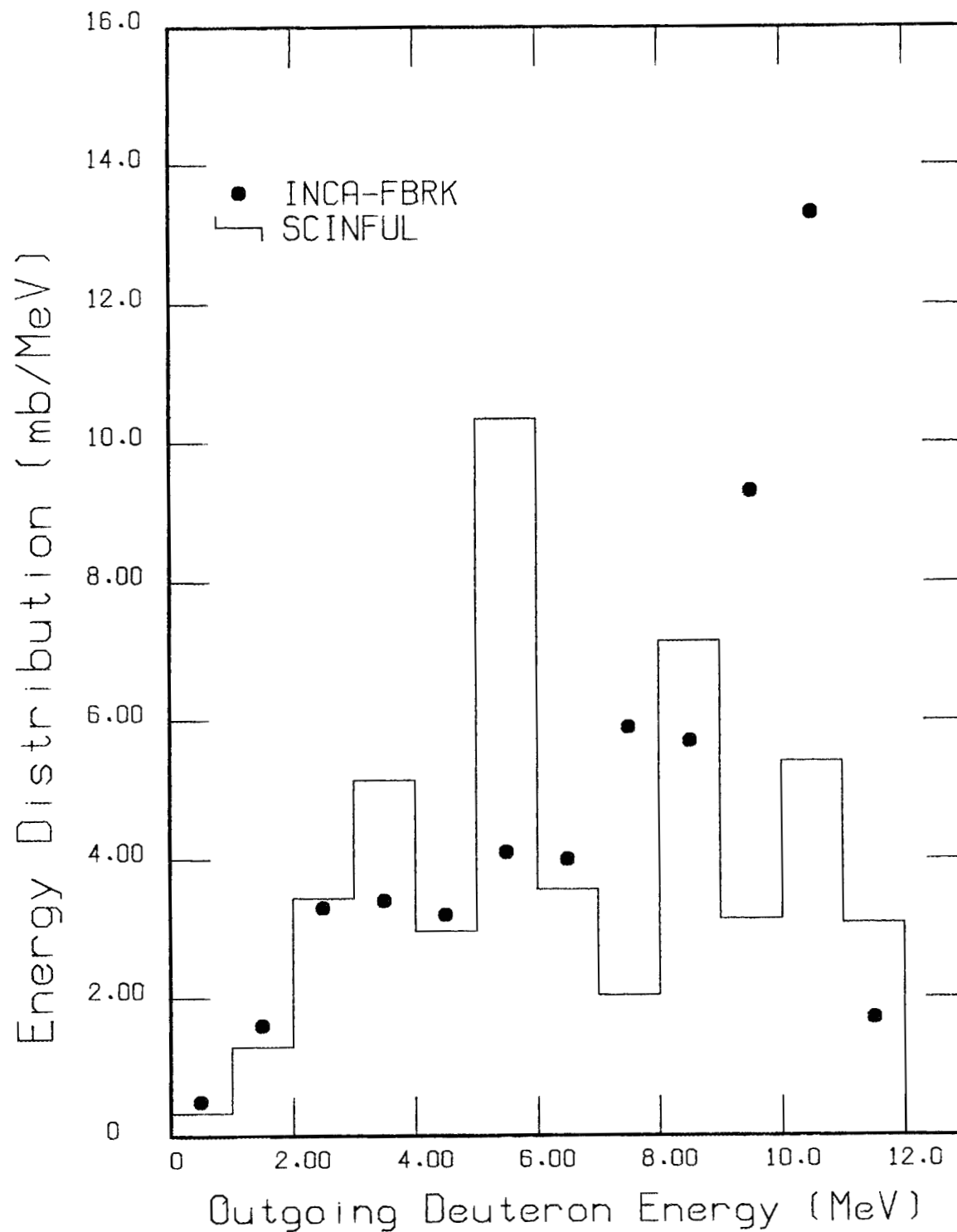


Fig. 10. Comparison of outgoing secondary-deuteron energy spectra for an incident neutron energy of 25 MeV. The solid points represent the spectrum computed using the intranuclear-cascade model code family INCA-FBRK; the data shown for this spectrum are reported in ref. 1. The histogram represents the same spectrum computed using the author's SCINFUL code which is described in ref. 3.

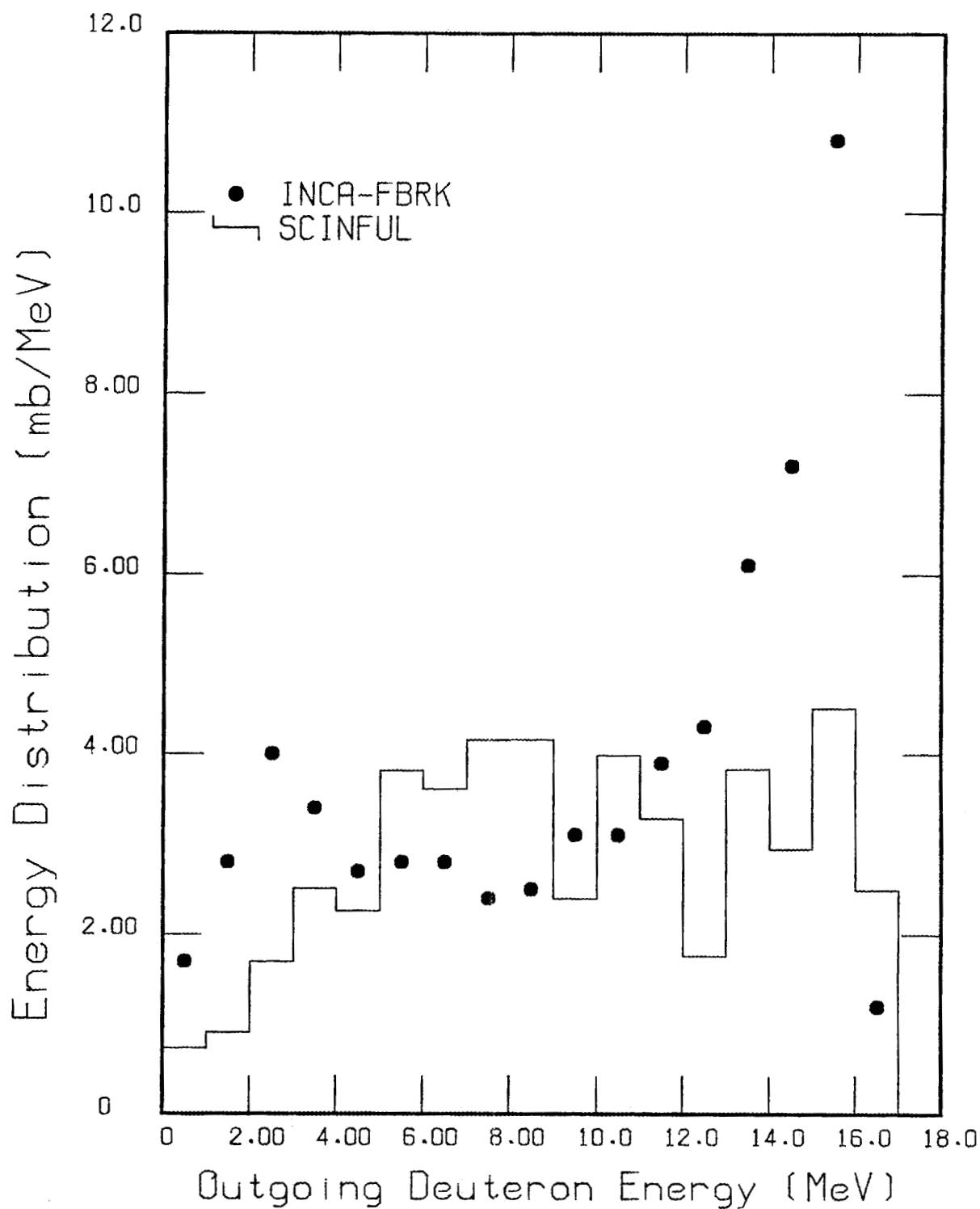


Fig. 11. Comparison of outgoing secondary-deuteron energy spectra for an incident neutron energy of 30 MeV. The solid points represent the spectrum computed using the intranuclear-cascade model code family INCA-FBRK; the data shown for this spectrum are reported in ref. 1. The histogram represents the same spectrum computed using the author's SCINFUL code which is described in ref. 3.

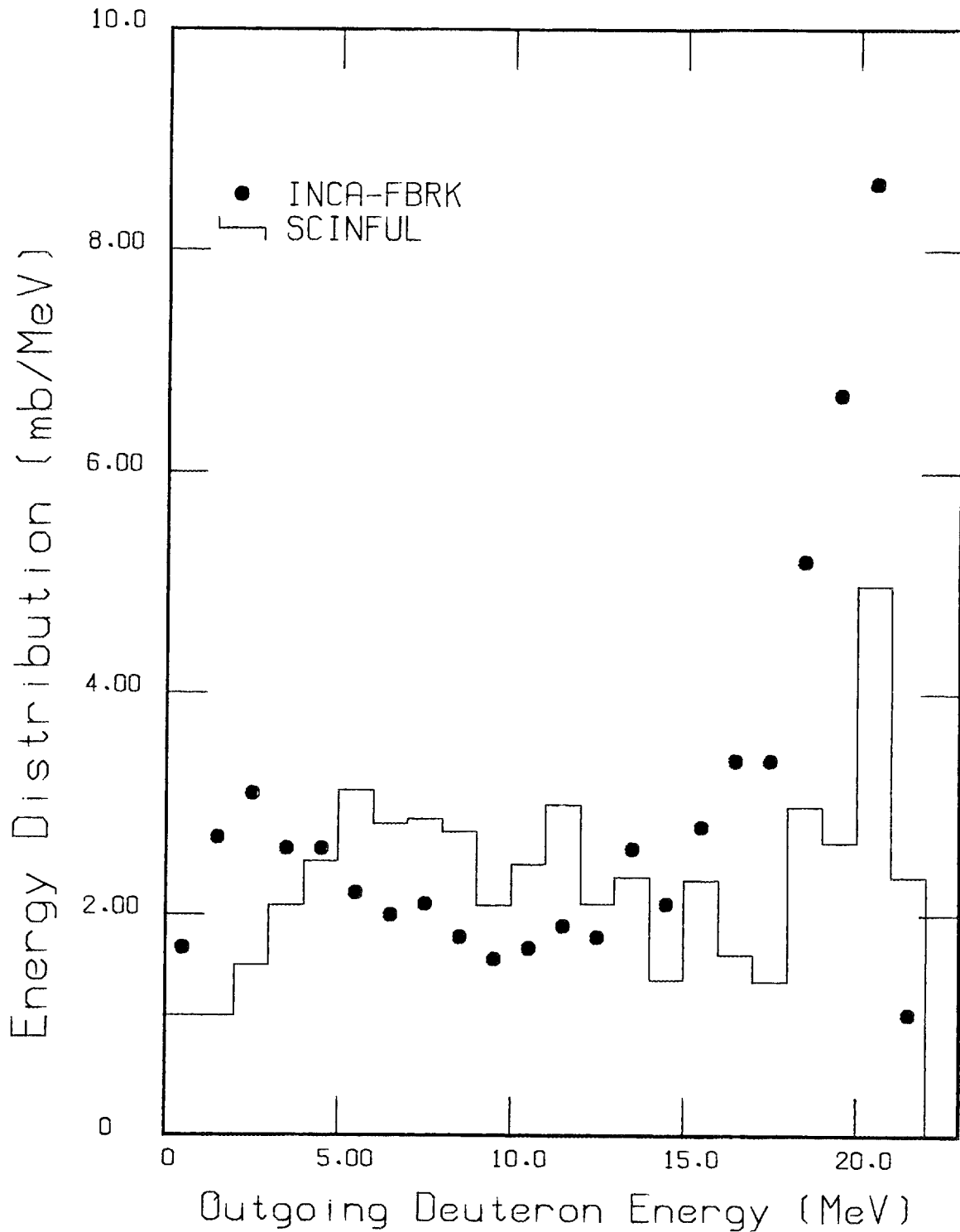


Fig. 12. Comparison of outgoing secondary-deuteron energy spectra for an incident neutron energy of 35 MeV. The solid points represent the spectrum computed using the intranuclear-cascade model code family INCA-FBRK; the data shown for this spectrum are reported in ref. 1. The histogram represents the same spectrum computed using the author's SCINFUL code which is described in ref. 3.

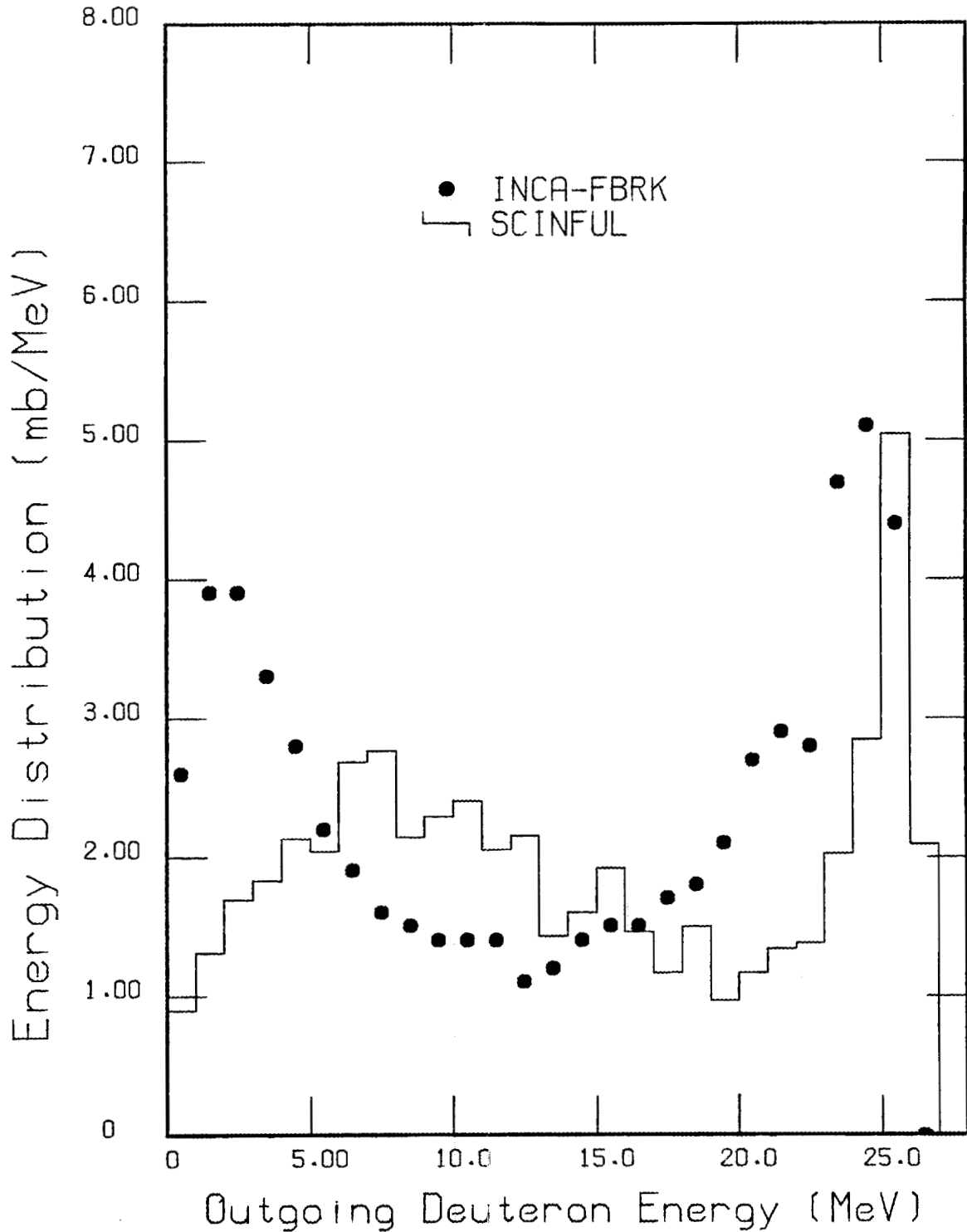


Fig. 13. Comparison of outgoing secondary-deuteron energy spectra for an incident neutron energy of 40 MeV. The solid points represent the spectrum computed using the intranuclear-cascade model code family INCA-FBRK; the data shown for this spectrum are reported in ref. 1. The histogram represents the same spectrum computed using the author's SCINFUL code which is described in ref. 3.

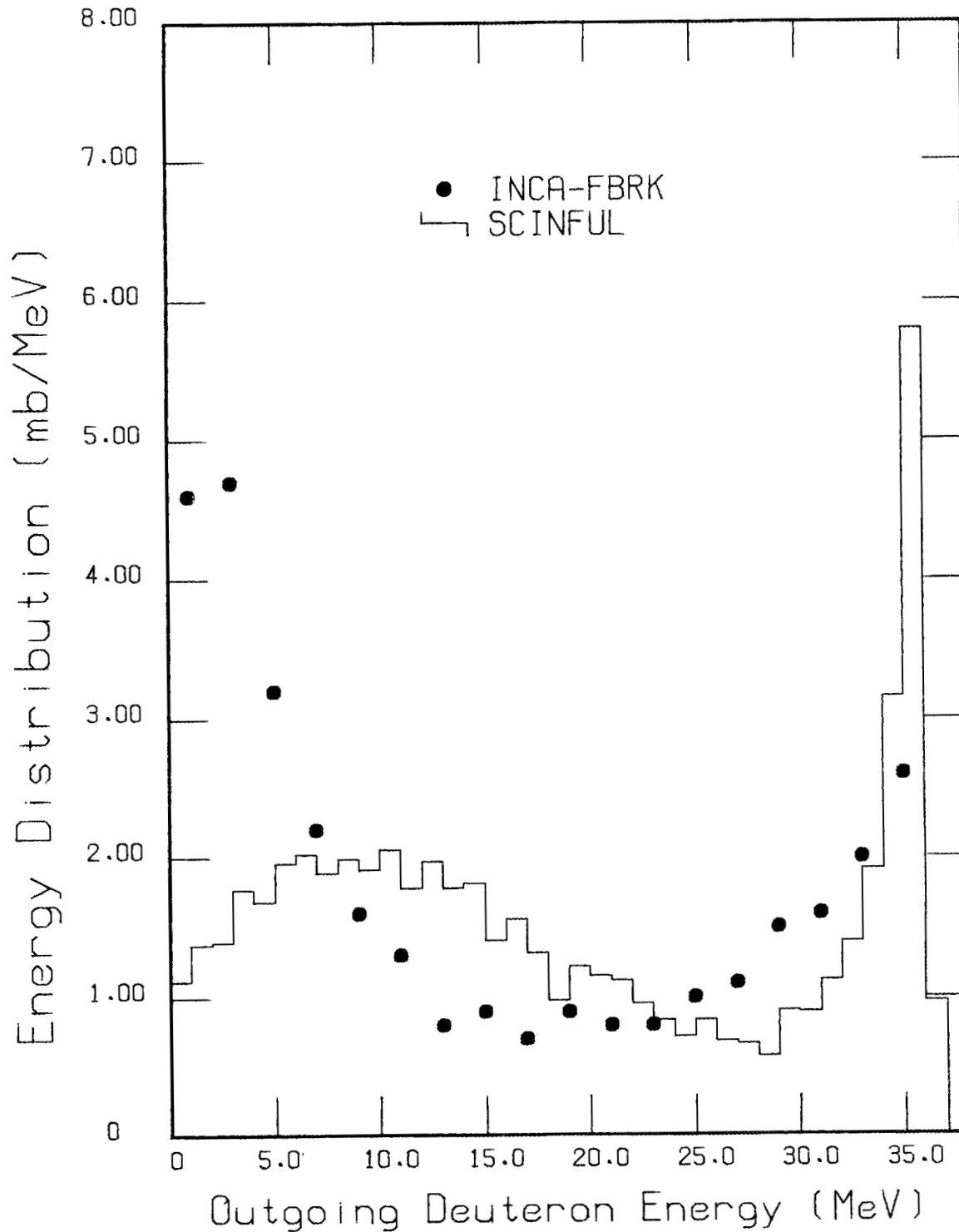


Fig. 14. Comparison of outgoing secondary-deuteron energy spectra for an incident neutron energy of 50 MeV. The solid points represent the spectrum computed using the intranuclear-cascade model code family INCA-FBRK; the data shown for this spectrum are reported in ref. 1. The histogram represents the same spectrum computed using the author's SCINFUL code which is described in ref. 3.

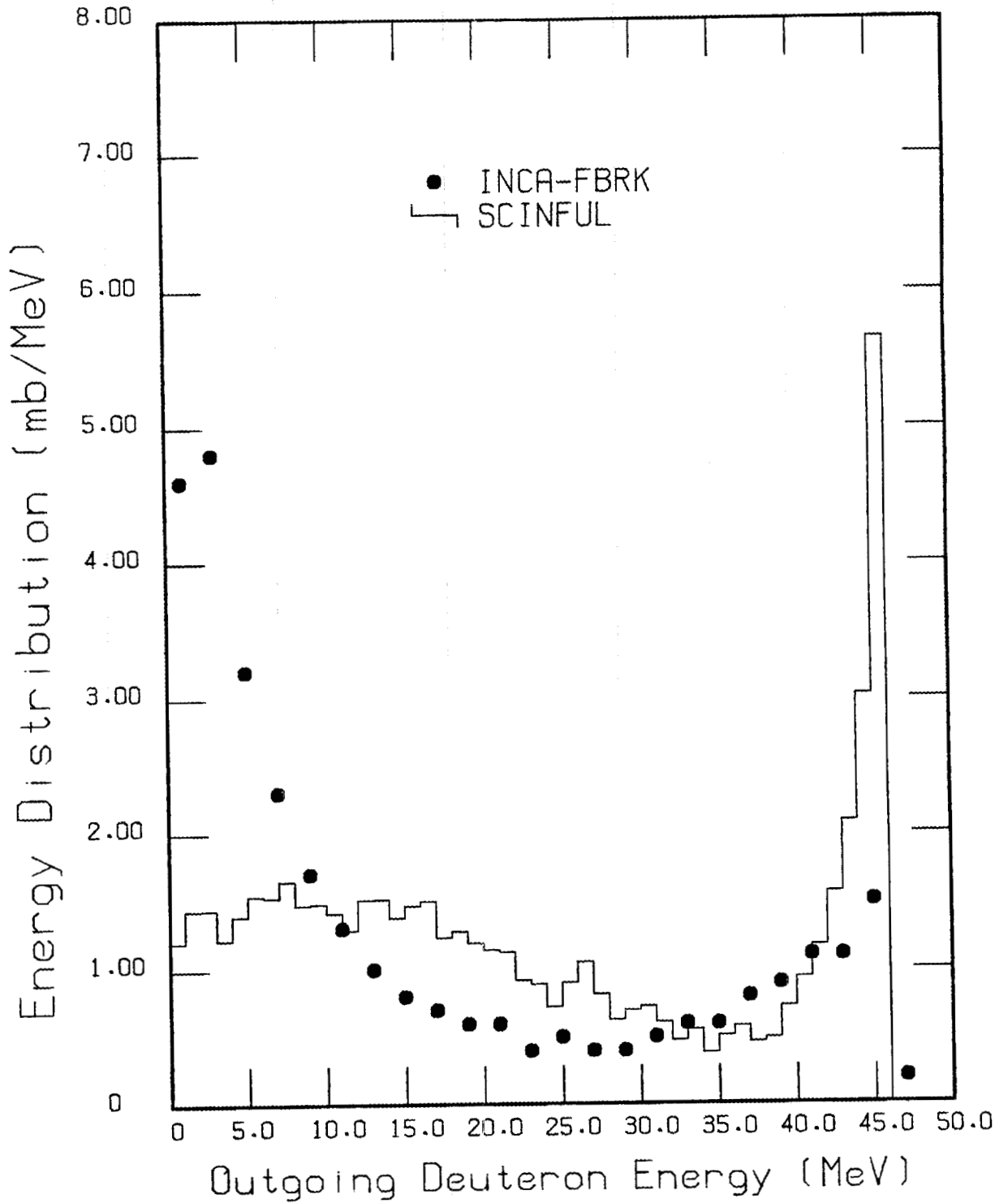


Fig. 15. Comparison of outgoing secondary-deuteron energy spectra for an incident neutron energy of 60 MeV. The solid points represent the spectrum computed using the intranuclear-cascade model code family INCA-FBRK; the data shown for this spectrum are reported in ref. 1. The histogram represents the same spectrum computed using the author's SCINFUL code which is described in ref. 3.

5. COMPARISONS OF SECONDARY TRITON PRODUCTION

As exhibited in Figs. 16 to 21 agreement between the two calculations is somewhat poorer than observed above for secondary protons and deuterons. In SCINFUL the energy distributions and cross sections were guided by the data of Subramanian et al.⁴ for E_n between 27.4 and 60.7 MeV. One may note that the production cross sections are small. Triton fluorescent light response cannot be distinguished from lower-energy proton response in a total experimental detector response, and so less effort was expended in the SCINFUL programming of secondary triton production. In SCINFUL, a small portion (5%) of the total $^{12}\text{C}(n,t)^{10}\text{B}$ reaction was assumed *ad hoc* to populate the ground state of ^{10}B ; the rest of the triton production was assumed to be continuum governed by the functional relationship give in Eq. (4) with the variable $Temp$ given by:

$$Temp = 0.5 + 0.04 * E_n \quad (7)$$

Comparing the two sets of calculations shows that the intranuclear cascade definitely predicts a softer triton spectrum than does SCINFUL. The triton energy spectra of Subramanian et al.⁴ definitely exhibit high-energy tritons, and the SCINFUL computation approximates the high-energy portion of the experimental spectra reasonably well. However, the continuum portion of the experimental spectra are also somewhat softer than the SCINFUL computations which may indicate that the SCINFUL parametrization of Eq. (4) for secondary tritons should be reinvestigated.

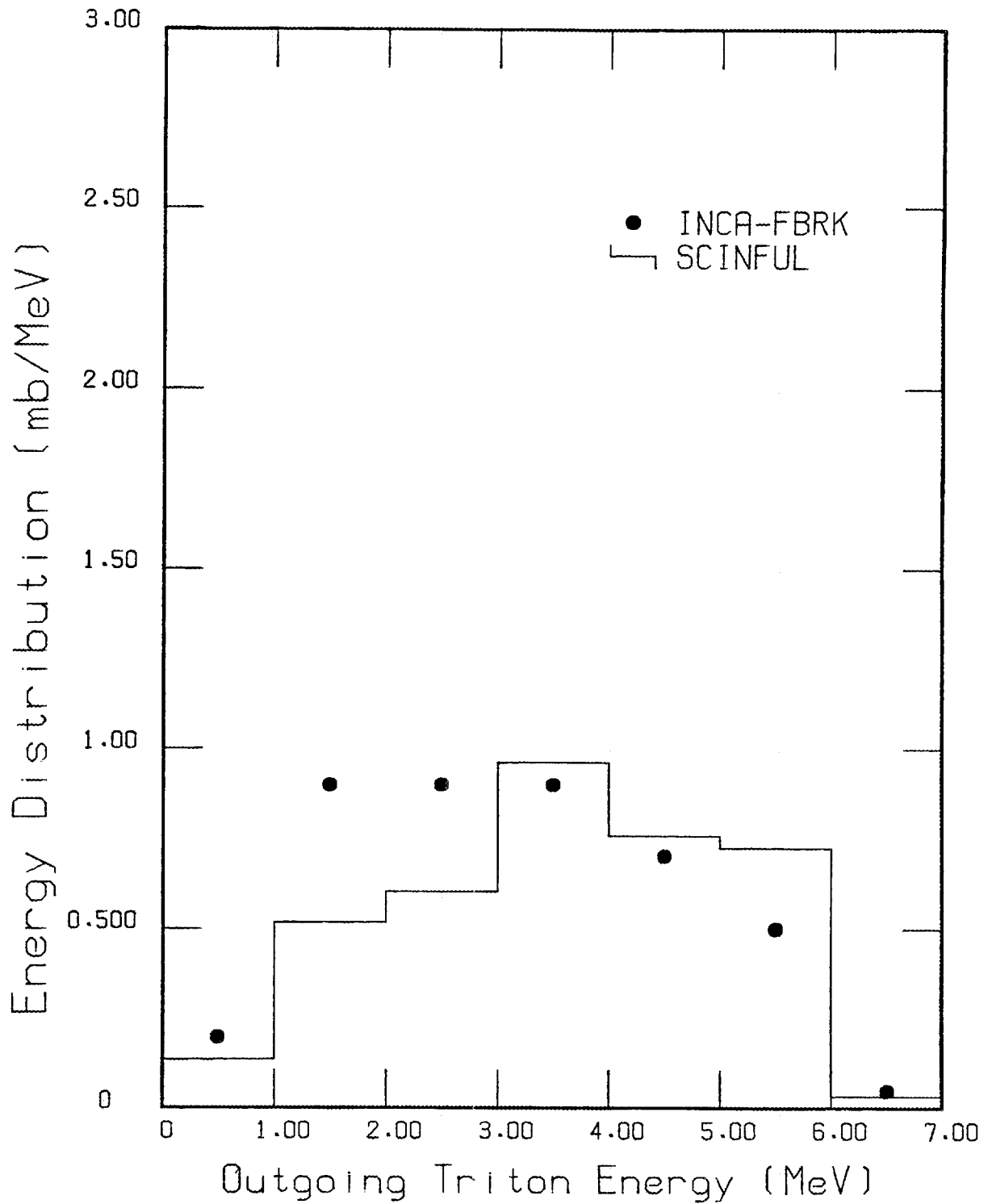


Fig. 16. Comparison of outgoing secondary-triton energy spectra for an incident neutron energy of 25 MeV. The solid points represent the spectrum computed using the intranuclear-cascade model code family INCA-FBRK; the data shown for this spectrum are reported in ref. 1. The histogram represents the same spectrum computed using the author's SCINFUL code which is described in ref. 3.

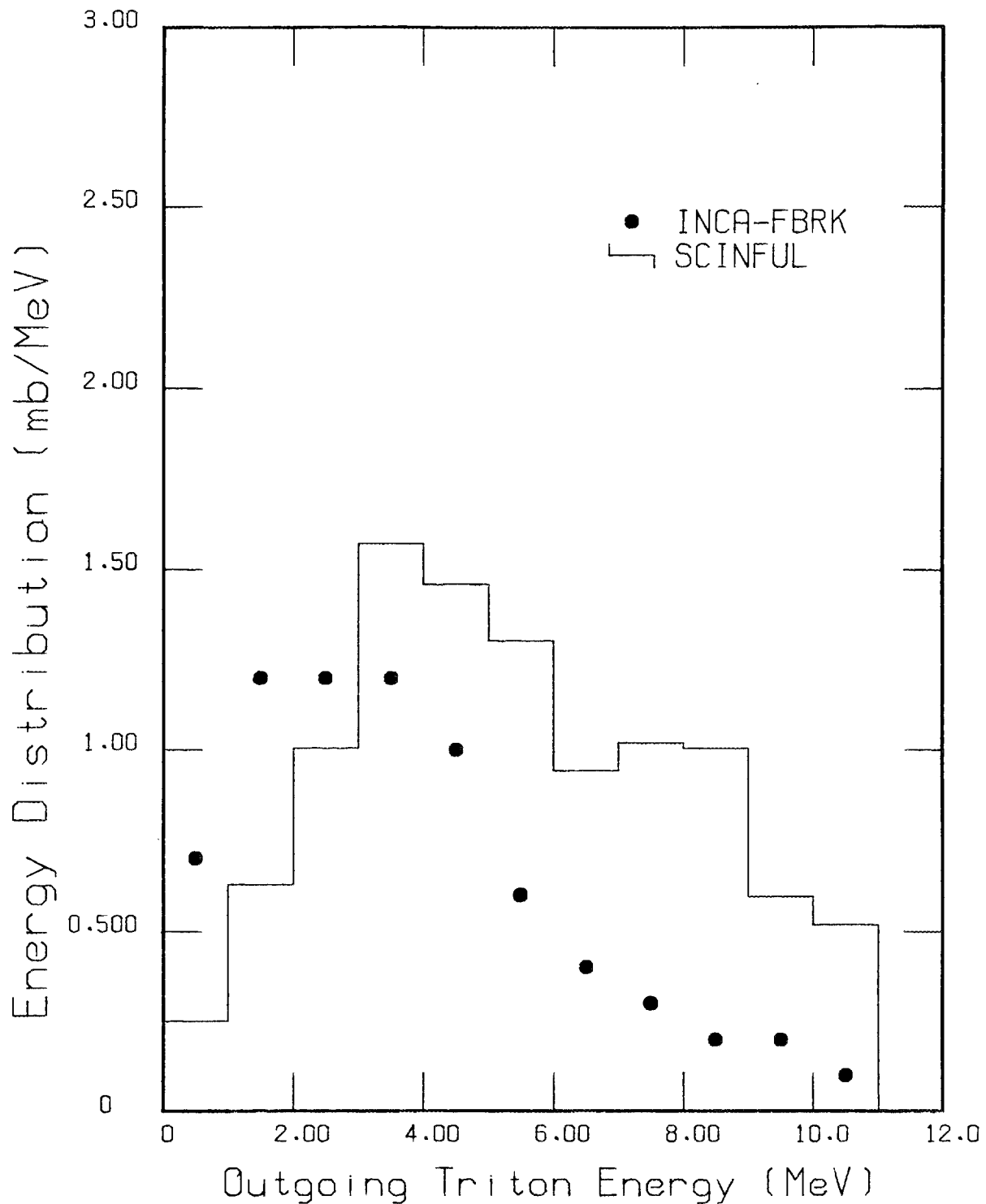


Fig. 17. Comparison of outgoing secondary-triton energy spectra for an incident neutron energy of 30 MeV. The solid points represent the spectrum computed using the intranuclear-cascade model code family INCA-FBRK; the data shown for this spectrum are reported in ref. 1. The histogram represents the same spectrum computed using the author's SCINFUL code which is described in ref. 3.

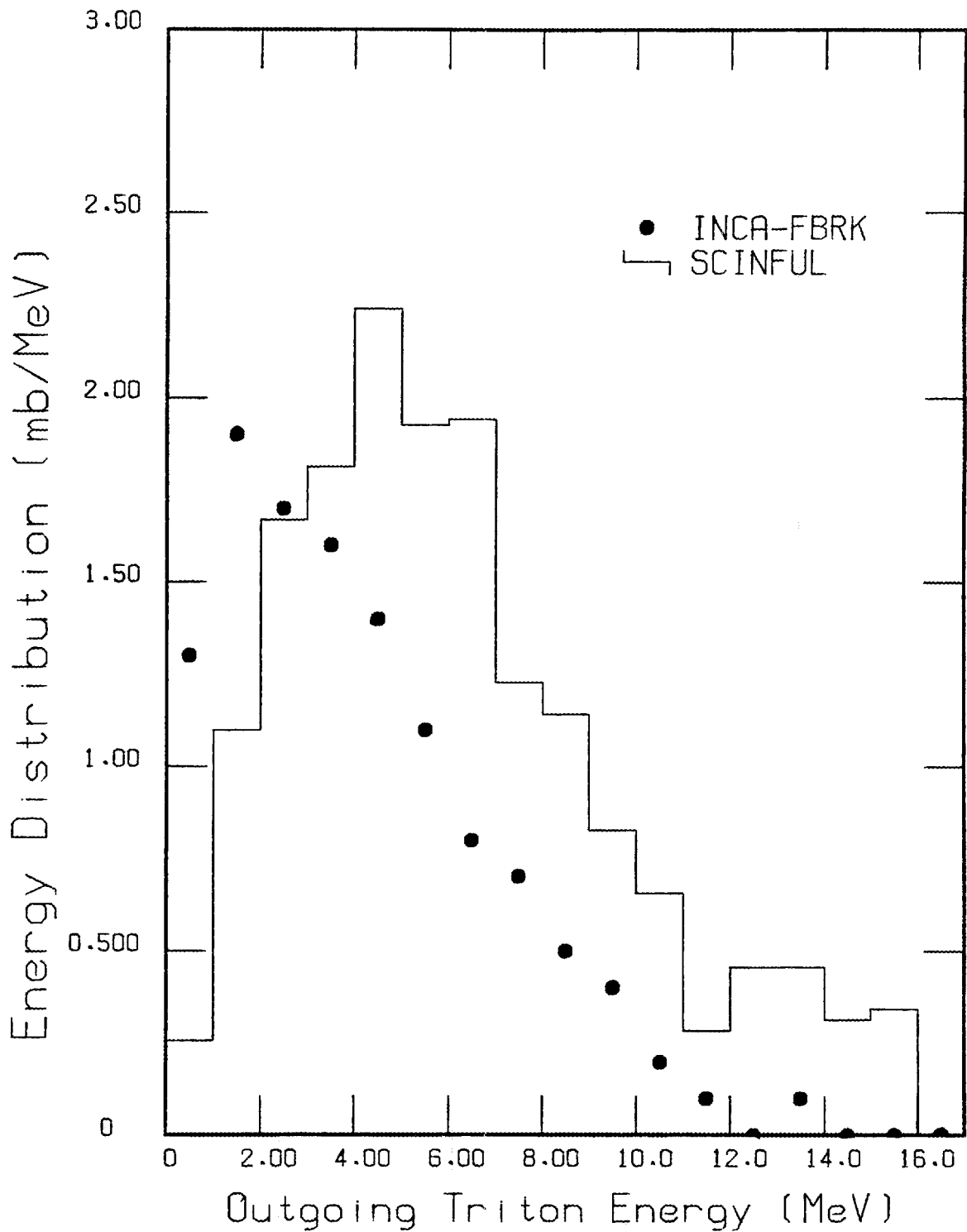


Fig. 18. Comparison of outgoing secondary-triton energy spectra for an incident neutron energy of 35 MeV. The solid points represent the spectrum computed using the intranuclear-cascade model code family INCA-FBRK; the data shown for this spectrum are reported in ref. 1. The histogram represents the same spectrum computed using the author's SCINFUL code which is described in ref. 3.

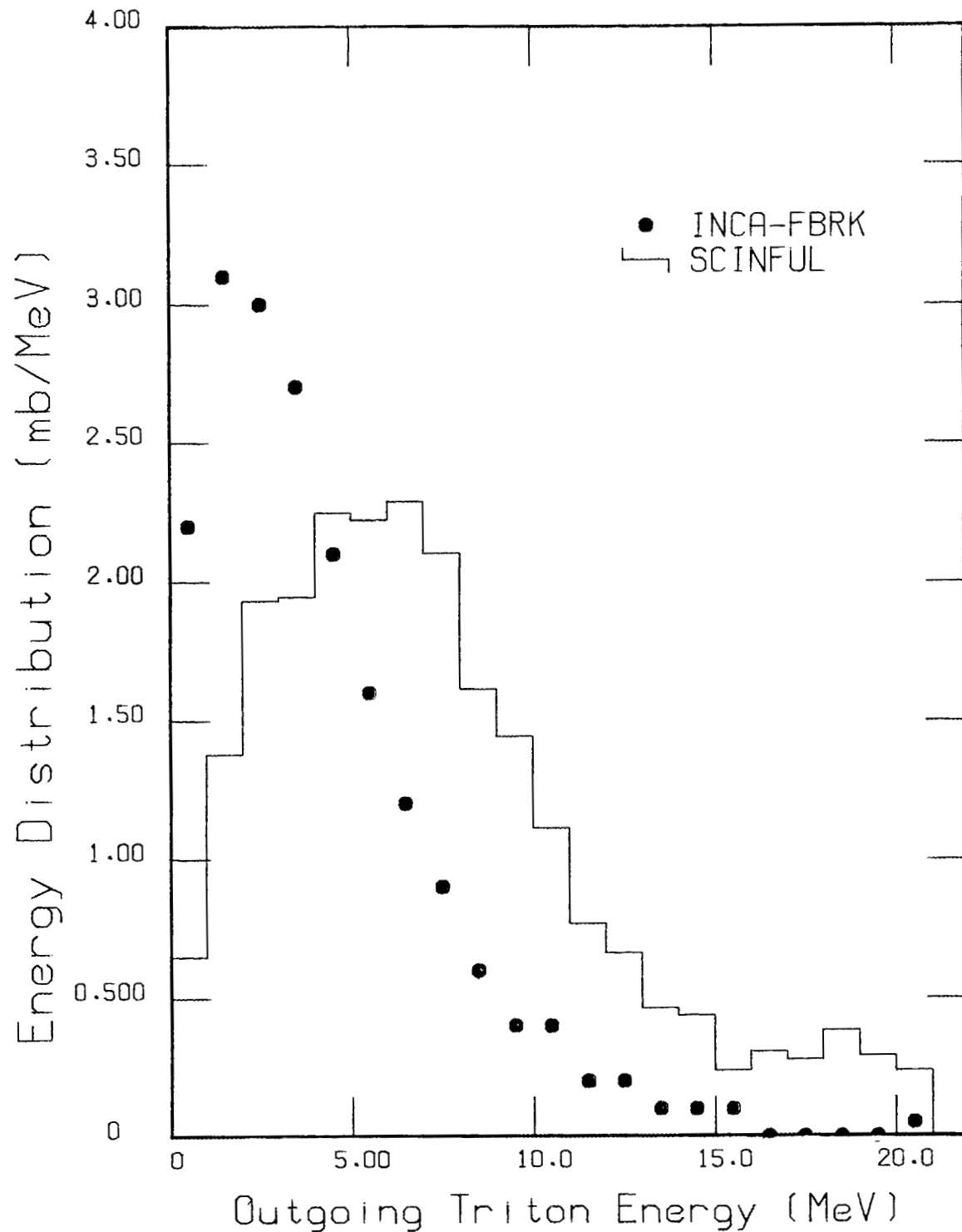


Fig. 19. Comparison of outgoing secondary-triton energy spectra for an incident neutron energy of 40 MeV. The solid points represent the spectrum computed using the intranuclear-cascade model code family INCA-FBRK; the data shown for this spectrum are reported in ref. 1. The histogram represents the same spectrum computed using the author's SCINFUL code which is described in ref. 3.

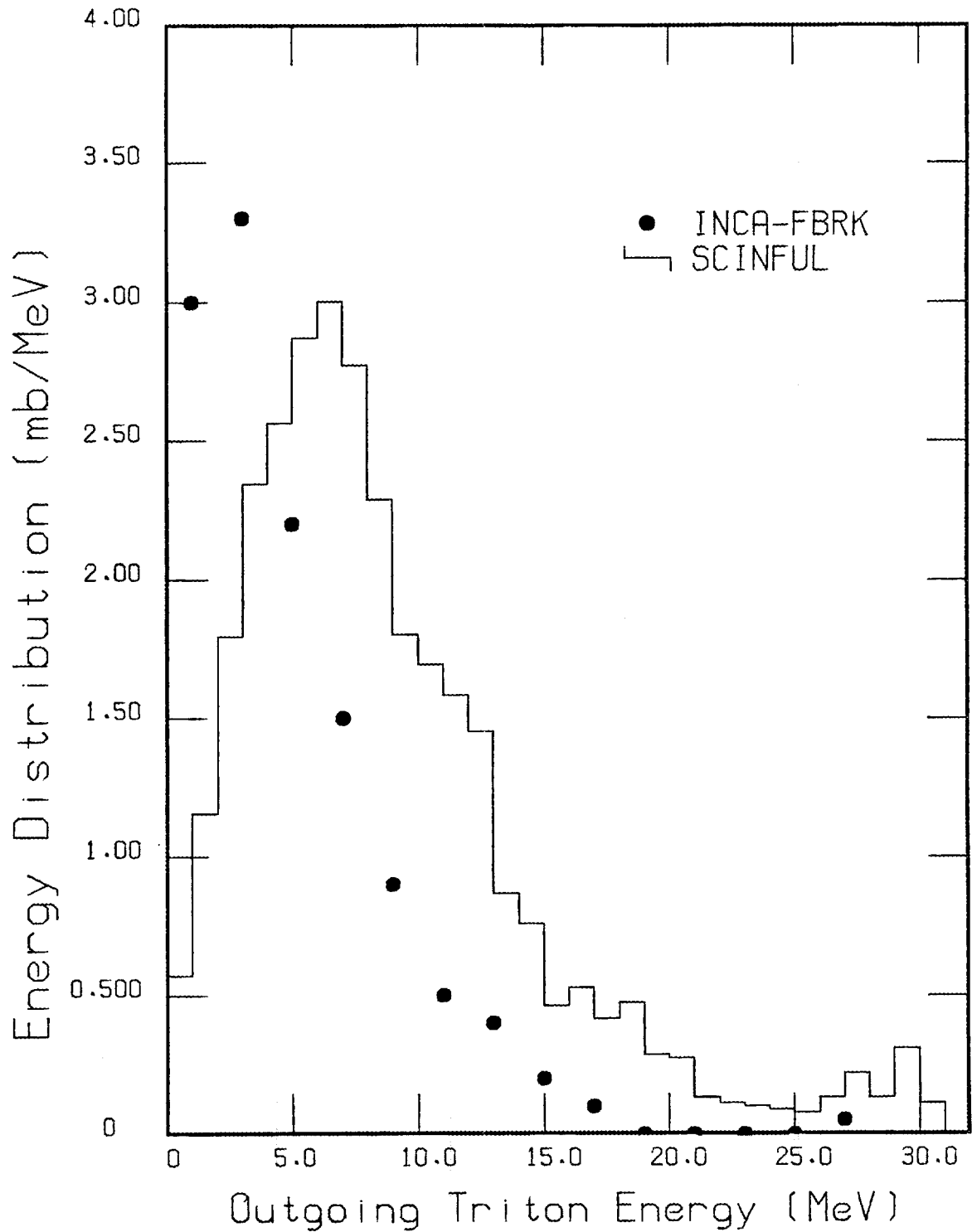


Fig. 20. Comparison of outgoing secondary-triton energy spectra for an incident neutron energy of 50 MeV. The solid points represent the spectrum computed using the intranuclear-cascade model code family INCA-FBRK; the data shown for this spectrum are reported in ref. 1. The histogram represents the same spectrum computed using the author's SCINFUL code which is described in ref. 3.

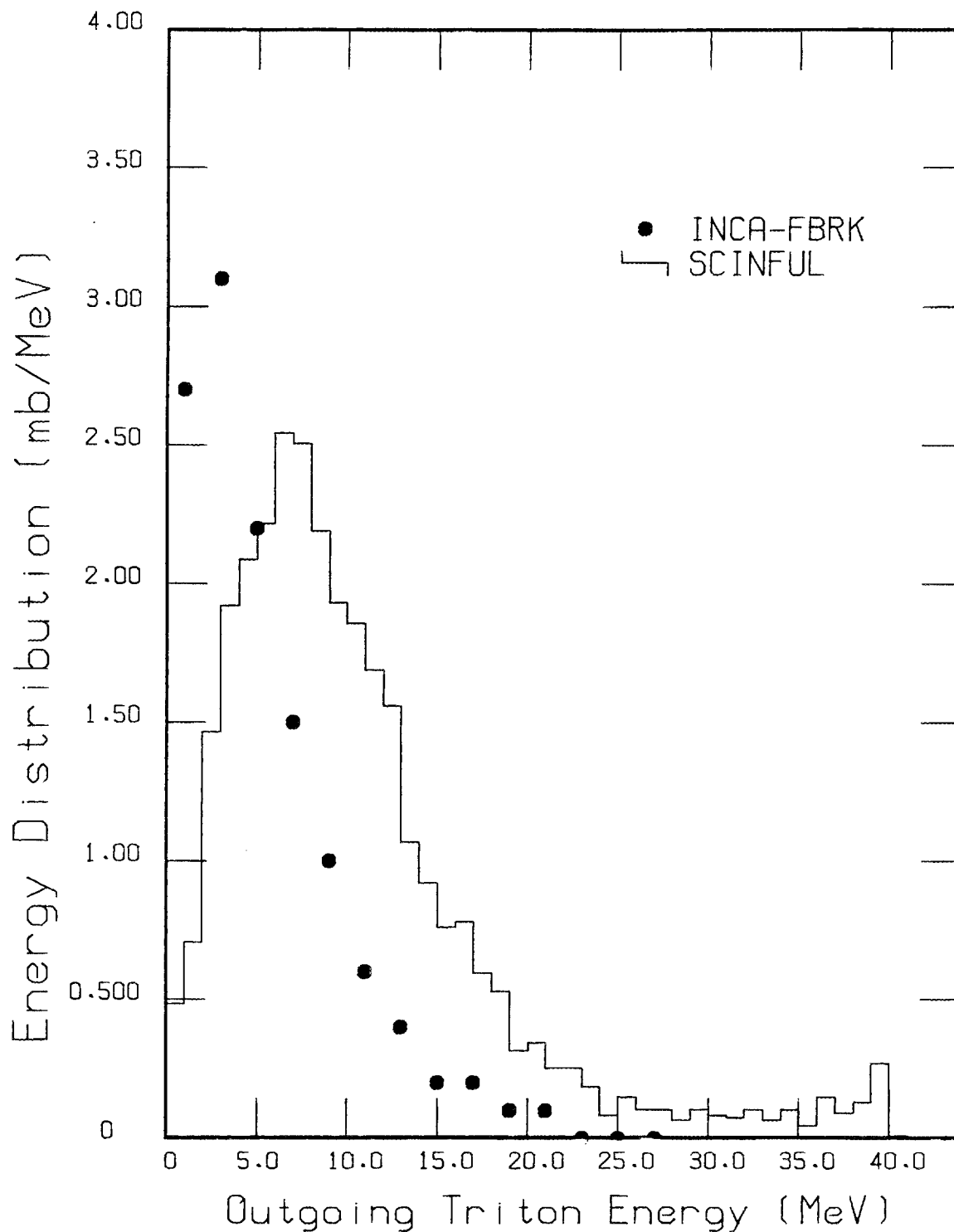


Fig. 21. Comparison of outgoing secondary-triton energy spectra for an incident neutron energy of 60 MeV. The solid points represent the spectrum computed using the intranuclear-cascade model code family INCA-FBRK; the data shown for this spectrum are reported in ref. 1. The histogram represents the same spectrum computed using the author's SCINFUL code which is described in ref. 3.

6. COMPARISONS OF ^3He -ION PRODUCTION

The cross sections for ^3He -ion production are small, very small compared to the cross sections for α -particle production. Fluorescent light output due to ^3He ions is similar to that for α particles, and cannot be distinguished in experimental detector responses. The programming in SCINFUL for ^3He -ion production in SCINFUL was the last to be done. So, as in the case of triton production just discussed, mostly what was done for ^3He -ion production was to obtain energy spectra which approximated the experimental data of Subramanian et al.⁴ A small fraction (4%) of the total ^3He -ion production was assumed *ad hoc* to populate the ground state of ^{10}Be ; the remaining ^3He -ion production was assumed to be governed by the proton continuum function given in Eq. (4), where $Temp = 3.0$ was set for all neutron energies.

As shown in Figs. 22 to 27, the INCA-FBRK calculations exhibit even fewer ^3He ions than do SCINFUL calculations, and the energy spectra are much softer than those computed using SCINFUL. Other than to indicate the small production cross sections for ^3He ions, the experimental data of Subramanian et al.⁴ are no help in determining a preference for either set of computed spectra. Very possibly, as in the triton production, the use of Eq. (4) to estimate the ^3He -ion continuum could be reinvestigated.

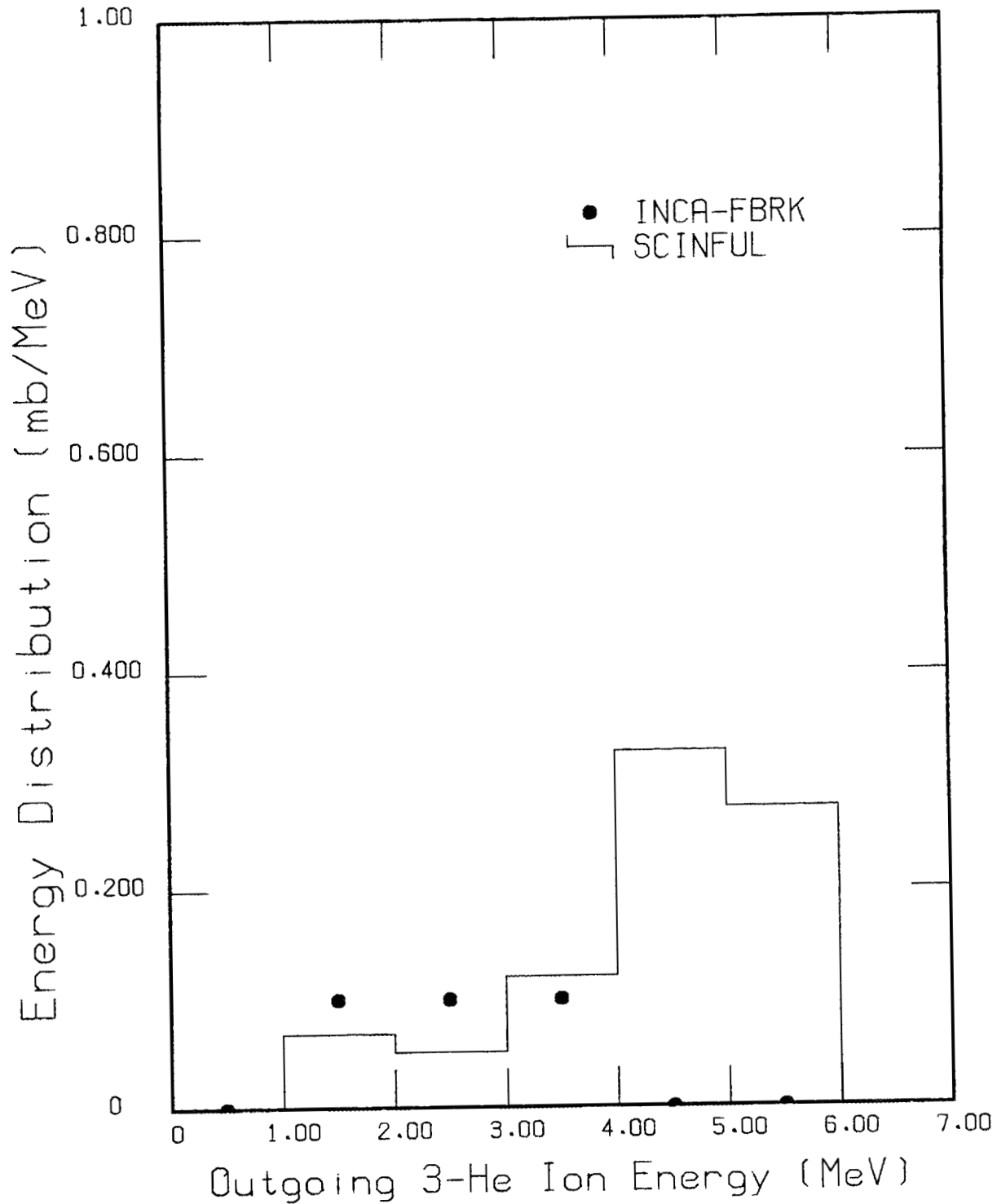


Fig. 22. Comparison of outgoing secondary- ^3He -ion energy spectra for an incident neutron energy of 25 MeV. The solid points represent the spectrum computed using the intranuclear-cascade model code family INCA-FBRK; the data shown for this spectrum are reported in ref. 1. The histogram represents the same spectrum computed using the author's SCINFUL code which is described in ref. 3.

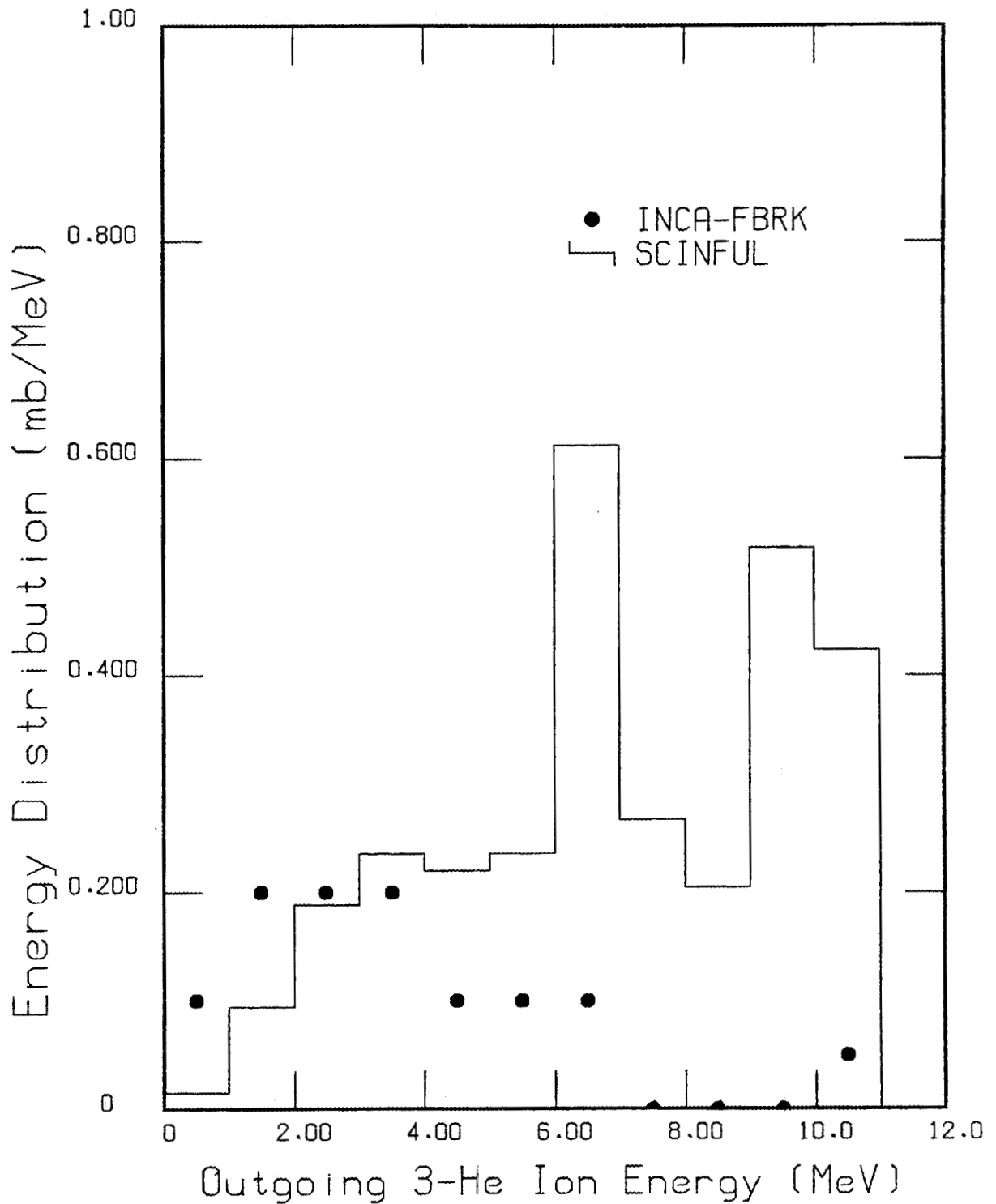


Fig. 23. Comparison of outgoing secondary ^3He -ion energy spectra for an incident neutron energy of 30 MeV. The solid points represent the spectrum computed using the intranuclear-cascade model code family INCA-FBRK; the data shown for this spectrum are reported in ref. 1. The histogram represents the same spectrum computed using the author's SCINFUL code which is described in ref. 3.

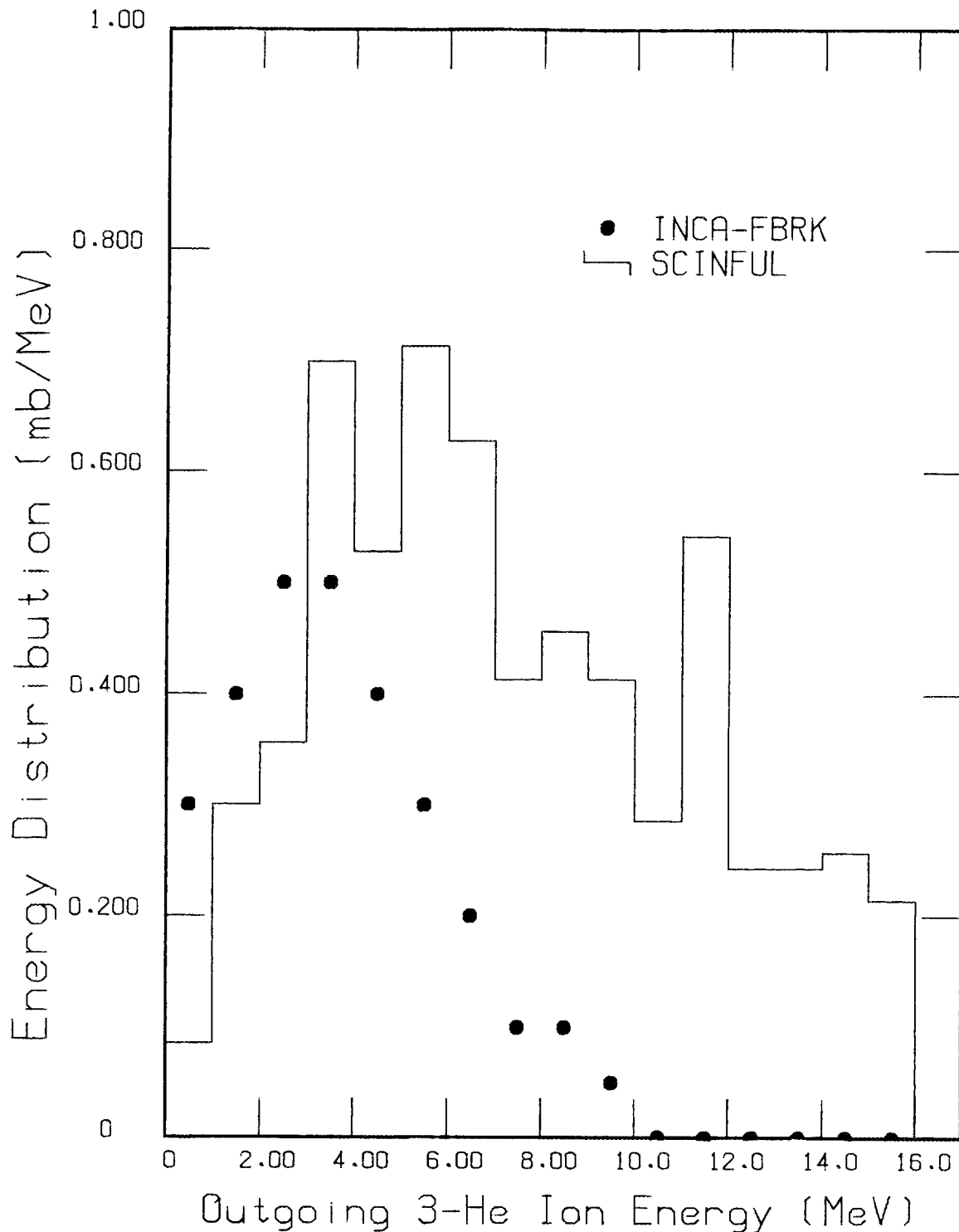


Fig. 24. Comparison of outgoing secondary- ^3He -ion energy spectra for an incident neutron energy of 35 MeV. The solid points represent the spectrum computed using the intranuclear-cascade model code family INCA-FBRK; the data shown for this spectrum are reported in ref. 1. The histogram represents the same spectrum computed using the author's SCINFUL code which is described in ref. 3.

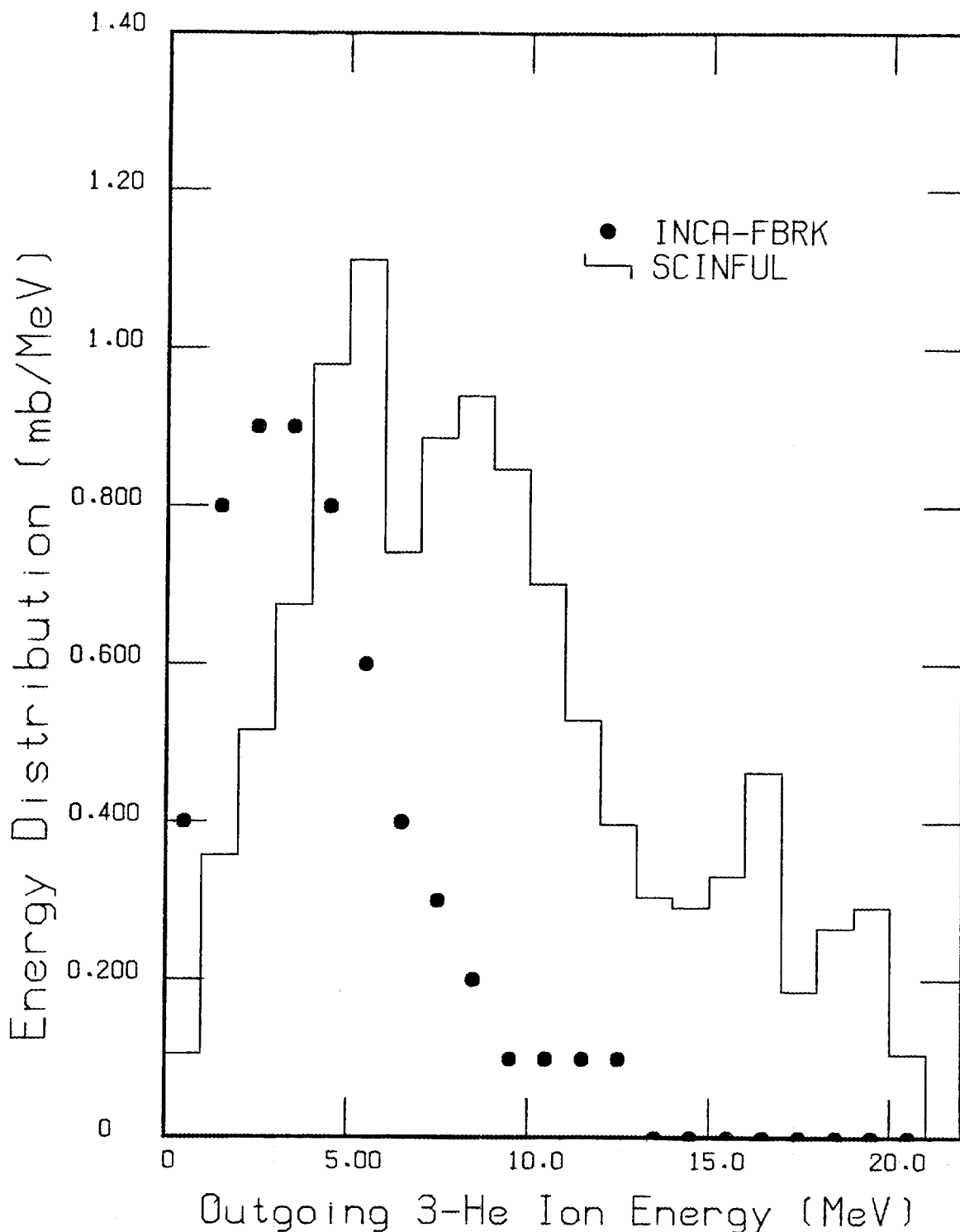


Fig. 25. Comparison of outgoing secondary- ^3He -ion energy spectra for an incident neutron energy of 40 MeV. The solid points represent the spectrum computed using the intranuclear-cascade model code family INCA-FBRK; the data shown for this spectrum are reported in ref. 1. The histogram represents the same spectrum computed using the author's SCINFUL code which is described in ref. 3.

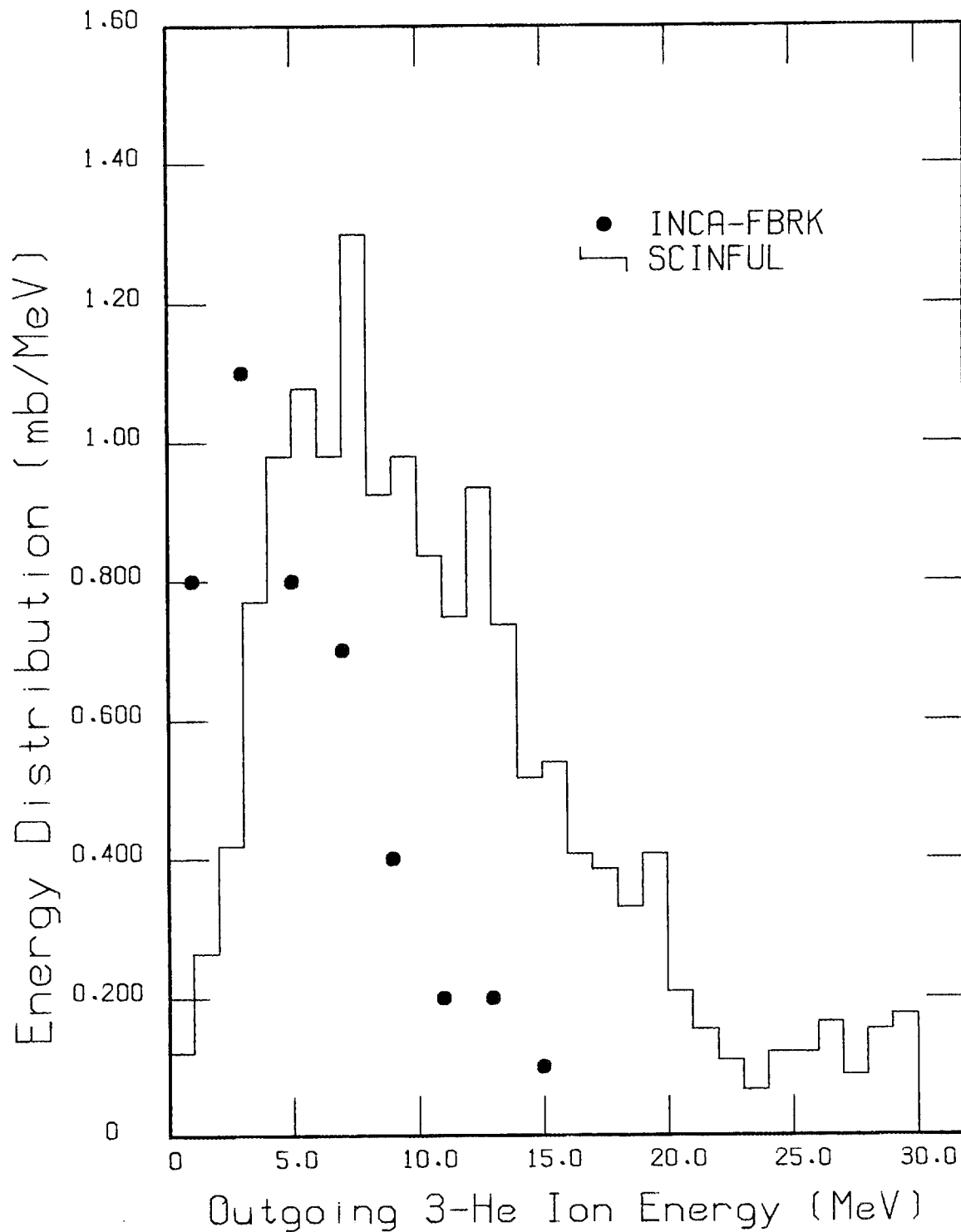


Fig. 26. Comparison of outgoing secondary- ^3He -ion energy spectra for an incident neutron energy of 50 MeV. The solid points represent the spectrum computed using the intranuclear-cascade model code family INCA-FBRK; the data shown for this spectrum are reported in ref. 1. The histogram represents the same spectrum computed using the author's SCINFUL code which is described in ref. 3.

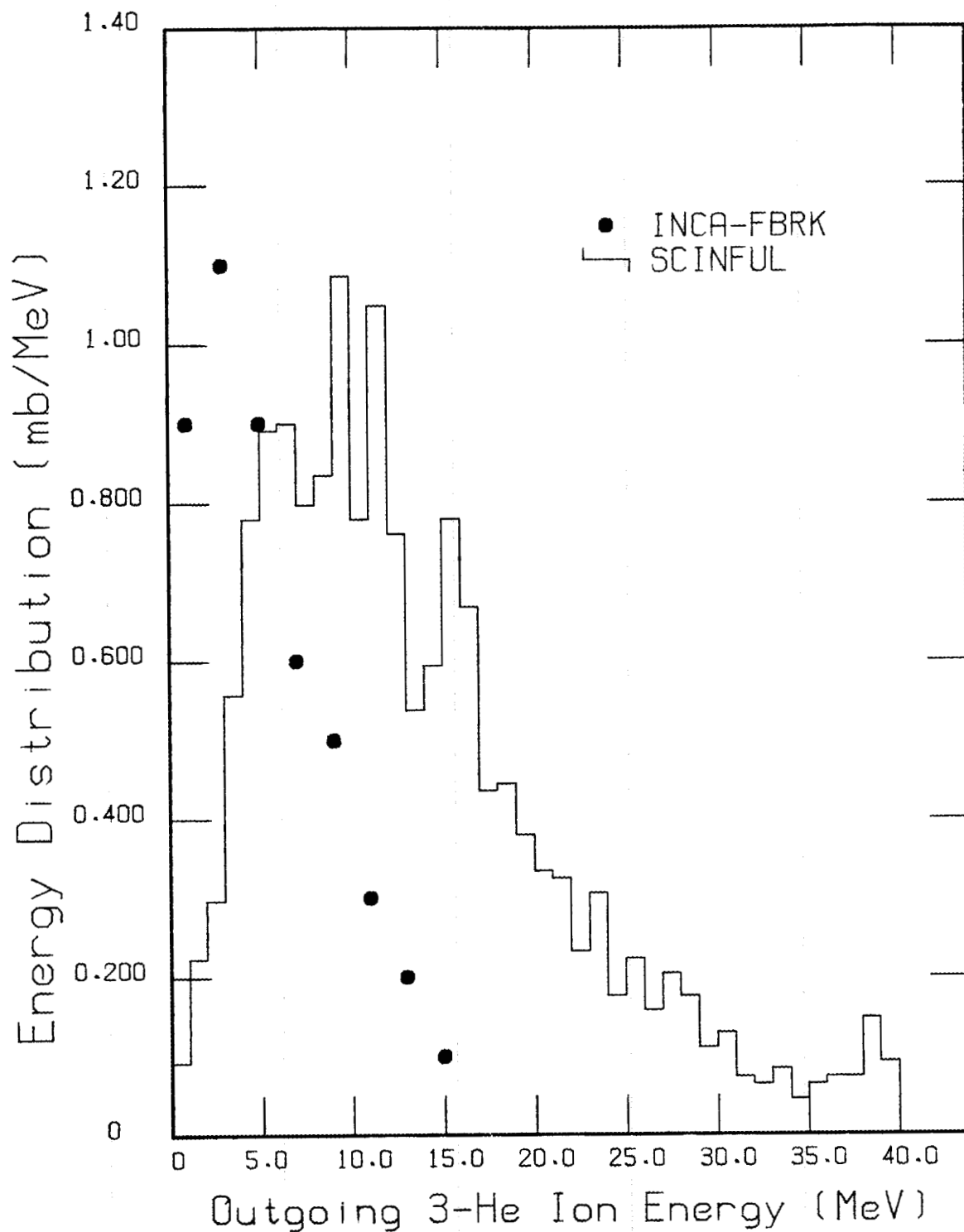


Fig. 27. Comparison of outgoing secondary- ^3He -ion energy spectra for an incident neutron energy at 60 MeV. The solid points represent the spectrum computed using the intranuclear-cascade model code family INCA-FBRK; the data shown for this spectrum are reported in ref. 1. The histogram represents the same spectrum computed using the author's SCINFUL code which is described in ref. 3.

7. COMPARISONS OF ALPHA PARTICLE PRODUCTION

To a considerable extent, the comparisons of the α -particle energy spectra with experiment represent the most important challenge of the computing capabilities of both INCA-FBRK and SCINFUL. In both codes, some adjustments can be made to parameters governing computations of any of the other secondary-particle spectra (i.e., those for p , d , t , and ${}^3\text{He}$) without much disturbing the computations of any of the others. What must be treated with care are those parameters affecting the α -particle portion of the calculation. For the INCA-FBRK code, the important parameter is that associated with the fraction of the ${}^{12}\text{C}$ nucleus as alpha clustering. For the SCINFUL code, it is the fraction of the total $n + {}^{12}\text{C}$ cross section assigned to alpha production.

There are several small adjustments in the SCINFUL code that can be made to slightly modify the α -particle energy spectrum at a given incident neutron energy. A small, incident-energy dependent fraction of the α production is assumed to populate the ground state of ${}^9\text{Be}$, and hence is treated as a two-body reaction. For $E_n < 20$ MeV, the cross section for the ground-state reaction is reasonably well known, and angular distributions of the reactions alphas have been measured¹³ and have been included in parametric form in SCINFUL. Indeed, the fluorescent light output of the α particles is easily defined in experimental responses measured in this incident neutron energy regime. For $E_n > 20$ MeV, the fraction of the reaction populating the ground state was estimated from the Subramanian et al.⁴ data at $E_n = 27, 40$ and 60 MeV, and from the Kellogg data¹⁴ data at 90 MeV. Another adjustment in the SCINFUL code is the fraction of the total alpha reaction that is treated as a three-body breakup of the excited ${}^{12}\text{C}$ ion after inelastic neutron scattering. For E_n up to 35 MeV, the experimental data of Antolkovic et al.¹⁵ give some indication of this fraction. In SCINFUL this fraction ranges from 0% for the lower-energy neutrons to about 55% at the upper end of the neutron range. Indeed, during the development of the code use was made of the α -particle spectrum of Subramanian et al.⁴ at $E_n = 60.7$ MeV to aid in determining about how much of the reaction should be designated as the three-body breakup portion at this neutron energy. It should be pointed out, however, that the effect of including three-body breakup has only a moderate effect on the calculated α -particle energy spectrum. Other parameters, such as how much of the reaction proceeds through well-known highly-excited states of ${}^{12}\text{C}$ or of ${}^9\text{Be}$ have probably as much effect. However, again boundary conditions and experimental knowledge must be satisfied, and so adjustments to these parameters are comparatively small and affect the computed α -particle spectrum only in detail.

Comparisons of the two sets of calculations of α -particle spectra are shown in Figs. 28 to 35. Differences for $E_n = 15$ and 20 MeV are quite small, and reflect mostly the amount of ${}^9\text{Be}$ bound state reaction included in SCINFUL. For $E_n = 25, 30$ and 35 MeV the differences in the spectra for the upper half of the secondary-particle energy are probably due to the cross sections given in SCINFUL for the reaction to proceed through a specific intermediate state in either ${}^{12}\text{C}$ or

⁹Be. However, already at $E_n = 30$ MeV the low-energy response of the INCA-FBRK calculation is definitely larger than the SCINFUL-computed response. Very definitely, the experimental data of Subramanian et al.⁴ at $E_n = 60.7$ MeV favor the INCA-FBRK calculations at the low-energy portion of the response. For the purpose for which SCINFUL was developed this discrepancy is not very important. However, if, in the future, the code is extended to compute responses for $E_n > 80$ MeV, a study of this portion of the program should be made.

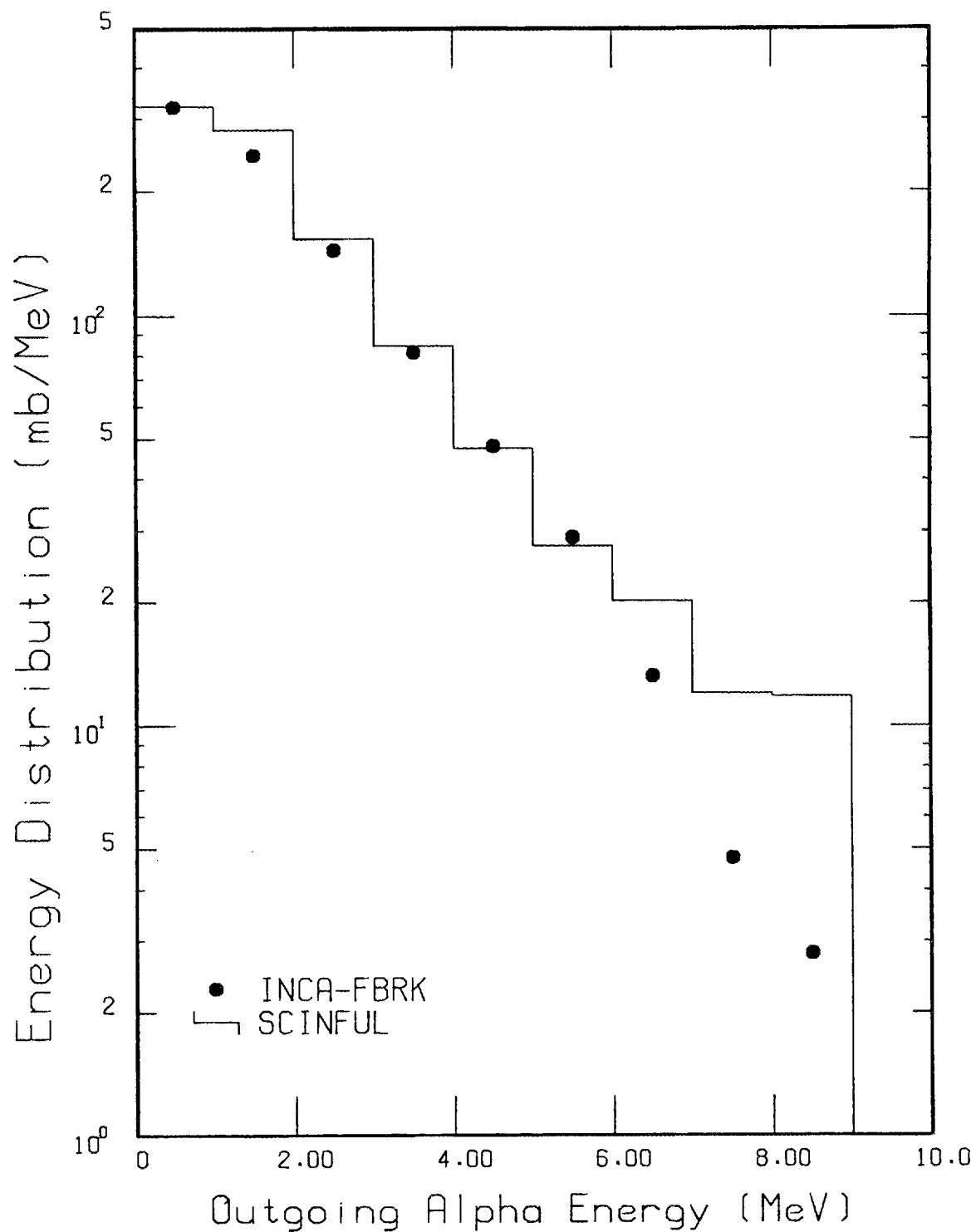


Fig. 28. Comparison of outgoing secondary-alpha energy spectra for an incident neutron energy of 15 MeV. The solid points represent the spectrum computed using the intranuclear-cascade model code family INCA-FBRK; the data shown for this spectrum are reported in ref. 1. The histogram represents the same spectrum computed using the author's SCINFUL code which is described in ref. 3.

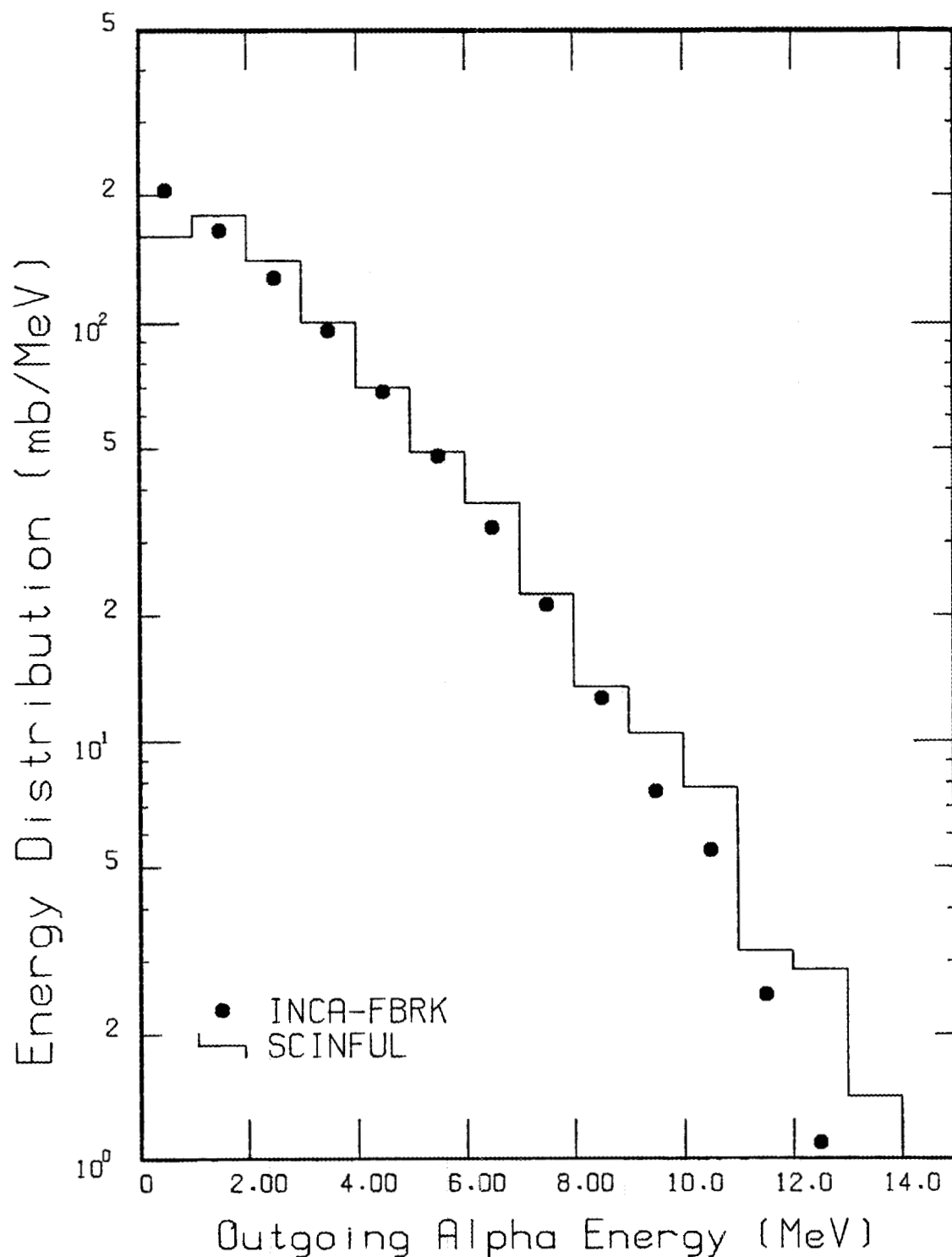


Fig. 29. Comparison of outgoing secondary-alpha energy spectra for an incident neutron energy of 20 MeV. The solid points represent the spectrum computed using the intranuclear-cascade model code family INCA-FBRK; the data shown for this spectrum are reported in ref. 1. The histogram represents the same spectrum computed using the author's SCINFUL code which is described in ref. 3.

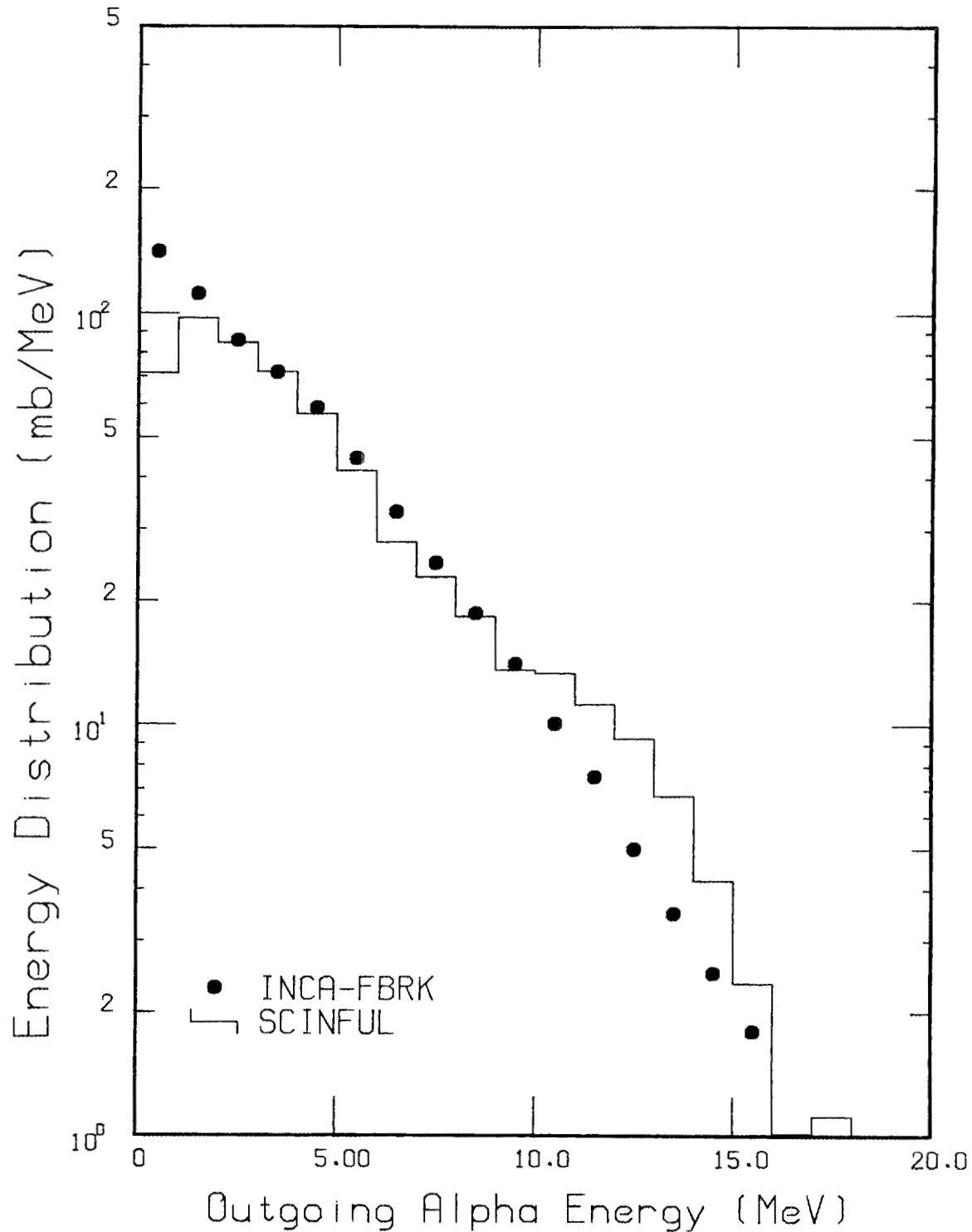


Fig. 30. Comparison of outgoing secondary-alpha energy spectra for an incident neutron energy of 25 MeV. The solid points represent the spectrum computed using the intranuclear-cascade model code family INCA-FBRK; the data shown for this spectrum are reported in ref. 1. The histogram represents the same spectrum computed using the author's SCINFUL code which is described in ref. 3.

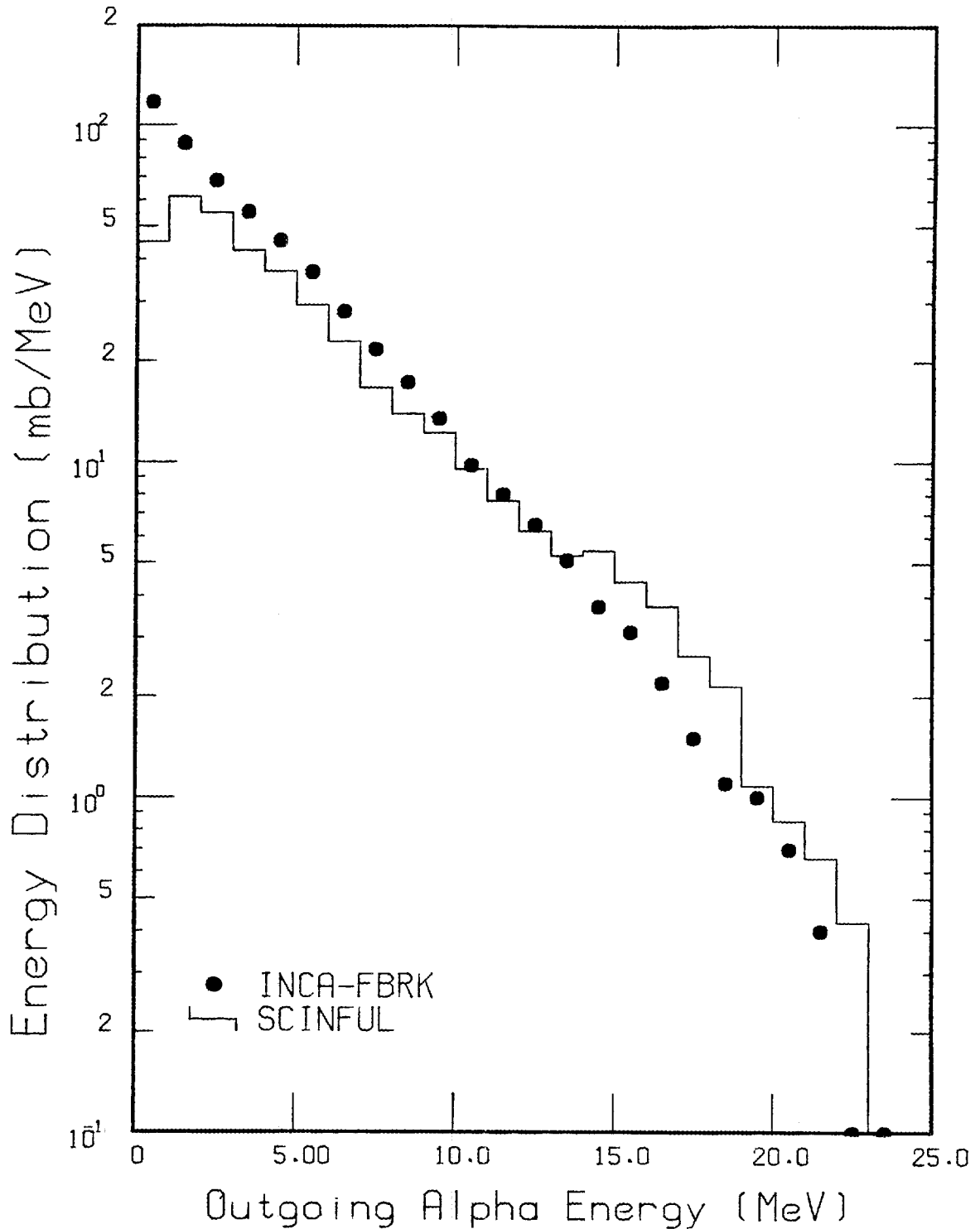


Fig. 31. Comparison of outgoing secondary-alpha energy spectra for an incident neutron energy of 30 MeV. The solid points represent the spectrum computed using the intranuclear-cascade model code family INCA-FBRK; the data shown for this spectrum are reported in ref. 1. The histogram represents the same spectrum computed using the author's SCINFUL code which is described in ref. 3.

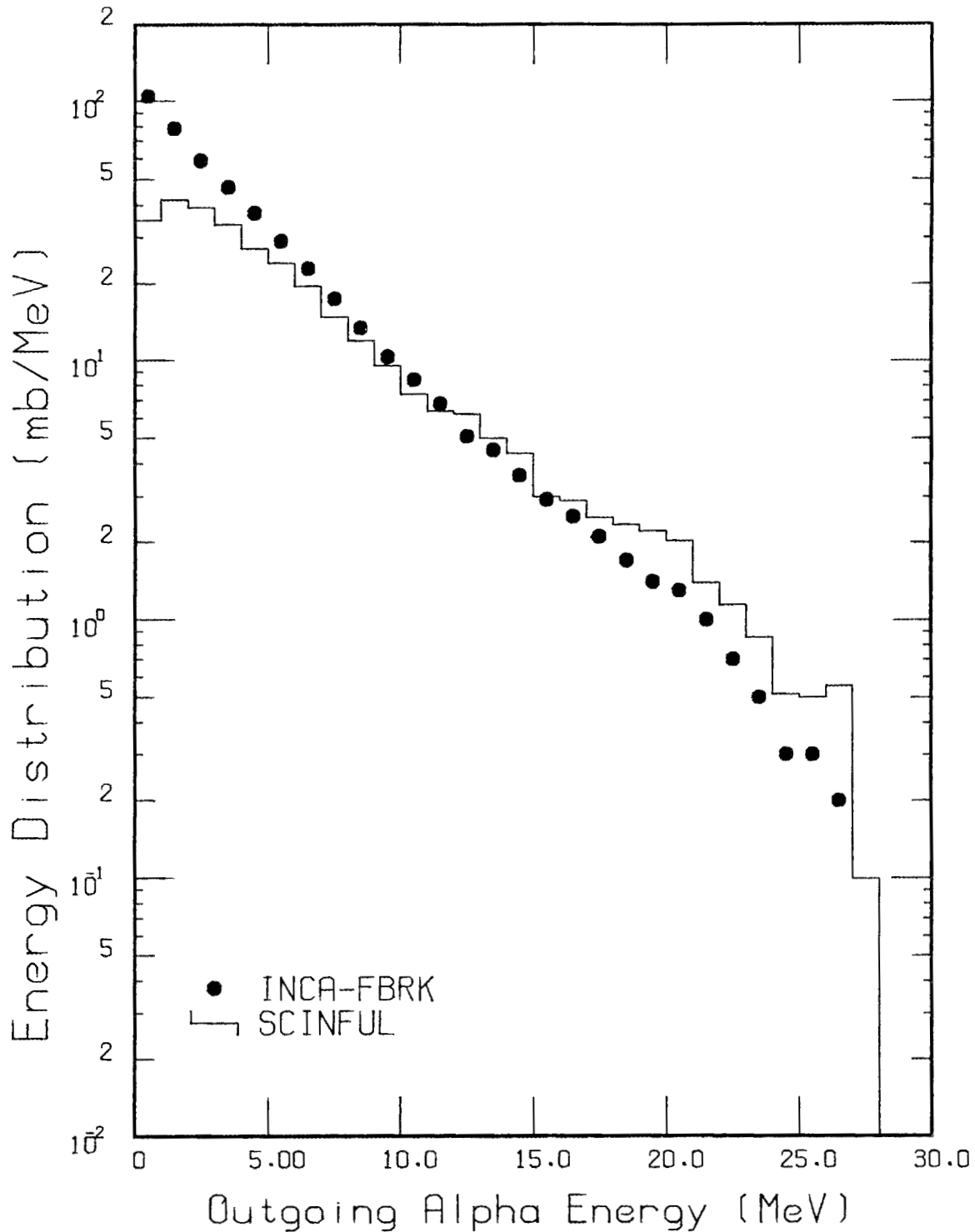


Fig. 32. Comparison of outgoing secondary-alpha energy spectra for an incident neutron energy of 35 MeV. The solid points represent the spectrum computed using the intranuclear-cascade model code family INCA-FBRK; the data shown for this spectrum are reported in ref. 1. The histogram represents the same spectrum computed using the author's SCINFUL code which is described in ref. 3.

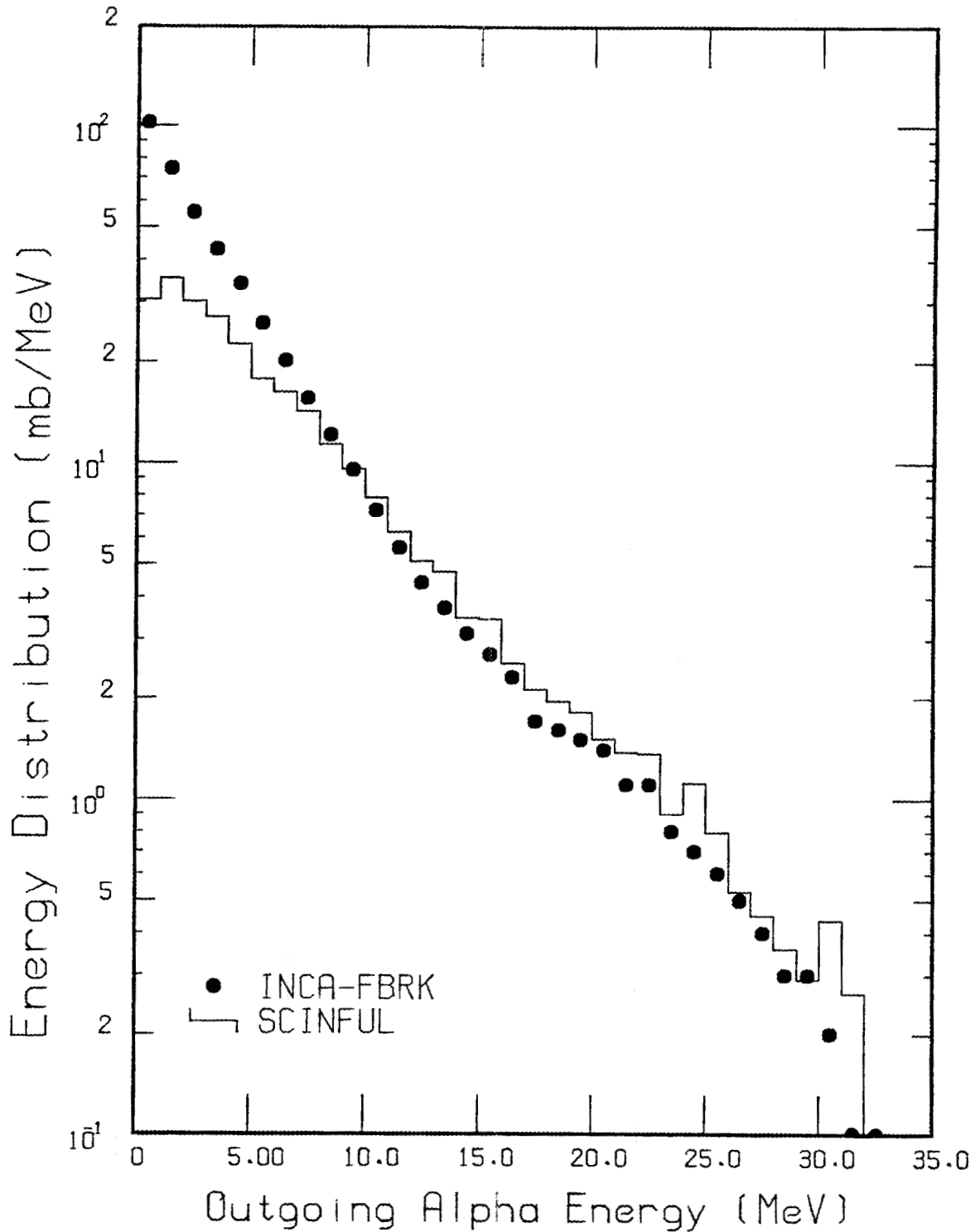


Fig. 33. Comparison of outgoing secondary-alpha energy spectra for an incident neutron energy of 40 MeV. The solid points represent the spectrum computed using the intranuclear-cascade model code family INCA-FBRK; the data shown for this spectrum are reported in ref. 1. The histogram represents the same spectrum computed using the author's SCINFUL code which is described in ref. 3.

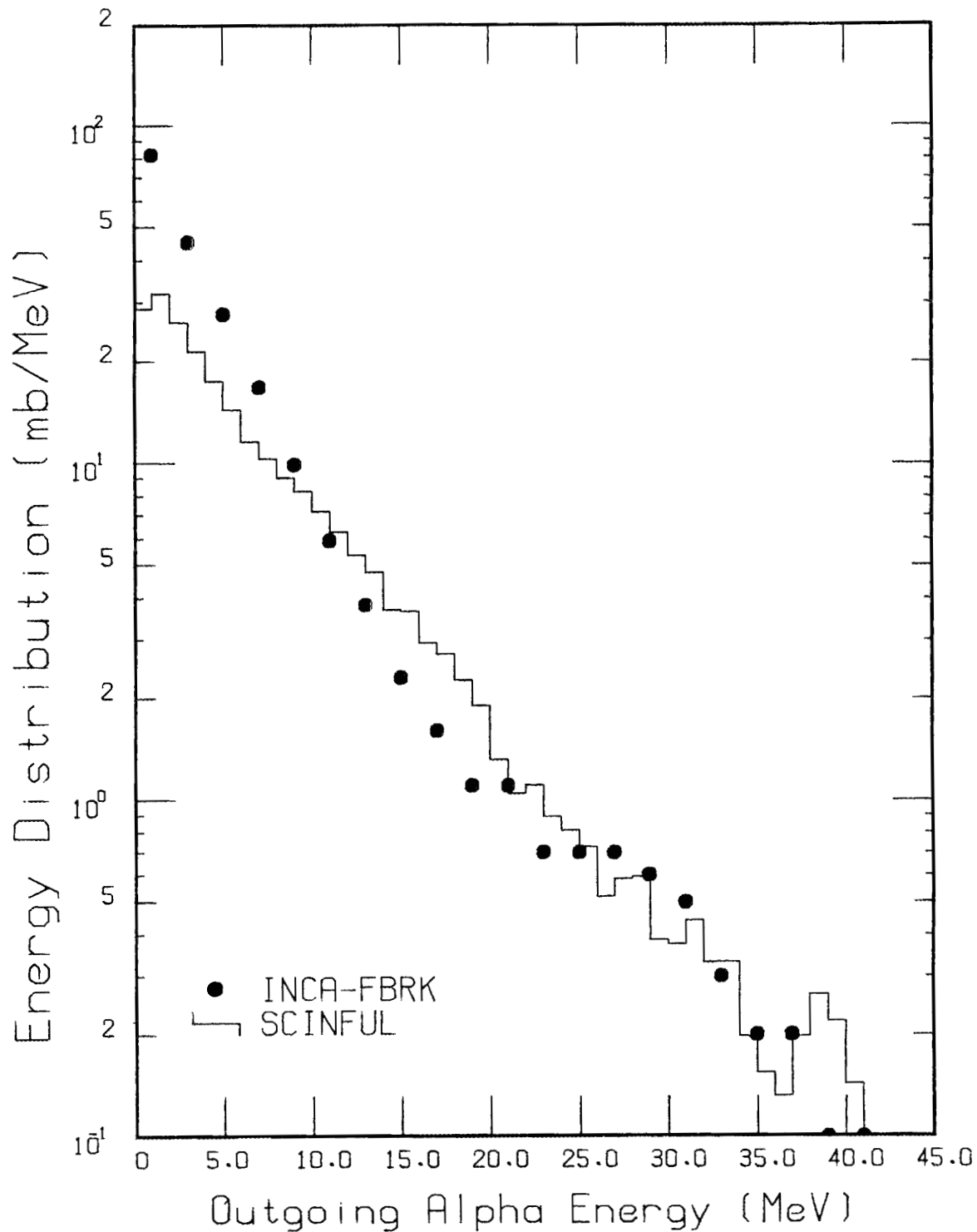


Fig. 34. Comparison of outgoing secondary-alpha energy spectra for an incident neutron energy of 50 MeV. The solid points represent the spectrum computed using the intranuclear-cascade model code family INCA-FBRK; the data shown for this spectrum are reported in ref. 1. The histogram represents the same spectrum computed using the author's SCINFUL code which is described in ref. 3.

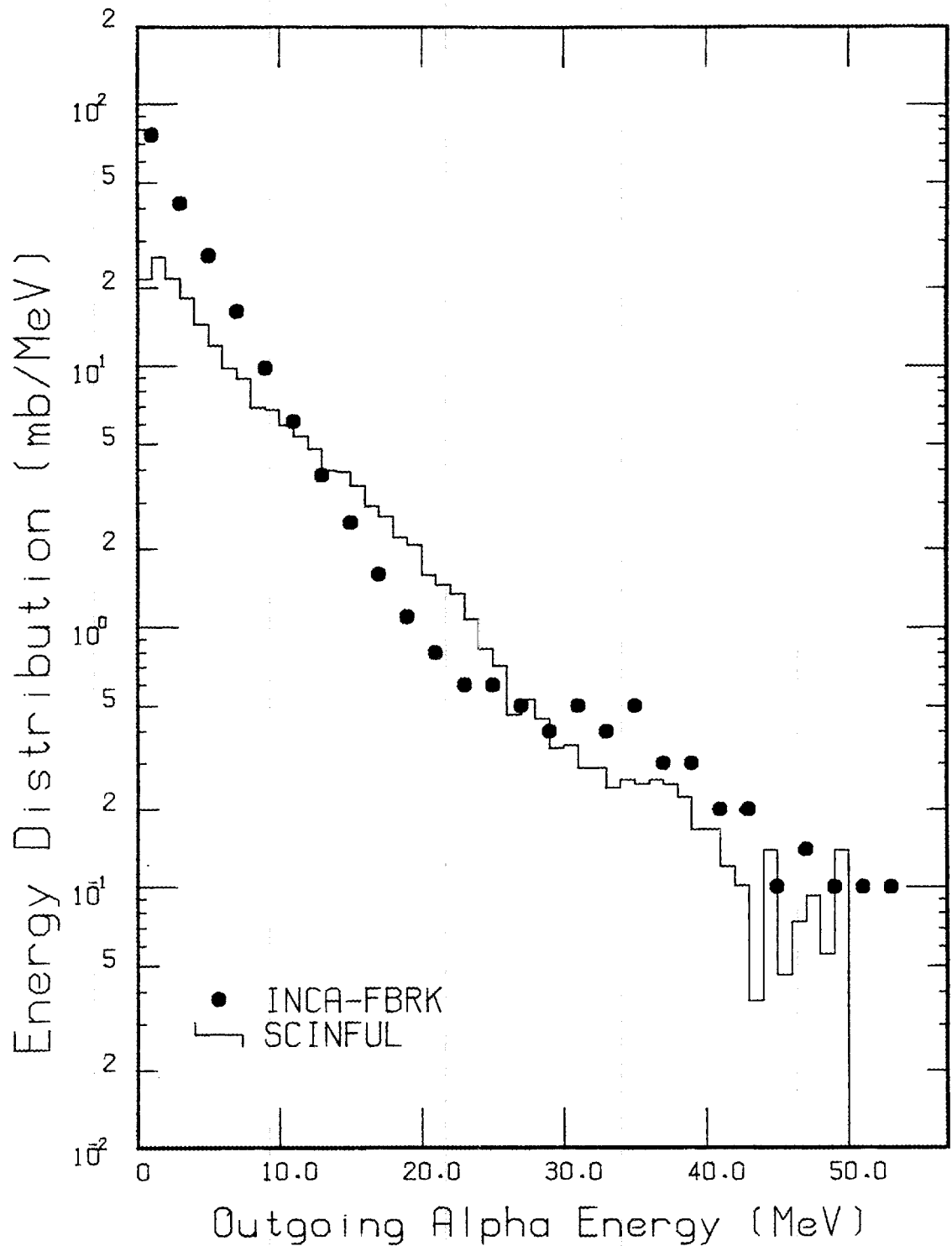


Fig. 35. Comparison of outgoing secondary-alpha energy spectra for an incident neutron energy of 60 MeV. The solid points represent the spectrum computed using the intranuclear-cascade model code family INCA-FBRK; the data shown for this spectrum are reported in ref. 1. The histogram represents the same spectrum computed using the author's SCINFUL code which is described in ref. 3.

8. COMPARISONS OF SECONDARY NEUTRON PRODUCTION

To a large extent in SCINFUL, once the charged-particle reactions had been developed the secondary neutron characteristics were fixed. The main reason that the secondary neutron characteristics were fixed was the boundary condition imposed by the total $n + {}^{12}\text{C}$ cross section, and the fact that the elastic scattering cross section is reasonably well known.

For the INCA-FBRK intranuclear cascade calculations, the “missing” ingredient is apparently the lack of a “direct-interaction” component to the inelastic-scattering channels. This code includes, however, compound-elastic scattering, and these results are shown in the figures to be discussed. The SCINFUL code includes elastic scattering via the elastic-scattering cross section and does not differentiate between compound-elastic scattering and shape-elastic scattering. For the purposes of comparison in this report, the results attributed to SCINFUL computations simply omitted all elastic scattering contributions.

The two sets of computed secondary-neutron energy spectra are shown in Figs. 36 to 43. For the lowest incident-neutron energies the differences are not too great, but as the incident neutron energy increases the differences become more pronounced. For the portion of the energy distribution corresponding to the lower half of the outgoing neutron energy, the observed differences could be related to the parametrized function used by SCINFUL for distribution of kinetic energies of outgoing continuum neutrons. In this code, this distribution is given a rather simple description taken from the code O5S:¹¹

$$\Phi(E_n) = EXP(-E_n/Temp) * E_n^{1.5} \quad (8)$$

where

$$Temp = 0.065 * E_n + 0.001 * E_n^2 \quad (9)$$

However, as noted in the document describing the code⁶ as well as in ref. 5, and as exhibited in Fig. 44, this relation does not reproduce the continuum neutron calculation of the statistical-model code TNG⁸ as well as, say, the formula given in Eq. (4) reproduces the continuum proton calculation of TNG as exhibited in Fig. 1. Except for the very lowest portion of the outgoing neutron energy spectra at $E_n = 50$ and 60 MeV, the SCINFUL computation is larger than the INCA-FBRK computation in the region where the SCINFUL computation is larger than the TNG-computed distribution. What this observation suggests is that the INCA-FBRK code, which uses an intranuclear cascade treatment, gives results similar to the TNG code, which uses a statistical-model treatment, for low-energy secondary neutrons.

The differences between the upper portions of the energy spectra computed using the INCA-FBRK code and those using the SCINFUL code are due to the use of explicitly included cross sections in SCINFUL for neutron excitation of levels in ${}^{12}\text{C}$ up to 18 MeV, whereas the INCA-FBRK code is, in effect, computing these cross sections. For incident neutron energies $E_n \leq 30$ MeV, the inelastic scattering

cross sections in SCINFUL have an experimental basis.¹⁶ At higher neutron energies, inelastic-scattering cross sections were estimated by extrapolation within the boundary condition provided by the total $n+^{12}\text{C}$ cross section. Lacking directly comparable experimental secondary neutron spectra for comparison with the calculated spectra it is difficult to be unequivocally in favor of one calculational result over the other. About all that can be said is that the harder neutron spectra computed using the INCA-FBRK code for $E_n = 50$ and 60 MeV are consistent with the softer secondary charged-particle spectra also computed using this code. For $E_n = 60.7$ MeV, as shown in ref. 5, the charged-particle energy spectra computed using SCINFUL are in reasonable agreement with the data of Subramanian et al.⁴ The agreement of the SCINFUL calculations with these data is, however, imperfect. A conservative conclusion would be that, should SCINFUL be further extended, some consideration should be given to the computation of the secondary neutron scattering. In particular, perhaps a parametrized formula giving a better reproduction of the continuum portion of the secondary neutron energy spectra computed using either the statistical model or the intranuclear cascade model should be determined to replace the current formula given in Eq. (8).

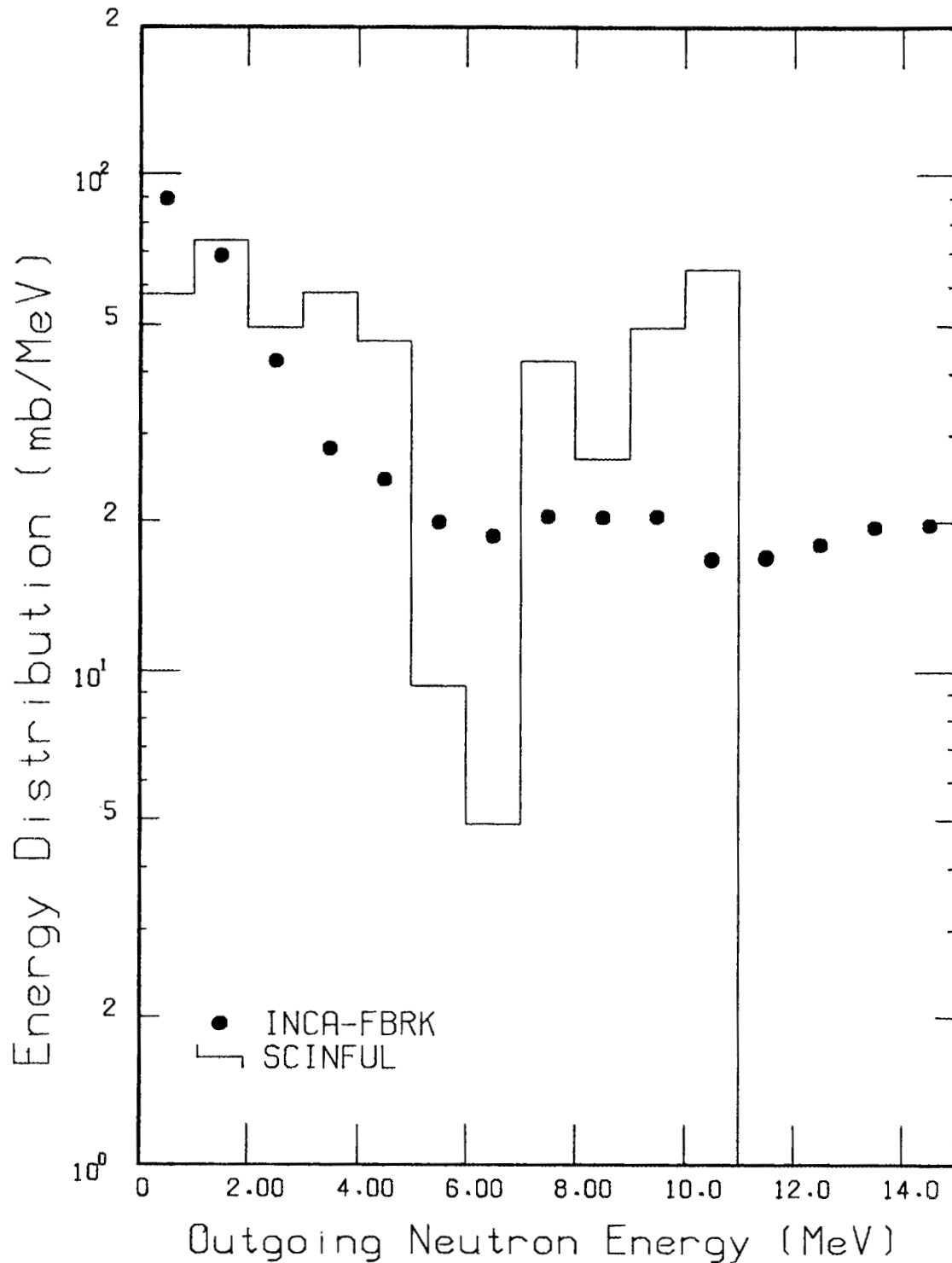


Fig. 36. Comparison of outgoing secondary-neutron energy spectra for an incident neutron energy of 15 MeV. The solid points represent the spectrum computed using the intranuclear-cascade model code family INCA-FBRK; the data shown for this spectrum are reported in ref. 1. The histogram represents the same spectrum computed using the author's SCINFUL code which is described in ref. 3.

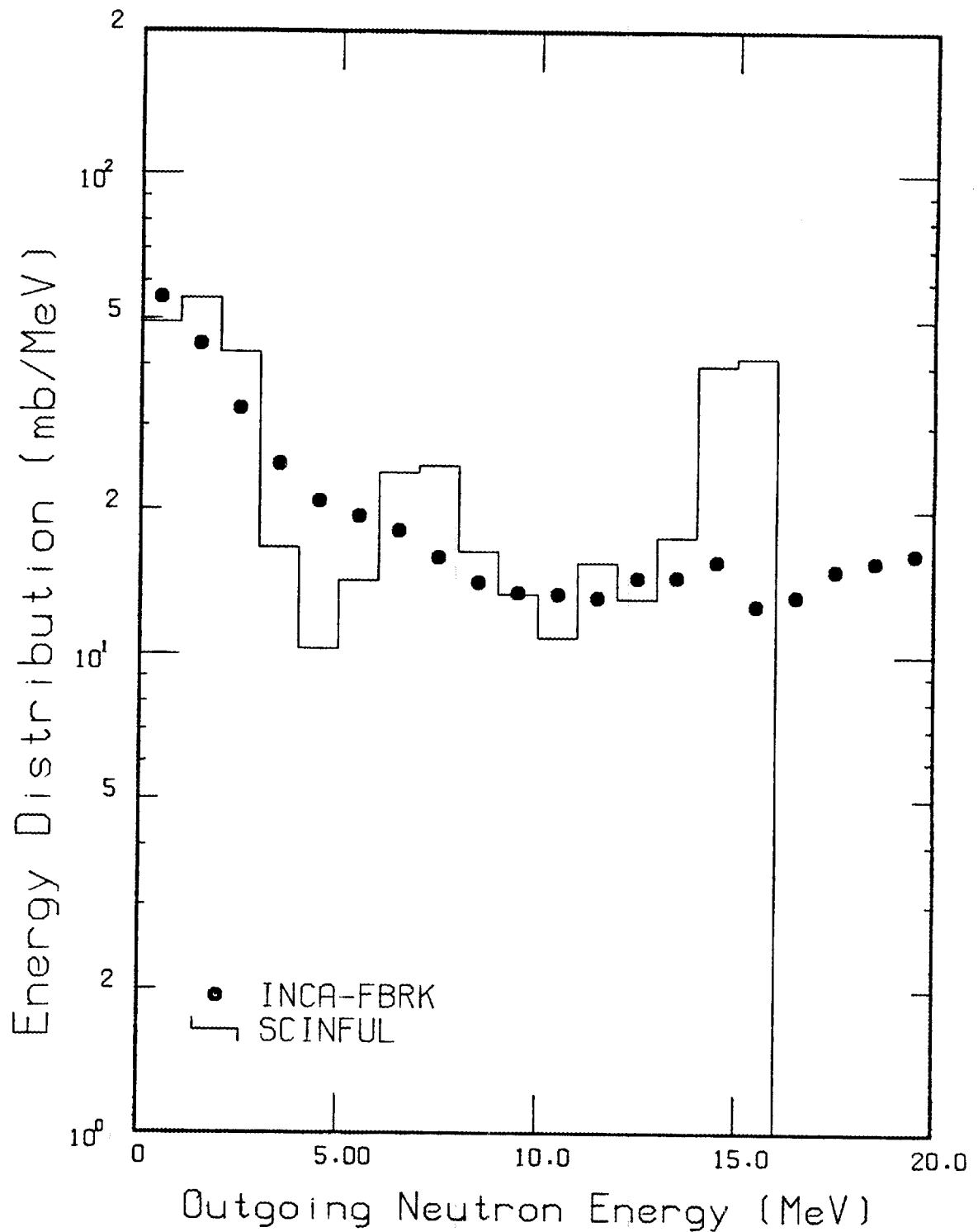


Fig. 37. Comparison of outgoing secondary-neutron energy spectra for an incident neutron energy of 20 MeV. The solid points represent the spectrum computed using the intranuclear-cascade model code family INCA-FBRK; the data shown for this spectrum are reported in ref. 1. The histogram represents the same spectrum computed using the author's SCINFUL code which is described in ref. 3.

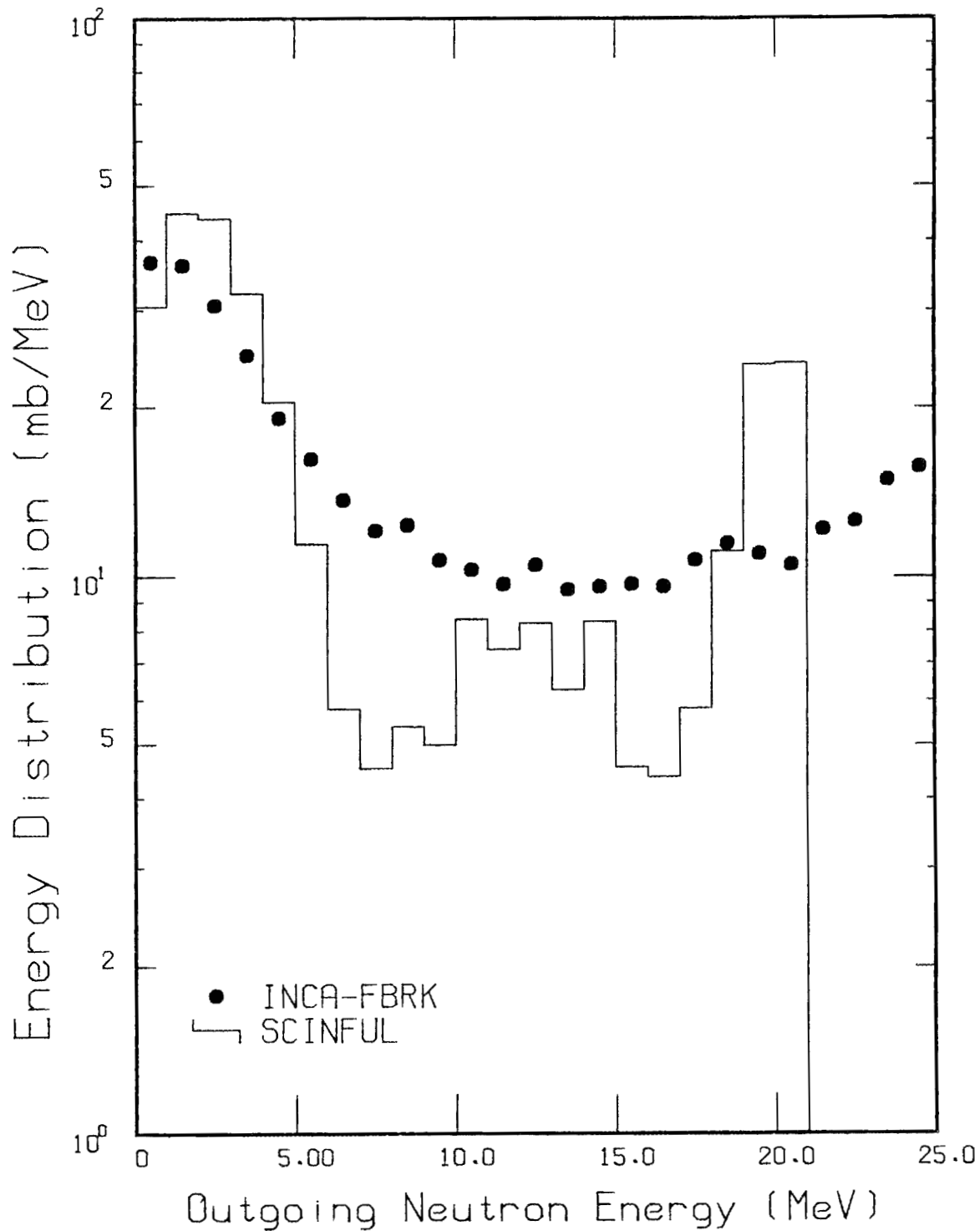


Fig. 38. Comparison of outgoing secondary-neutron energy spectra for an incident neutron energy of 25 MeV. The solid points represent the spectrum computed using the intranuclear-cascade model code family INCA-FBRK; the data shown for this spectrum are reported in ref. 1. The histogram represents the same spectrum computed using the author's SCINFUL code which is described in ref. 3.

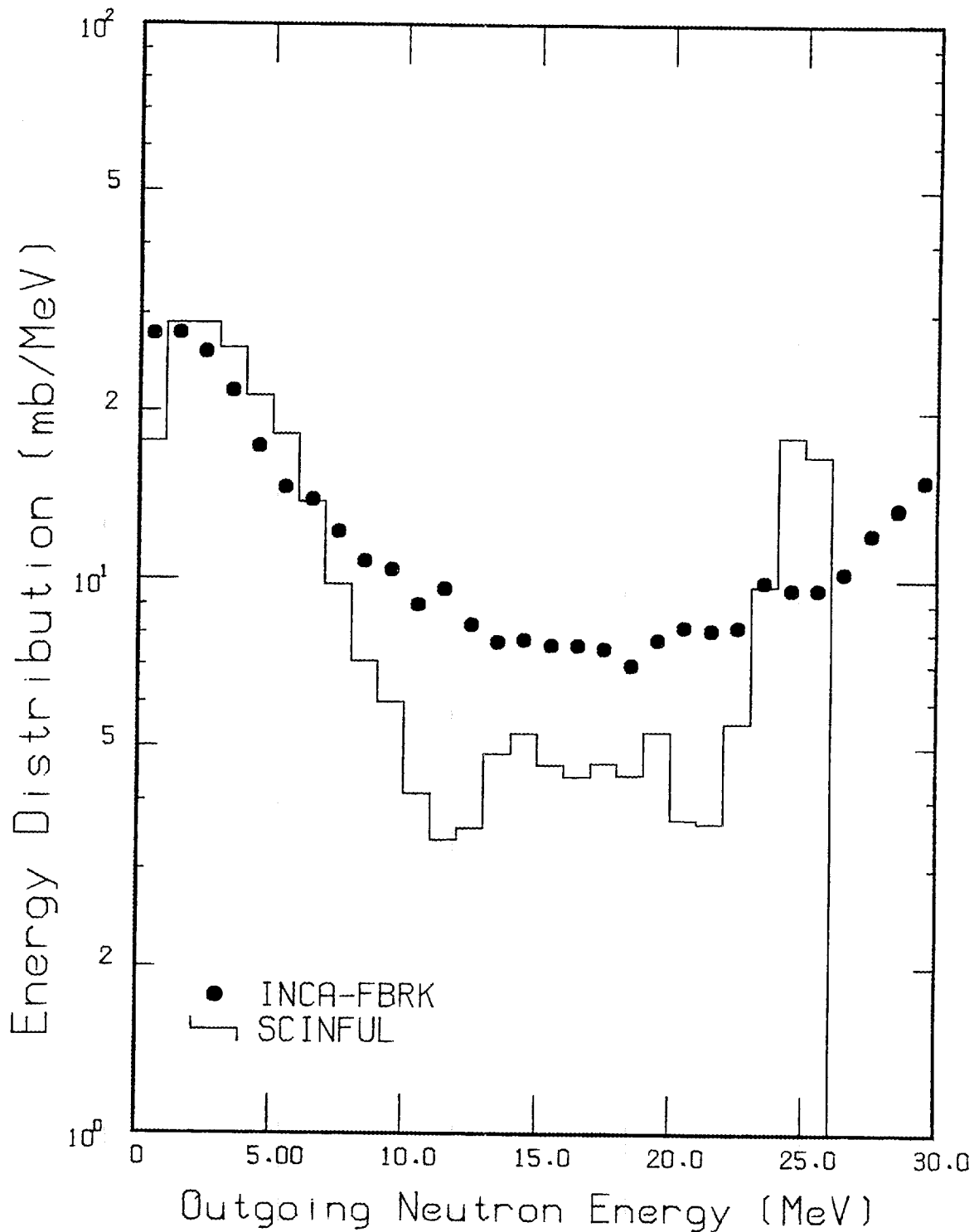


Fig. 39. Comparison of outgoing secondary-neutron energy spectra for an incident neutron energy of 30 MeV. The solid points represent the spectrum computed using the intranuclear-cascade model code family INCA-FBRK; the data shown for this spectrum are reported in ref. 1. The histogram represents the same spectrum computed using the author's SCINFUL code which is described in ref. 3.

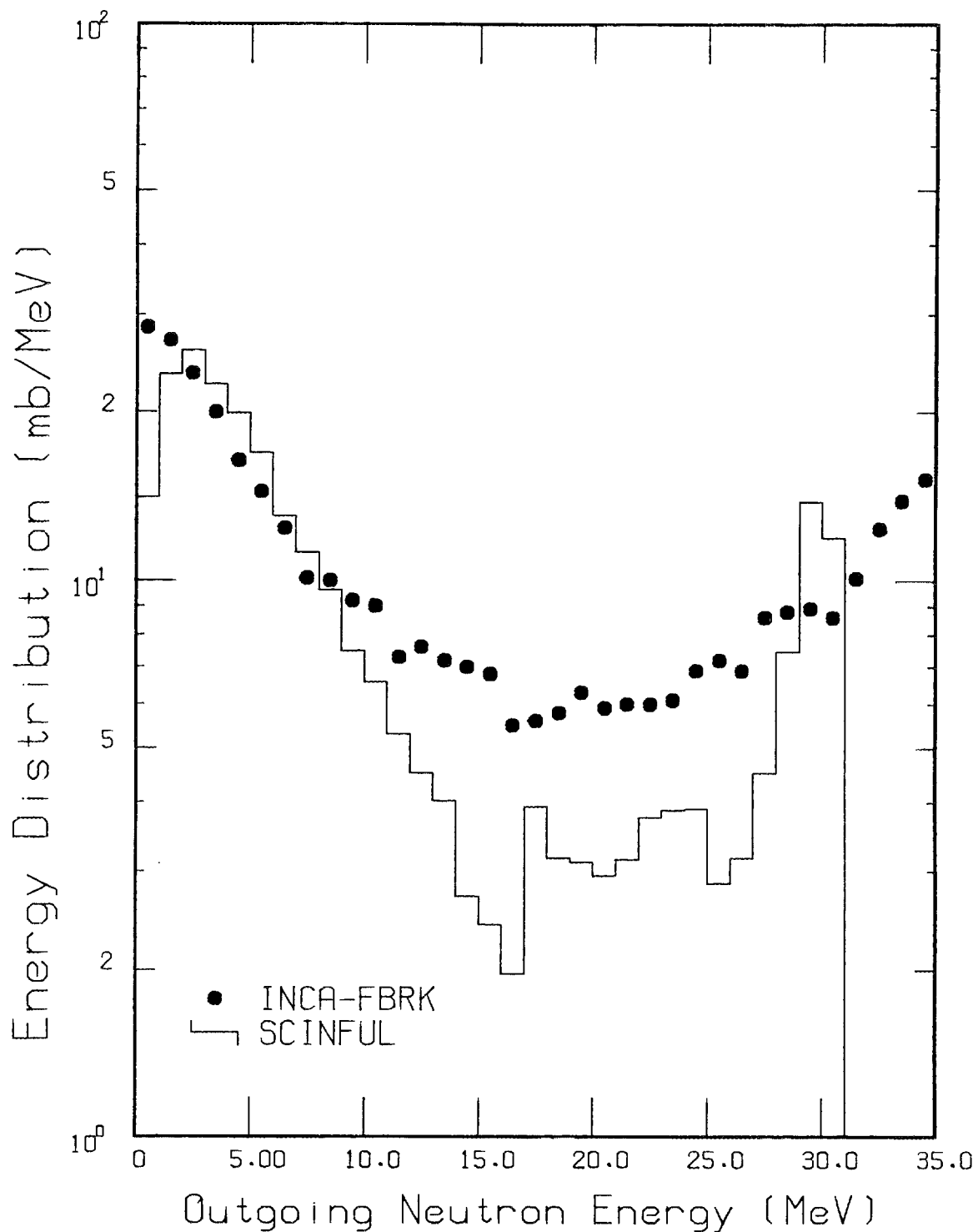


Fig. 40. Comparison of outgoing secondary-neutron energy spectra for an incident neutron energy of 35 MeV. The solid points represent the spectrum computed using the intranuclear-cascade model code family INCA-FBRK; the data shown for this spectrum are reported in ref. 1. The histogram represents the same spectrum computed using the author's SCINFUL code which is described in ref. 3.

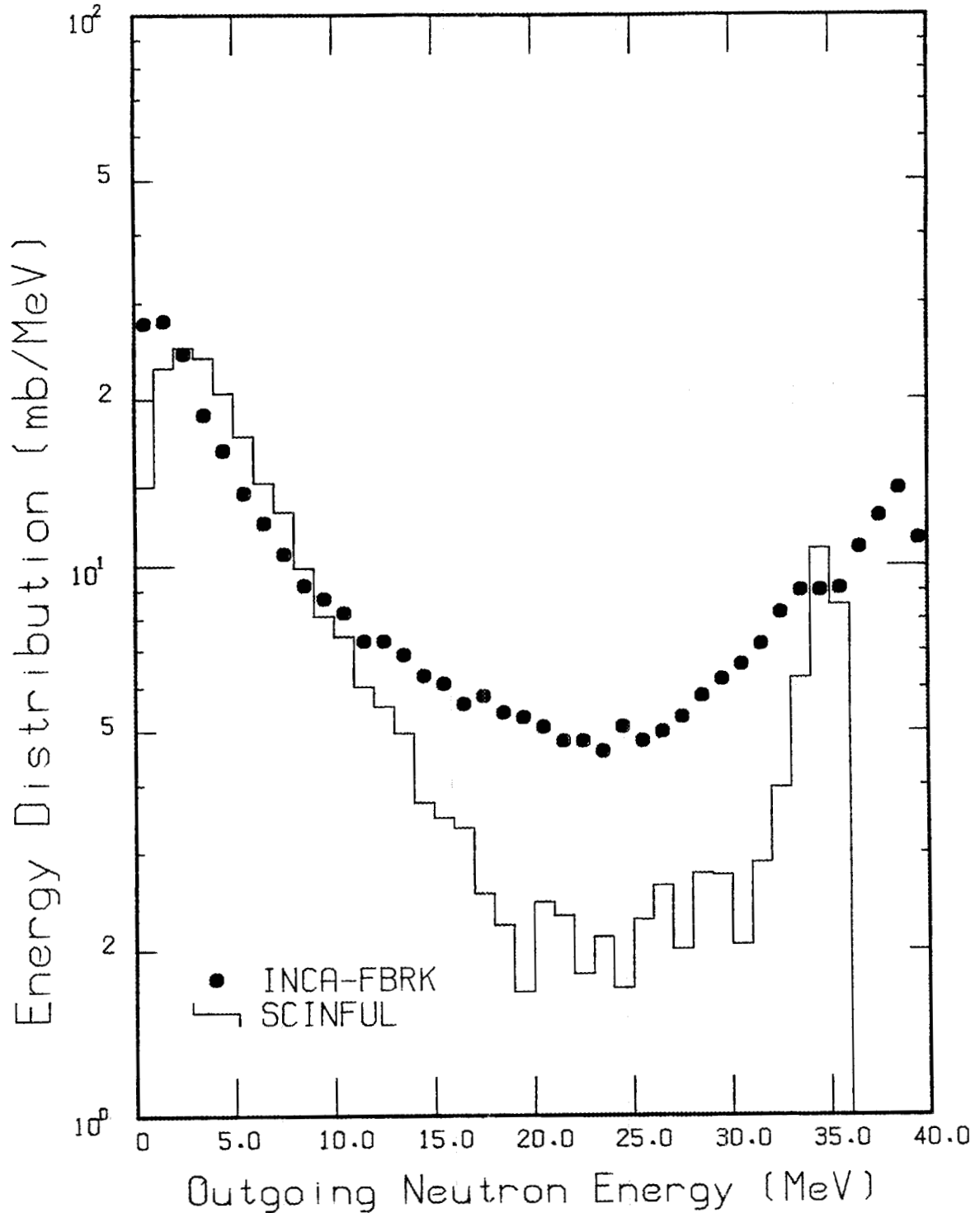


Fig. 41. Comparison of outgoing secondary-neutron energy spectra for an incident neutron energy of 40 MeV. The solid points represent the spectrum computed using the intranuclear-cascade model code family INCA-FBRK; the data shown for this spectrum are reported in ref. 1. The histogram represents the same spectrum computed using the author's SCINFUL code which is described in ref. 3.

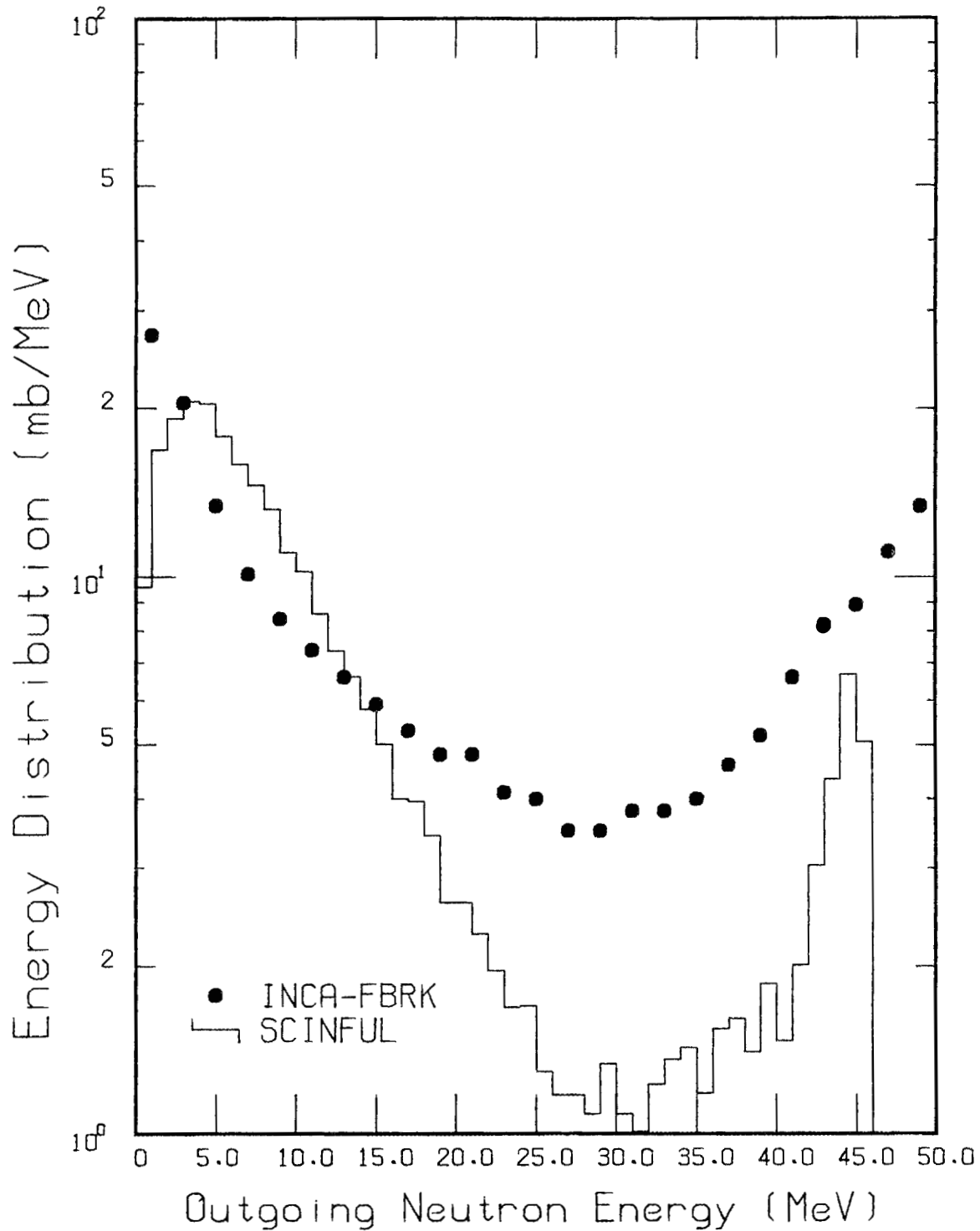


Fig. 42. Comparison of outgoing secondary-neutron energy spectra for an incident neutron energy of 50 MeV. The solid points represent the spectrum computed using the intranuclear-cascade model code family INCA-FBRK; the data shown for this spectrum are reported in ref. 1. The histogram represents the same spectrum computed using the author's SCINFUL code which is described in ref. 3.

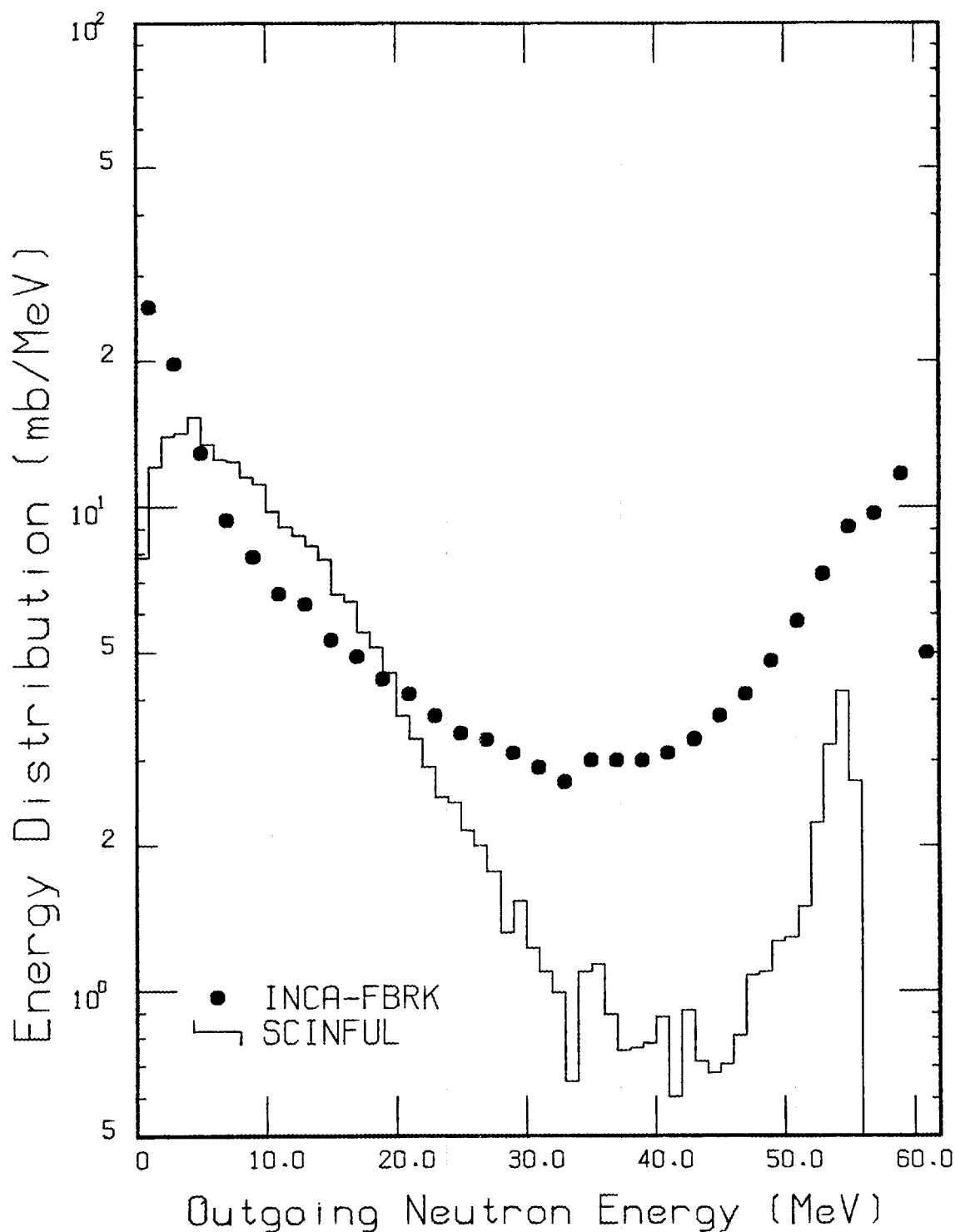


Fig. 43. Comparison of outgoing secondary-neutron energy spectra for an incident neutron energy of 60 MeV. The solid points represent the spectrum computed using the intranuclear-cascade model code family INCA-FBRK; the data shown for this spectrum are reported in ref. 1. The histogram represents the same spectrum computed using the author's SCINFUL code which is described in ref. 3.

ORNL - DWG 88-6094

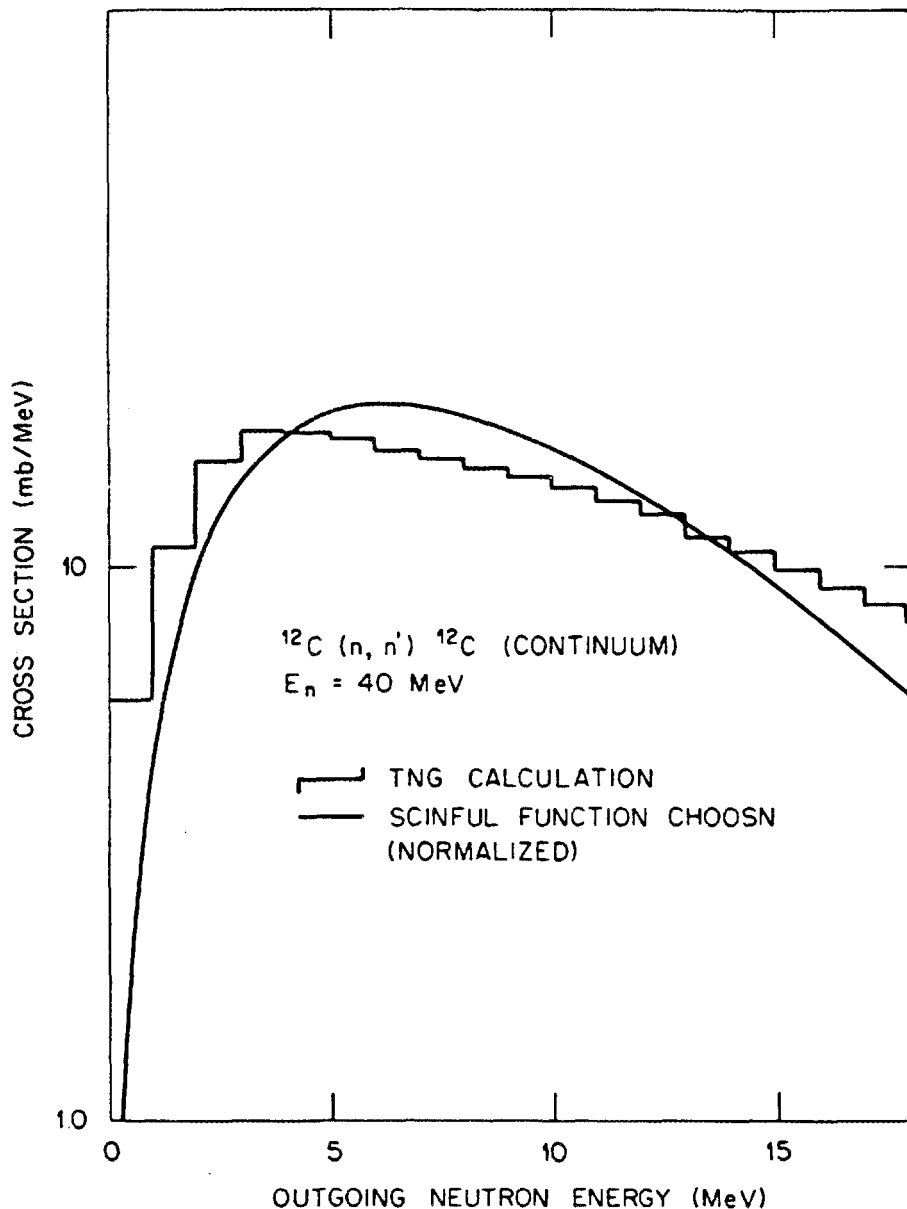


Fig. 44. Distribution of kinetic energies of the outgoing secondary neutron in a $^{12}\text{C}(n, n')^{12}\text{C}$ reaction for $E_n = 40 \text{ MeV}$ and for the residual ^{12}C in a highly excited continuum state. The histogram was computed using the statistical-model code TNG (ref. 8). The normalized curve represents the analytic function used in the author's code SCINFUL (ref. 3) and is the function given in Eqs. (8) and (9) in the text.

9. COMPARISONS OF TOTAL PARTICLE PRODUCTION CROSS SECTIONS

The report by Brenner and Prael¹ also gives double differential spectra for secondary particles of masses 6 through 12. In principle, the same information could be output from SCINFUL. However, for the practical purpose of SCINFUL, detailed knowledge of the energy spectra of these heavier mass secondary particles is not very important.

At least as meaningful a comparison is the total particle production cross section. The cross sections are given in the Brenner-Prael report¹ and they were extracted from the SCINFUL calculations. The comparisons of these cross sections is given in Table 2. The uncertainties given for both sets of data are "typical" statistical one-standard-deviation uncertainties. For the INCA-FBRK output, typical uncertainties are given only for $E_n = 15$ MeV. Brenner and Prael state¹ that production cross sections errors are less than 1%.

Qualitatively the two sets of integral secondary-particle production cross sections are in good agreement. Studying this table in some detail, however, reveals important differences. In particular, as the incident neutron energy increases the differences in the integral yields for secondary neutrons and secondary α -particles diverge; the INCA-FBRK program predicts almost twice as many α -particles as does SCINFUL for $E_n = 60$ MeV. Most of this difference, as indicated in Fig. 35, is for small outgoing α -particle energies. The differences in mass 12 must be related to the inclusion of compound-elastic scattering in INCA-FBRK which is not included in SCINFUL. The differences in masses 9 and 10 must be related to the inclusion in SCINFUL of small percentage requirements, as already discussed, of ground-state reactions in the $(n, t) + (n, {}^3\text{He})$ and (n, α) channels, requirements which are not in the INCA-FBRK codes. Reducing these small percentage requirements in SCINFUL would result in increasing the integral secondary α -particle production cross section by, perhaps, 75 mb at $E_n = 60$ MeV. The discrepancy in secondary α -particle production at this E_n would be reduced but it would still be rather large.

Table 2. Integral production cross sections (mb) for $n + {}^{12}\text{C}$ reactions: comparisons of INCA-FBRK values with SCINFUL results grouped by incident neutron energy.

Particle Identification	SCINFUL ^a Values	INCA-FBRK ^b Values
A. Incident neutron energy = 15 MeV:		
Neutrons	483.32 ± 4.56	446.0 ± 1.8
Protons	0.86 ± 0.19	1.8 ± 0.1
Alphas	962.04 ± 6.43	890.5 ± 1.4
Mass 9	63.04 ± 1.65	17.9 ± 0.2
Mass 12	184.51 ± 2.82	156.9 ± 0.8
B. Incident neutron energy = 20 MeV:		
Neutrons	406.77 ± 2.87	405.8
Protons	28.91 ± 0.77	35.9
Deuterons	53.19 ± 1.04	30.0
Alphas=	799.03 ± 4.03	795.2
Mass 9	23.83 ± 0.70	5.9
Mass 11	69.63 ± 1.19	49.7
Mass 12	144.39 ± 1.71	139.2
C. Incident neutron energy = 25 MeV:		
Neutrons	316.07 ± 2.33	380.5
Protons	50.52 ± 0.93	63.1
Deuterons	47.85 ± 0.91	56.1
Tritons	3.73 ± 0.25	4.0
3-He ions	0.84 ± 0.12	0.3
Alphas	555.32 ± 3.09	635.4
Mass 6	0.0	0.8
Mass 7	0.0	0.8
Mass 9	12.69 ± 0.47	2.9
Mass 10	4.58 ± 0.28	4.2
Mass 11	97.63 ± 1.30	115.5
Mass 12	86.15 ± 1.22	114.0
D. Incident neutron energy = 30 MeV		
Neutrons	279.79 ± 2.10	366.3
Protons	66.94 ± 1.03	81.6
Deuterons	49.08 ± 0.88	64.7
Tritons	10.30 ± 0.40	7.2
3-He ions	3.01 ± 0.22	1.1
Alphas	386.11 ± 2.46	534.4
Mass 6	1.76 ± 0.17	5.7
Mass 7	6.41 ± 0.32	18.6
Mass 8	2.81 ± 0.21	3.9
Mass 9	10.57 ± 0.41	1.8
Mass 10	11.84 ± 0.43	6.4
Mass 11	114.23 ± 1.34	131.3
Mass 12	71.56 ± 1.06	99.2

Table 2. Continued

Particle Identification	SCINFUL ^a Values	INCA-FBRK ^b Values
E. Incident neutron energy = 35 MeV:		
Neutrons	263.25 ± 1.94	372.5
Protons	77.51 ± 1.05	103.4
Deuterons	51.54 ± 0.86	63.9
Tritons	16.65 ± 0.49	11.7
3-He ions	6.38 ± 0.30	3.0
Alphas	305.61 ± 2.09	461.5
Mass 6	3.23 ± 0.21	5.7
Mass 7	9.30 ± 0.36	42.3
Mass 8	4.65 ± 0.26	4.8
Mass 9	15.88 ± 0.48	4.0
Mass 10	21.38 ± 0.55	11.7
Mass 11	105.27 ± 1.23	118.9
Mass 12	59.28 ± 0.92	97.8
F. Incident neutron energy = 40 MeV:		
Neutrons	266.13 ± 1.88	381.4
Protons	94.17 ± 1.12	116.6
Deuterons	52.30 ± 0.83	62.7
Tritons	22.99 ± 0.55	19.1
3-He ions	11.02 ± 0.38	5.9
Alphas	263.50 ± 1.87	433.2
Mass 6	3.98 ± 0.23	10.0
Mass 7	11.38 ± 0.39	47.2
Mass 8	5.33 ± 0.27	3.9
Mass 9	17.25 ± 0.48	4.2
Mass 10	34.44 ± 0.67	15.5
Mass 11	94.03 ± 1.12	102.3
Mass 12	49.08 ± 0.81	94.8
G. Incident neutron energy = 50 MeV:		
Neutrons	269.62 ± 1.72	398.1
Protons	108.68 ± 1.09	136.0
Deuterons	56.70 ± 0.79	65.0
Tritons	31.37 ± 0.59	24.4
3-He ions	15.02 ± 0.41	8.8
Alphas	231.04 ± 1.59	402.2
Mass 6	4.51 ± 0.22	16.5
Mass 7	8.79 ± 0.31	40.9
Mass 8	2.77 ± 0.17	2.4
Mass 9	14.22 ± 0.40	5.1
Mass 10	45.49 ± 0.71	16.9
Mass 11	77.32 ± 0.92	79.4
Mass 12	36.83 ± 0.64	93.2

Table 2. Continued

Particle Identification	SCINFUL ^a Values	INCA-FBRK ^b Values
H. Incident neutron energy = 60 MeV:		
Neutrons	253.29 ± 1.53	406.3
Protons	113.12 ± 1.02	150.6
Deuterons	57.04 ± 0.73	60.7
Tritons	30.87 ± 0.54	24.3
3-He ions	15.99 ± 0.39	9.7
Alphas	196.32 ± 1.35	380.9
Mass 6	4.77 ± 0.21	17.0
Mass 7	5.94 ± 0.23	33.3
Mass 8	1.68 ± 0.12	2.2
Mass 9	14.53 ± 0.37	5.4
Mass 10	43.19 ± 0.63	15.0
Mass 11	71.08 ± 0.81	65.8
Mass 12	27.00 ± 0.50	90.5

^a Ref. 3.^b Ref. 1.

10. CONCLUSIONS AND RECOMMENDATIONS

The computational results of secondary particle energy spectra and integral production cross sections obtained by two rather different calculational methods have been compared. Qualitatively the agreement is quite good; both methods lead to small yields of tritons and ^3He ions, intermediate yields of deuterons and protons, and large yields of neutrons and α particles. Comparable qualitative agreement is good for integral production cross sections of mass-6 to mass-12 secondary particles.

Quantitatively, the agreement for both secondary-particle energy spectra and integral production cross sections is quite good for $E_n = 15$ and 20 MeV; moderate differences are observed in both spectra and integral cross sections for $E_n = 25$ MeV, and the differences increase as the incident neutron energy increases. The existing experimental data of Subramanian et al.⁴ are in reasonably good agreement with the SCINFUL computations, but they are also in reasonably good agreement with the INCA-FBRK computations.

For the purpose for which SCINFUL was written, namely computing organic scintillator responses to incident neutron detection, the present comparisons provide a good corroboration of the SCINFUL program. Listing the secondary charged particles in order of importance, α , p , d , t , and ^3He , one may observe that for the first two the principle important differences from a nuclear physics point of view are for the smallest $\sim 15\%$ of maximum energy of the energy spectra, where the INCA-FBRK code predicts a significantly larger yield at larger incident neutron energies than does SCINFUL. However, these low-energy particles have very low fluorescent light amplitudes, and so at most would have only a minor effect on the total response calculation. The last two secondary charged particles in the list, t and ^3He , have such small yields as to hardly matter in the total response calculation.

For the secondary deuterons, the different predicted energy distributions of the INCA-FBRK code could be significant, especially for the larger incident neutron energies. In SCINFUL total deuteron yields and energy distributions were tailored to approximately reproduce not only the Subramanian et al.⁴ data but also the response data of Lockwood et al.¹² for E_n up to 75 MeV. One should not construe that these comparisons of secondary-deuteron energy spectra in some fashion imply an inadequacy in the intranuclear cascade method. In the first place, as mentioned in the Introduction, such is not the purpose of this study; and in the second place, much, if not most, of the secondary-deuteron production in INCA-FBRK is computed using a pickup model added to the intranuclear cascade program.

The only differences between INCA-FBRK and SCINFUL calculations that might be of concern are those exhibited for the secondary neutron spectra, especially for the larger incident neutron energies. These differences become important for the multiple scattering and geometrical aspects of the total response calculation problem, i.e., the *second* phase of the total SCINFUL calculation mentioned in the second paragraph of the Introduction. For a small detector, these differences in calculated neutron spectra would be of little concern; the higher-energy neutrons would simply escape the detector. However, for a large detector, wherein the total response involves multiple interactions of the incident neutron with the nuclear

62 CONCLUSIONS AND RECOMMENDATIONS

constituents of the detector, the differences in the yields of the higher-energy secondary neutrons could be important, perhaps as much as 10 to 15% for a very large detector in the largest-amplitude portion of detector response for $E_n \sim 60$ MeV. Present-day experimental response data are not sufficiently accurate to discriminate between a response computed using the secondary neutron spectrum for $E_n = 60$ MeV computed using INCA-FBRK from a response computed using SCINFUL. Indeed, a better experimental determination would be a secondary-neutron spectrum similar to the secondary-charged-particle spectra of Subramanian, et al.⁴

As presently written, SCINFUL provides a good tool for computing organic scintillator responses to incident monoenergetic neutrons for the incident neutron energy region between 0.1 and 80 MeV. However, if, in the future, programmatic needs should encourage the extension of these response calculations to neutron energies greater than 80 MeV, the methods utilized in SCINFUL to provide the nuclear characteristics of secondary charged particles – and neutrons — following nonelastic neutron interactions with ^{12}C should be reviewed.

ACKNOWLEDGMENTS

I wish to thank C. Y. Fu for a careful review of this report. I also appreciate the effort of S. Damewood in preparing the document.

REFERENCES

1. D. J. Brenner and R. E. Prael, *At. Data and Nucl. Data Tables* **41**, 71 (1989).
2. E. Fermi, *Prog. Theor. Phys.* **5**, 570 (1950).
3. J. K. Dickens, *SCINFUL: A Monte-Carlo-Based Computer Program to Determine a Scintillator Full Energy Response to Neutron Detection for E_n Between 0.1 and 80 MeV: User's Manual and FORTRAN Program Listing*, ORNL-6462 (1988).
4. T. S. Subramanian, J. L. Romero, F. P. Brady, J. W. Watson, D. H. Fitzgerald, R. Barrett, G. A. Needham, J. L. Ullman, C. I. Zanelli, D. J. Brenner, and R. E. Prael, *Phys. Rev. C* **28**, 521 (1983).
5. J. K. Dickens, *Comp. in Phys.* **3**, 62 (1989).
6. J. K. Dickens, *SCINFUL: A Monte Carlo Based Computer Program to Determine a Scintillator Full Energy Response to Neutron Detection for E_n Between 0.1 and 80 MeV: Program Development and Comparisons of Program Predictions with Experimental Data*, ORNL-6463 (1988).
7. C. Y. Fu, *Summary of ENDF/B-V Evaluations for Carbon, Calcium, Iron, Copper, and Lead and ENDF/B-V Revision 2 for Calcium and Iron*, ORNL/TM-8283 (1982).
8. C. Y. Fu, *At. Data Nucl. Data Tables* **17**, 127 (1976); also *Nucl. Sci. Eng.* **100**, 61 (1988).
9. F. Ajzenberg-Selove, *Nucl. Phys. A* **413**, 1 (1984); *Nucl. Phys. A* **433**, 1 (1985).
10. J. L. Romero, private communication (1987).
11. R. E. Textor and V. V. Verbinski, *O5S: A Monte Carlo Code for Calculating Pulse Height Distributions due to Monoenergetic Neutrons Incident on Organic Scintillators*, ORNL-4160 (1968). See also M. A. Cleemput, *O5S — A Version Suitable for Use on the DEC System-10*, ORNL/CF-82/268/R1 (1982).
12. J. A. Lockwood, C. Chen, L. A. Friling, D. Swartz, N. St. Onge, A. Galonsky and R. R. Doering, *Nucl. Instrum. Meth.* **138**, 353 (1976).
13. G. Dietze, H. J. Brede, H. Klein and H. Schölermann, in *Nuclear Data for Science and Technology, Proc. of Int. Conf. 6-10 Sept. 1982, Antwerp*, K. H. Böckhoff, ed. (D. Reidel Publ. Co., Dordrecht/Boston/London, 1983), p. 930; M. Brendle, M. Morike, G. Staudt, and G. Steidle, *Z. Naturforsch* **23a**, 1229 (1968); R. C. Haight, S. M. Grimes, R. G. Johnson, and H. H. Barshall, *Nucl. Sci. Eng.* **17**, 41 (1984).
14. D. A. Kellogg, *Phys. Rev.* **90**, 224 (1953).
15. B. Antolkovic, I. Slaus, D. Plenkovic, P. Macq, and J. P. Meulders, *Nucl. Phys. A* **394**, 87 (1983).
16. A. S. Meigoni, J. S. Petler, and R. W. Finlay, *Phys. Med. Bio.* **29**, 643 (1984); see also R. W. Finlay, A. S. Meigoni, J. S. Petler, and J. P. Delaroche, *Nucl. Instrum. Meth. Phys. Res. B* **10/11**, 396 (1985).

INTERNAL DISTRIBUTION

- | | |
|---------------------|--------------------------------|
| 1. B. R. Appleton | 28. R. C. Ward |
| 2-6. J. K. Dickens | 29. J. J. Dorning (consultant) |
| 7-11. C. Y. Fu | 30. R. M. Haralick(consultant) |
| 12. T. A. Gabriel | 31. J. E. Leiss (consultant) |
| 13. D. M. Hetrick | 32. N. Moray (consultant) |
| 14. N. W. Hill | 33. M. F. Wheeler (consultant) |
| 15. D. T. Ingersoll | 34. EPMD Reports Office |
| 16. R. W. Ingle | 35-36. Laboratory Records |
| 17-21. D. C. Larson | Department |
| 22. J. W. McConnell | 37. Laboratory Records, |
| 23. R. W. Peelle | ORNL-RC |
| 24. F. G. Perey | 38. Document Reference |
| 25. R. W. Roussin | Section |
| 26. R. T. Santoro | 39. Central Research Library |
| 27. R. R. Spencer | 40. ORNL Patent Section |

EXTERNAL DISTRIBUTION

41. G. F. Auchampaugh, Los Alamos National Laboratory, P. O. Box 1663, MS D449-P3, Los Alamos, NM 87545
42. P. Binns, National Accelerator Center, P. O. Box 72, Faure 7131, South Africa
43. D. J. Brenner, Radiological Research Laboratories, College of Physicians and Surgeons of Columbia University, 630 W. 168 Street, New York City, NY 10032
44. W. K. Brooks, Department of Physics and Astronomy, University of Pittsburgh, 100 Allen Hall, 3941 O'Hara Street, Pittsburgh, PA 15260
45. F. E. Cecil, Colorado School of Mines, Department of Physics, Golden, CO 80401
46. Satoshi Chiba, Department of Physics, Japan Atomic Energy Research Institute, Tokai-mura, Naka-gun, Ibaraki-ken 319-11, Japan
47. A. Dauchy, Institut des Sciences Nucleaires, 53 Avenue des Martyrs, 38026 Grenoble Cedex, France
48. D. R. Edwards, Department of Nuclear Engineering, 102 Fulton Hall, Rolla, MO 65401
49. Roger W. Finlay, Department of Physics and Astronomy, Ohio University, Athens, OH 45701
50. S. M. Grimes, Department of Physics and Astronomy, Ohio University, Athens, OH 45701
51. Chris Hartmann, Department of Medical Physics, 1530 MSC, 1300 University Avenue, Madison, WI 53706
52. R. R. Keziah, Department of Physics, Air Force Academy, Colorado Springs, CO 80840
53. Horst Klein, Physikalisch-Technische Bundesanstalt, Braunschweig und Berlin, Bundesalle 100, Postfach 3345, D-3300 Braunschweig, Germany
54. Jeffrey Leavey, IBM Research Division, Thomas J. Watson Research Center, P. O. Box 218, Yorktown Heights, NY 10598

55. R. Madey, Department of Physics, Kent State University, Kent, OH 44242
56. Don Marshlenski, Ohio State University, Van de Graaff Accelerator Laboratory, 1302 Kinnear Road, Columbus, OH 43212
57. Capt. J. B. Martin, Department of the Air Force, Air Force Weapons Laboratory, Kirtland Air Force Base, NM 87117-6008
58. G. L. Morgan, Los Alamos National Laboratory, P. O. Box 1663, Group P-15, MS D406, Los Alamos, NM 87545
59. J. S. O'Connell, RADP/B109, National Institute for Science and Technology, Gaithersburg, MD 20899
60. Nils Olsson, Uppsala Universitet, Neutronforsknings Laboratoriet, Studsvik, S-611 82 Nyköping, Sweden
61. R. E. Prael, Los Alamos National Laboratory, Los Alamos, NM 87545
62. J. A. Reafsnyder, Deputy Assistant Manager, Energy Research and Development, Department of Energy, Oak Ridge Operations, Post Office Box 2008, Oak Ridge, TN 37831-6269
63. J. L. Romero, Crocker Nuclear Laboratory, University of California at Davis, Davis, CA 95616
64. D. L. Smith, Argonne National Laboratory, Applied Physics Division, Building 314, 9700 South Cass Avenue, Argonne, IL 60439
65. R. W. Tayloe, Jr., Battelle Columbus Division, 505 King Avenue, Columbus, OH 43201-2693
66. F. Y. Tsang, Idaho National Engineering Laboratory, EG&G Idaho Inc., TRA652, P. O. Box 1652, Idaho Falls, ID 83415
67. Yoshitomo Uwamino, Institute for Nuclear Study, University of Tokyo, Midori-cho 3-2-1, Tanashi, Tokyo 188, Japan
68. Thiraphat Vilaithong, Physics Department, Chiang Mai University, Faculty of Science, Chiang Mai 50002, Thailand
69. S. Wender, Los Alamos National Laboratory, P. O. Box 1663, Group P-3, MS D449, Los Alamos, NM 87545
70. S. L. Whetstone, Department of Energy, ER-23/GTN, 19901 Germantown Rd., Germantown, MD 20874
71. Warren Wilson, AFWL/SWYW, Building 416, Kirtland Air Force Base, NM 87117-5008
72. M. S. Zucker, Department of Nuclear Energy, Brookhaven National Laboratory, Upton, NY 11973
- 73-82. Office of Scientific and Technical Information, P. O. Box 62, Oak Ridge, TN 37831